Influence of Crystallographic Orientation on Friction and Fretting Fatigue Behavior of Ni-base Superalloys

(Ni基超合金の摩擦とフレッティング疲労特性に及ぼす結晶方位の影響)

by

RENGARAJ BALAVENKATESH

A Dissertation Submitted to the Graduate School of Engineering
in Partial Fulfillment of the Requirements for the Degree of

Doctor of Engineering

at the

Nagaoka University of Technology

May 2018

Influence of Crystallographic Orientation on Friction and Fretting Fatigue Behavior of Ni-base Superalloys

Abstract

Heat resistant materials such as Ni-base superalloys possess a remarkable capability to hold their properties at elevated temperature conditions. They have been widely used in the hot section components of modern aircraft and power generation gas turbine engines. Especially, turbine blades are one of the most sophisticated components of a gas turbine which convert the thermal energy of combustion gases into mechanical energy. Here, turbine blades are casted as single crystals of Ni-base superalloys due to their higher tolerance to creep and low cycle fatigue exposure. Consequently, single crystal blades exhibit high elastic anisotropy, i.e. their mechanical properties vary with crystallographic orientation.

Single crystal blades are mounted on turbine disks, manufactured from polycrystalline Ni-base superalloys by means of dovetail connections or fir-tree arrangements. Cyclic friction and fretting between the single crystal blade and polycrystalline disk occur due to small oscillating relative displacements during engine operation. Key research focus should be laid on the clarification of crystallographic orientation dependence on high temperature strength of single crystal superalloy. Specifically, the effect of secondary crystallographic orientation of rotor blades with respect to disk contact surface on the mechanical strength and reliability needs to be clarified to achieve further improvements in microstructure design and development of advanced superalloys.

The aim of the present study is to investigate the influence of crystallographic orientation of contacting single crystal (SC) vs polycrystalline (PC) superalloys used in gas turbine blades and disks, respectively. To achieve this, the role of crystallographic orientation of single crystal rotor blade material (CMSX-2/4) with respect to polycrystalline disk material (IN718) on the cyclic sliding friction (CSF) and fretting fatigue (FF) behavior was investigated at ambient and high temperatures.

First, anisotropic frictional response of contacting superalloys during cyclic sliding under gross slip conditions has been investigated. A significant influence of crystallographic contact plane (crystallographic orientation of sliding surface) and sliding orientation (crystallographic orientation toward the sliding direction) on the coefficient of friction (COF) was found. At room temperature, a normal load depended anisotropic tribological behavior was observed. On a given contact surface orientation, a specific effect of sliding direction was also established. This anisotropic behavior was found to be independent of test temperature. Discussions were made on the above experimental results. It was shown that both the stress and the deformation field near the contact area which are closely influenced by the anisotropic mechanical properties in longitudinal and transverse elastic moduli and in yield strength would play extrinsic roles there.

Second, fretting fatigue tests were carried out under partial slip conditions. Significant differences in fretting fatigue lives with respect to contacting superalloy combinations were found experimentally. These differences were found to be controlled by material dependent tangential force coefficient (TFC) evolution during fretting fatigue loading. A slight improvement of life at 600 °C was observed under lower stress amplitudes. Significant changes in the fretting induced subsurface microstructure was characterized using SEM and EBSD techniques. Experimentally measured TFC values were correlated with an analytical approach based on a crack analogue model for the estimation of fretting fatigue crack propagation life. Also, the influence of secondary crystallographic orientation of single crystal superalloy on the TFC, and in turn, the fretting fatigue life was highlighted. Notable differences in fretting contact stress field induced multiple slip systems and crack initiation behavior were observed.

With respect to the above experimental investigations, a mechanism-based numerical model was proposed to analyze the crack initiation stress state due to fretting forces on single crystal slip systems. A competition between resolved shear stresses (shear mode) and resolved normal stresses (opening mode) was found to be controlled by the secondary crystallographic orientation. It was also found by quantitative calculation

that the magnitude of *TFC* at the contact interface and resolved normal stresses on slip planes play a critical role in accelerating crack initiation and propagation with increasing misorientation angle. An equivalent stress range parameter was proposed to incorporate the effect of varying resolved normal stresses with secondary orientation and *TFC*. The proposed model enables us to estimate the effect of crystallographic orientation on *TFC* and resolved normal stresses acting on single crystal slip planes. Those estimations are in agreement with the experimental results.

The present experimental and analytical studies on the crystallographic orientation based on the variation of surface tractions and sub-surface stress state under the influence of fretting forces can be useful in fretting fatigue strength design of SC/PC mating parts such as gas turbine SC blades and PC disk assemblies, where friction/fretting induced stress concentration leads to early fatigue crack nucleation and growth, resulting in premature failure of components.

DEDICATION

To My Parents

G. RENGARAJ & ***R. RAJALAKSHMI***

To My Wife

NG. VANMATHI SINDHU

Acknowledgments

With great pleasure, I would like to express my deep sense of thankfulness and profound gratitude to my respected supervisor, Professor Masakazu Okazaki, for his vital guidance, everlasting professional advice, continuous encouragement and dedicated mentorship with personal care. I would like to thank Prof. Gnanamoorthy (IITM, formerly at IIITDM) for recommending me to study in Japan. I express my sincere and heartiest thanks to Dr. Jayaprakash and Dr. Yamagishi for their motivational approach, timely help, and valuable discussions during my research. I would also like to thank my doctoral committee; Prof. Nanko, Prof. Ihara, Prof. Miyashita, Prof. Taura and Prof. Koguchi (NIIT) for their review and recommendations to improve this dissertation. I extend my gratitude to Prof. Otsuka, Prof. Homma and Prof. Masaki (Okinawa Kosen) for their valuable inputs to my study.

Furthermore, I am greatly appreciative of my colleague Mr. S. Baba for his help and involvement in experimental studies; without which this work would not have been possible. Also, I am grateful to all my colleagues, former and current members of Okazkai lab, my tutor Mr. Sekiguchi, Dr. Rajiv gandhi, Dr. Milton, Mr. Siddharth, Mr. Devidatta and fellow PhD students; Mr. Hayashi, Mr. Tai Bui, Mr. Hao and Mr. Yonaguni. I would like to acknowledge National Institute for Materials Science (NIMS), Tsukuba for the help in using CSF test equipment and Prof. Yamazaki (Chiba University) and Dr. Yamagishi (NIIT) for their help in EBSD analysis.

I would like to acknowledge all administrative and academic staffs of Nagaoka University of Technology, especially Mrs. Hoshi and all staffs of International affairs division and machine shop, for their kind cooperation during the course of my study. Special thanks to all my Japanese host families and International friends, who made my stay in Nagaoka a memorable one.

Last but not least, I would like to thank my family, especially my parents and my wife, for their love, support, constant encouragement and for always believing in me.

This study program was supported by the Japanese Government (MEXT) Scholarship.

Contents

THIS PAGE INTENTIONALLY LEFT BLANK

List of Figures

List of Tables

Chapter 1

Introduction

A brief introduction to the Ni-base superalloys, anisotropic properties of single crystals, fretting fatigue behavior of engineering alloys and objectives of this research work are presented in this Chapter. The advantages of single crystal Ni-base superalloys over polycrystalline superalloys are discussed. Also, based on the previous studies on single crystal Ni-base superalloys, the uncertainties in failure behavior with respect to crystallographic orientation of single crystals are highlighted. Furthermore, fretting fatigue failure studies on engineering alloys are reviewed with particular focus on anisotropic contact configurations. Finally, the objectives and the approach of this dissertation are outlined.

1.1 Advanced Ni-base superalloys for gas turbines

Nickel based superalloys are widely used in hot section of aircraft and power-generation gas turbines which can hold to their strength and properties at high temperatures. They are mainly used in the turbine and combustor sections of aircraft engines which constitute 40-50% of the total weight [1–3]. Continuous improvement of high temperature strength and properties of Ni-base superalloys used in advanced gas turbines is inevitable for better fuel economy thereby reducing CO_2 emission in order to prevent global warming [4, 5]. This can be achieved by increasing the turbine inlet temperature (TIT) of combustion gases. At the same time, it is necessary to select the materials that can withstand these high temperatures without any degradation in their performance. Gas turbine blades are one of the most sophisticated components of a gas turbine which convert the thermal energy of combustion gases into mechanical energy. Significant developments are made in the manufacturing technologies of turbine blades [5, 6]. Fig. 1-1 shows the blades casted using three methods [6].

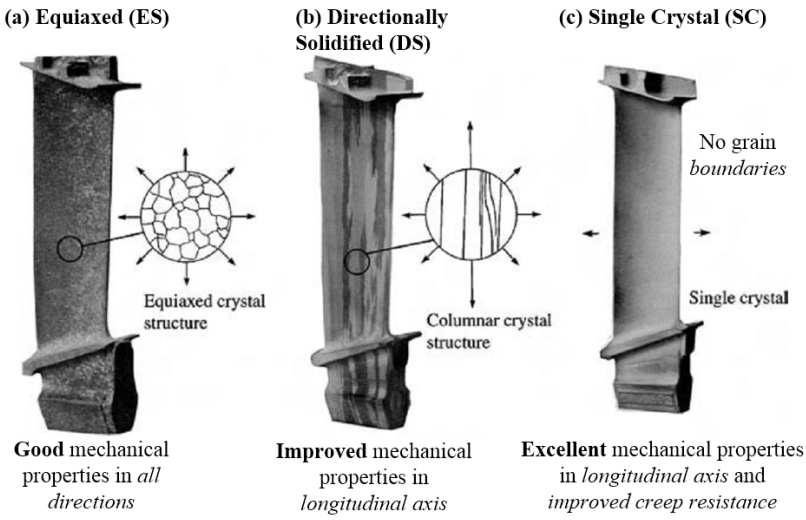

Figure 1-1: Investment casting methods (a) equiaxed, (b) directionally solidified and (c) single crystal structures [6]

Particularly, gas turbine blades are casted as single crystals of Ni-base superalloys due to their higher tolerance to creep and low cycle fatigue behavior [6]. This is achieved by aligning the <001> low Young's modulus primary crystallographic orientation with the blade axis [2]. However, the secondary crystallographic orientation

perpendicular to blade axis is generally not controlled but can be determined [7–10]. Single crystal blades are preferred over polycrystalline blades due to enhanced creep and fatigue properties. Since no grain boundaries are present in single crystals, grain boundary sliding during creep loading is avoided (Fig. 1-2). High temperature fatigue life can be improved maintaining lower stiffness along longitudinal axis of the single crystal blade, which result in significant improvement in turbine inlet temperature as shown in Fig. 1-3.

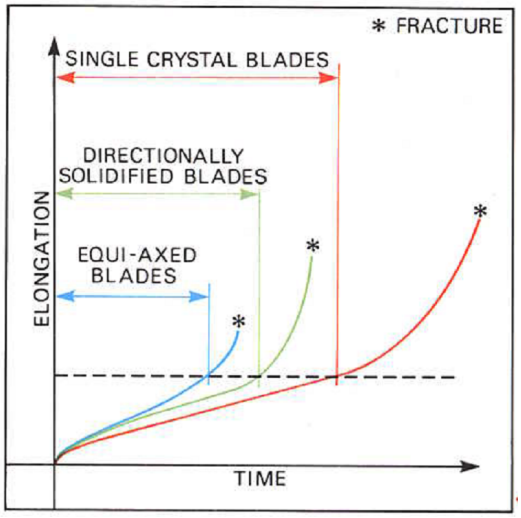

Figure 1-2: Stress rupture life of blades manufactured by different processing routes [6].

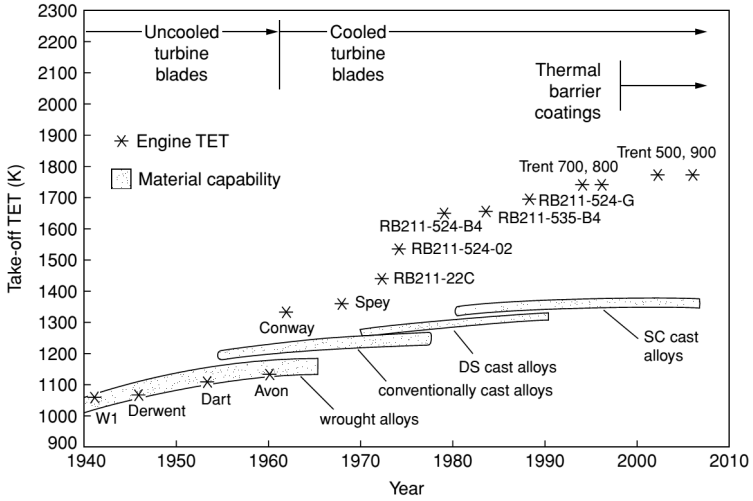

Figure 1-3: Evolution of turbine inlet temperature (TIT) of civil engines in the past seventy years [1].

1.2 Anisotropic properties of FCC single crystal material

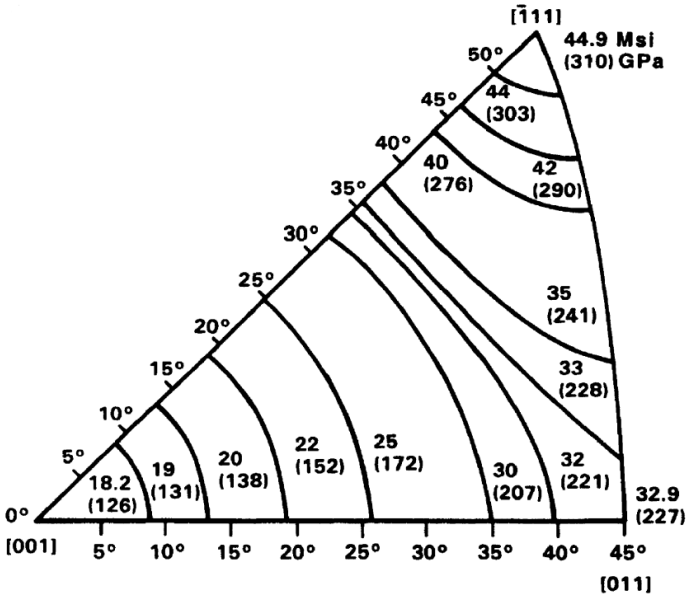

Figure 1-4: Elastic modulus of Ni-base superalloy at room temperature [11].

The fact that the blades are casted as single crystals means their mechanical properties are anisotropic in nature i.e. properties are dependent on crystallographic orientation [3, 12–16]. Fig. 1-4 shows the variation of elastic modulus of a single crystal Ni-base superalloy as a function of crystallographic orientation in the stereographic triangle [11]. The crystallographic orientation of single crystal Ni-base superalloy component with respect to loading directions could affect the mechanical strength properties such as high cycle fatigue (HCF) [5, 7, 17, 18], thermo-mechanical fatigue (TMF) [19, 20] and creep [11, 21] behavior. Recently, key research focus has been laid on the clarification of crystal orientation dependence on high temperature strength of single crystal superalloy for the design and development of next generation rotor blades. Particularly, effect of secondary crystal orientation of rotor blades on the reliability of high temperature strength needs to be clarified for further improvements in microstructure design and development [7, 14, 22, 23]. Here, the main focus is on the high temperature mechanical and metallurgical properties such as creep resis-

tance, thermo-mechanical fatigue strength, corrosion and oxidation resistance, plain fatigue strength and fretting fatigue strength. So far, studies on the crystal orientation dependence on creep strength, thermo-mechanical strength and environmental resistance have been reported. Combined knowledge of orientation effect on the high temperature properties is essential for unified design and development of advanced gas turbine engine systems.

1.3 Fretting fatigue of engineering alloys

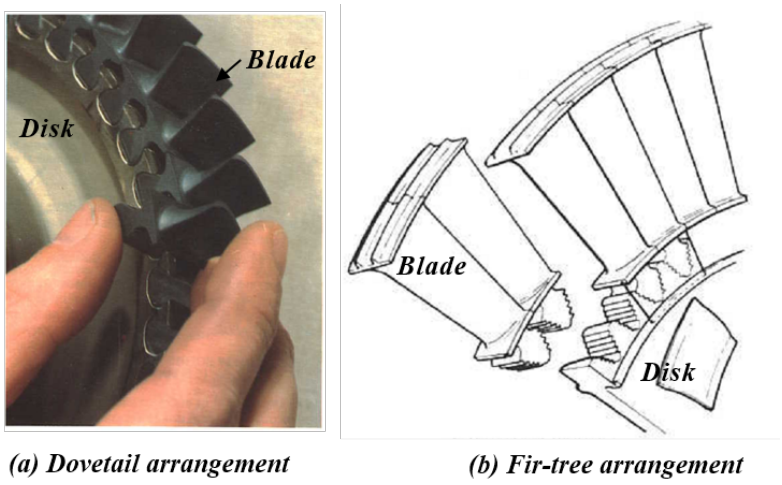

Figure 1-5: Methods of securing turbine blades to disks [6].

Turbine blades are mounted on turbine disks using either dovetail connections or fir tree arrangement, as shown in Fig. 1-5 [6]. Friction and fretting occur due to small oscillating relative displacement at the contact interface of mating components [24–26]. Fretting fatigue in gas turbine blade-disk attachment occurs due to small oscillating surface displacements (fretting) in addition to the bulk stress (fatigue) [26]. The addition of fretting induced stress concentration at the interface might aid in fretting damage and crack nucleation, as schematically shown in Fig. 1-6. When fretting occurs together with fatigue it accelerates the crack nucleation (within first several thousand cycles) and it can lead to drastic reduction in fatigue life of the component [24]. Thus, catastrophic failure under fretting conditions can occur at stress

levels well below the fatigue limit of a material. Fretting fatigue failure is particularly important in safety-critical industries such as aerospace and power generation. Several literatures are available on the fretting fatigue behavior of various steels [27–34], Al alloys [35–39] and Ti alloys [30, 40–43]. However, studies on the fretting fatigue behavior of heat resistant superalloys [44], more specifically, on the single crystal Ni-base superalloys are limited [45–47].

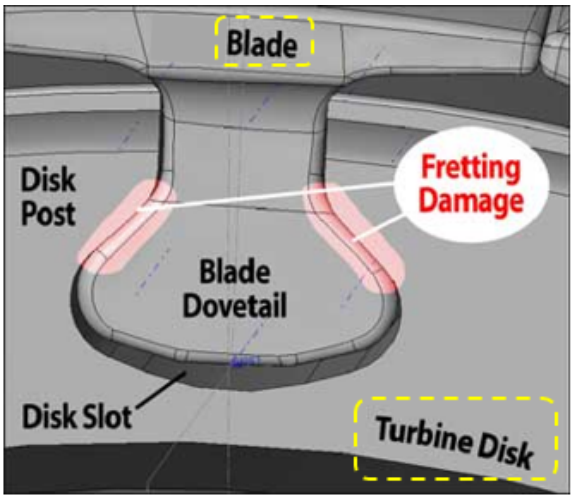

※https://www.lambdatechs.com/fretting-fatigue.html

Figure 1-6: Schematic of fretting fatigue damage in blade/disk assembly

Previous studies on fretting behavior of engineering alloys suggest that there are more than 50 variables of fretting process which can be divided into two groups: (i) primary variables and (ii) secondary variables [48]. Coefficient of friction (COF) is one of the primary variables which was identified as the important parameter affecting the fretting process [22, 24, 47, 48, 48]. Significant development on the application of fracture mechanics to fretting fatigue of polycrystalline materials has been made [49–59]. Giannakopoulos et al. [60] proposed a fretting fatigue life estimation methodology based on the analogy between contact mechanics and fracture mechanics, where crack initiation angle and effective stress intensity factors (SIFs) can be computed by knowing the COF under fretting contact. Many researchers have reported the importance of considering the frictional force between the mating parts for accurate estimation of fretting fatigue life [8, 22, 47, 61], which has been taken into account in

the current work on single crystal Ni-base superalloys.

1.4 Fretting fatigue of single crystal alloys

In comparison to polycrystalline alloys, fewer reports are available on fretting behavior of single crystal alloys. Early study by Hoeppner and Salivar [62] on the fretting fatigue of contacting Cu single crystals showed significant dependence of orientation on the amount of slip and fretting fatigue lives. Also, they have highlighted the possible changes in the the sub-surface stress field which altered the maximum value of shear stress away from the primary slip systems [62]. Arakere and Swanson [46] highlighted the influence of *COF* on the tangential normal stress at the critical contact location which controls fretting crack nucleation in a single crystal Ni-base superalloy. They also reported the preferential secondary orientations for which crack growth at the blade tip can be minimized. Murthy et al. [63] published a series of papers on contacting single crystal/polycrystalline Nickel subjected to blade/disk loading, in which fretting fatigue crack nucleation and growth lives of polycrystalline alloy (IN100) in contact with single crystal nickel were estimated based on multi-axial fatigue parameters. Furthermore, anisotropic stress field due to dissimilar contact have been derived based on singular integral equations [47, 63, 64]. Huang et al. [8] reported the crystallographic orientation effect on fretting at room temperature (RT) under different applied displacement amplitudes on (001) face, while there is a crystallographic effect under partial slip conditions, the effect of crystallographic orientation diminished with continued fretting due to plastic deformation and mechanical mixing of surface layer under gross slip conditions [8]. Few studies have been reported on the friction behavior and the formation of surface layers on polycrystalline Ni-base superalloys [65–68]. However, the gross sliding friction behavior of SC superalloy having different crystallographic surface orientations at high temperature has not been yet established.

Recently, Fleury et al. [22] investigated the effect of the crystal orientation of a single crystal contact pad on the fretting fatigue life of polycrystalline Ni-base

superalloy at high temperature. They also emphasized the need to study the influence of coefficient of friction of contacting superalloys at high temperature. However, for a more realistic understanding of fretting fatigue of turbine blade-disk attachment, it is necessary to apply the fatigue load on the single crystal specimen representative of blade material and contact pressure exerted by polycrystalline contact pads which are representative of the disk material.

1.5 Objectives of this study

The aim of the present study is to investigate the influence of crystallographic orientation of contacting single crystal vs polycrystalline superalloys used in gas turbine blades and disks, respectively. The results obtained from this study can be useful in understanding the effect of metallurgical aspect of materials on component design for high temperatures. The following are the objectives of this work:

- What is the influence of crystallographic contact orientation and crystallographic sliding orientation of single crystal material on sliding friction response at ambient and elevated temperatures?

- What is the effect of contacting superalloy combinations and tangential tractions on the fretting fatigue failure behavior of contacting superalloys?

- How does the secondary crystallographic orientation of single crystal blade material influence the performance against fretting fatigue?

- How to incorporate the experimentally measured contact tractions in to life prediction methodology for superalloys?

- How does the crystallographic orientation modify the sub-surface stress state induced by fretting stresses?

1.6 Approach

Experimental and analytical investigations were carried out in order to address the objectives set forth. The experimental study involves cyclic sliding friction tests and fretting fatigue tests at ambient and high temperatures. Here, the evolution of frictional tractions and fatigue lives under fretting conditions are studied. These experimental results are extensively analyzed in the analytical study. Analysis of crack propagation life estimation based on experimentally measure tangential tractions is proposed. Furthermore, the influence of secondary crystallographic orientation on the internal stress field in a FCC single crystal slip systems which control the deformation behavior in Ni-base superalloys is investigated.

Fretting and friction properties are known to be influenced by displacement modes such as partial slip, mixed mode and gross slip/sliding [8]. Here, the coefficient of friction between sliding/fretting contacts is one of the main factors that could control the failure mechanism, that is, either material removal by wear, crack nucleation from frictional interface or both [22, 63]. Thus it is important to consider not only the normal load direction and surface orientation but also the direction of sliding/fretting along which the tangential force is acting. In order to characterize the orientation induced anisotropy on normal and tangential load direction, the CSF tests were carried out under gross sliding conditions. Meanwhile, fretting fatigue (FF) failure tests were conducted on single crystal specimens having different secondary crystallographic orientations to estimate the fatigue life under fretting conditions. In addition to ambient temperature conditions, tests have also been conducted at 600 °C, typical temperature experienced in the gas turbine blade/disk attachment region during operation.

1.7 Dissertation outline

This section describes the individual topics that are covered in this dissertation as summarized in Fig. 1-7.

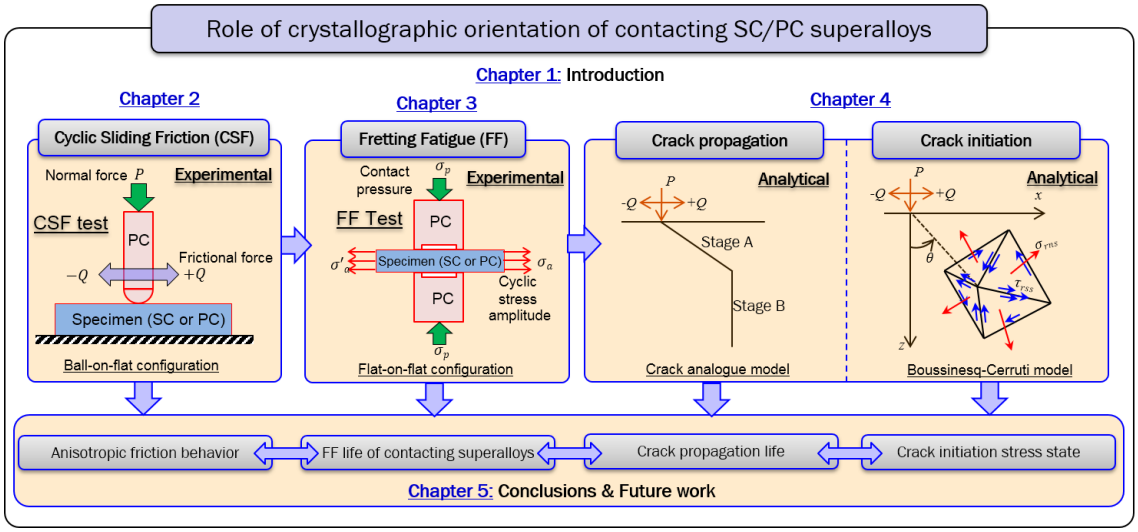

Figure 1-7: Dissertation outline

Chapter 1: The basics of Ni-base superalloys used in advanced gas turbine engines and their relevance to better performance in terms of significant developments in recent years are presented. Then the potential impact of fretting process on the fatigue behavior of these alloys are discussed, with particular focus to gas turbine blade/disk assembly. Background study on the effect of single crystal orientation on fretting process identified the limited knowledge and studies that have to be done. Based on that, objectives of the current study are defined and a systematic approach is utilized to achieve those objectives.

Chapter 2: Crystallographic aspects of contacting superalloys are investigated on the representative turbine blade and disk assembly. Major emphasis was put on the role of crystallographic orientation with respect to normal loading and tangential loading directions. The experimental observations are related to the elastic anisotropic mechanical properties of single crystal superalloy material.

Chapter 3: Fretting fatigue failure behavior of similar contacting superalloys is studied in order to estimate the fatigue strength of superalloys subjected to fretting

loading. The plain fatigue strength of the materials is compared with observed fretting fatigue strength and severity of fretting process is highlighted. Specific role of contact tractions which are controlled by secondary crystallographic orientations is characterized by means of stick-slip area fraction and fracture morphologies of failed specimens.

Chapter 4: Analytical study on the fretting fatigue crack propagation and crack initiation stress state is detailed. The influence of tangential tractions between the contacting superalloys on the crack propagation behavior are studied using a model based on crack analogue approach. Furthermore, the variation sub-surface stress state under the action of fretting stresses acting on different crystallographic orientations which control the crack nucleation process is formulated. The role of tangential force coefficient and orientation on the resolved stresses on single crystal slip systems are analyzed in detail. Correlations with experimental findings are made.

Chapter 5: The findings of the present study are summarized and suggestions for future research scope are presented.

1.8 Chapter references

[1] Reed, R.C.. The Superalloys. Cambridge: Cambridge University Press; 2006. doi:10.1017/CBO9780511541285.

[2] Pollock, T., Tin, S.. Nickel-Based Superalloys for Advanced Turbine Engines: Chemistry, Microstructure and Properties. Journal of Propulsion and Power 2006;22(2):361–374. doi:10.2514/1.18239.

[3] Shah, D., Duhl, D.. The Effect of Orientation, Temperature and Gamma Prime Size on the Yield Strength of a Single Crystal Nickel Base Superalloy. In: Et al., M.G., editor. Superalloys 1984 (Fifth International Symposium). TMS; 1984, p. 105–114. doi:10.7449/1984/Superalloys_1984_105_114.

[4] Davis, J.R.. ASM Specialty Handbook: Nickel, Cobalt, and Their Alloys. 2000. ISBN 978-0-87170-685-0. URL: http://books.google.com/?id=IePhmnbmRWkC. doi:10.1361/ncta2000p013.

[5] Okazaki, M.. High-temperature strength of Ni-base superalloy coatings. Science and Technology of Advanced Materials 2001;2(2):357–366. doi:10.1016/S1468-6996(00)00022-X.

[6] Rolls-Royce, . The jet engine. 1996. arXiv:0902121049.

[7] Kakehi, K.. Influence of Primary and Secondary Crystallographic Orientations on Strengths of Nickel-based Superalloy Single Crystals. Materials Transactions 2004;45(6):1824–1828. doi:10.2320/matertrans.45.1824.

[8] Huang, X., Gibson, T.E., Zhang, M., Neu, R.W.. Fretting on the cubic face of a single-crystal Ni-base superalloy at room temperature. Tribology International 2009;42(6):875–885. doi:10.1016/j.triboint.2008.12.003.

[9] Sakaguchi, M., Ike, M., Okazaki, M.. Microstructural Changes in a Single Crystal Ni-base Superalloy Induced by Plastic Straining. Materials Science and Engineering A 2012;534:253–259. doi:10.1016/j.msea.2011.11.066.

[10] Yang, C., Liu, L., Zhao, X., Li, Y., Zhang, J., Fu, H.. Dendrite Morphology and Evolution Mechanism of Nickel-based Single Crystal Superalloys Grown Along the <001> and <011> Orientations. Progress in Natural Science: Materials International 2012;22(5):407–413. doi:10.1016/j.pnsc.2012.10.001.

[11] MacKay, R.A., Maier, R.D.. The influence of orientation on the stress rupture properties of nickel-base superalloy single crystals. Metallurgical Transactions A 1982;13(10):1747–1754. doi:10.1007/BF02647830.

[12] Savage, M.W.R.. The Influence of Crystal Orientation on the Elastic Stresses of a Single Crystal Nickel-Based Turbine Blade. Journal of Engineering for Gas Turbines and Power 2012;134(1):012501: 1–7. doi:10.1115/1.4004129.

[13] Raabe, D., Ma, D., Roters, F.. Effects of initial orientation, sample geometry and friction on anisotropy and crystallographic orientation changes in single crystal microcompression deformation: A crystal plasticity finite element study. Acta Materialia 2007;55(13):4567–4583. doi:10.1016/j.actamat.2007.04.023.

[14] Sabnis, P.a., Mazière, M., Forest, S., Arakere, N.K., Ebrahimi, F.. Effect of secondary orientation on notch-tip plasticity in superalloy single crystals. International Journal of Plasticity 2012;28(1):102–123. doi:10.1016/j.ijplas.2011.06.003.

[15] Siebörger, D., Knake, H., Glatzel, U.. Temperature dependence of the elastic moduli of the nickel-base superalloy CMSX-4 and its isolated phases. Materials Science and Engineering: A 2001;298(1-2):26–33. doi:10.1016/S0921-5093(00)01318-6.

[16] Arakere, N.K., Siddiqui, S., Magnan, S., Ebrahimi, F., Forero, L.. Investigation of three-dimensional stress fields and slip systems for FCC single crystal superalloy notched specimens. Proceedings of the ASME Turbo Expo 2004 2004;6:207–215. doi:10.1115/GT2004-53938.

[17] Arakere, N.K., Swanson, G.. Effect of Crystal Orientation on Fatigue Failure of Single Crystal Nickel Base Turbine Blade Superalloys. Journal of Engineering for Gas Turbines and Power 2002;124(1):161. doi:10.1115/1.1413767.

[18] Hou, N.X., Gou, W.X., Wen, Z.X., Yue, Z.F.. The influence of crystal orientations on fatigue life of single crystal cooled turbine blade. Materials Science and Engineering A 2008;492(1-2):413–418. doi:10.1016/j.msea.2008.03.043.

[19] Okazaki, M., Sakaguchi, M., Yamagishi, S.. Subcritical Crack Growth on Crystallographic Planes in a Ni-base Superalloy: Relevance to Orientations. Procedia Engineering 2013;55:677–684. doi:10.1016/j.proeng.2013.03.314.

[20] Fleury, E., Rémy, L.. Behavior of nickel-base superalloy single crystals under thermal-mechanical fatigue. Metallurgical and Materials Transactions A 1994;25(1):99–109. doi:10.1007/BF02646679.

[21] Matan, N., Cox, D., Carter, P., Rist, M., Rae, C., Reed, R.. Creep of CMSX-4 superalloy single crystals: effects of misorientation and temperature. Acta Materialia 1999;47(5):1549–1563. doi:10.1016/S1359-6454(99)00029-4.

[22] Fleury, R.M.N., Paynter, R.J.H., Nowell, D.. The Influence of Contacting Ni-based Single-crystal Superalloys on Fretting Fatigue of Ni-based Polycrystalline Superalloys at High Temperature. Tribology International 2014;76:63–72. doi:10.1016/j.triboint.2014.01.011.

[23] Karadge, M., Preuss, M., Withers, P.J., Bray, S.. Importance of Crystal Orientation in Linear Friction Joining of Single Crystal to Polycrystalline Nickel-based Superalloys. Materials Science and Engineering A 2008;491(1-2):446–453. doi:10.1016/j.msea.2008.04.064.

[24] Waterhouse, R.. Fretting fatigue. Applied Science Publishers; 1981.

[25] Hoeppner, D., Adibnazari, S., Moesser, M.. Literature review and preliminary studies of fretting and fretting fatigue incuding special applications to aircraft joints. Tech. Rep.; 1994.

[26] Lindley, T.. Fretting fatigue in engineering alloys. International Journal of Fatigue 1997;19(93):39–49. doi:10.1016/S0142-1123(97)00039-X.

[27] Nix, K.J., Lindley, T.C.. The application of fracture mechanics to fretting fatigue. Fatigue & Fracture of Engineering Materials and Structures 1985;8(2):143–160. doi:10.1111/j.1460-2695.1985.tb01200.x.

[28] Tanaka, K., Mutoh, Y., Sakoda, S., Leadbeater, G.. Fretting Fatigue in 0. 55C Spring Steel and 0. 45C Carbon Steel. Fatigue and Fracture of Engineering Materials and Structures 1985;8(2):129–142. doi:10.1111/j.1460-2695.1985.tb01199.x.

[29] Lindley, T., Nix, K.. Fretting Fatigue in the Power Generation Industry: Experiments, Analysis, and Integrity Assessment. In: Standardization of Fretting Fatigue Test Methods and Equipment. 100 Barr Harbor Drive, PO Box C700, West Conshohocken, PA 19428-2959: ASTM International; 1992, p. 153–169. doi:10.1520/STP25828S.

[30] Nakazawa, K., Sumita, M., Maruyama, N.. Effect of Contact Pressure on Fretting Fatigue of High Strength Steel and Titanium Alloy. In: Standardization of Fretting Fatigue Test Methods and Equipment. 100 Barr Harbor Drive, PO Box C700, West Conshohocken, PA 19428-2959: ASTM International; 1992, p. 115–125. doi:10.1520/STP25824S.

[31] Nix, K.J., Lindley, T.C.. The influence of relative slip range and contact material on the fretting fatigue properties of 3.5NiCrMoV rotor steel. Wear 1988;125(1-2):147–162. doi:10.1016/0043-1648(88)90199-8.

[32] Okane, M., Shiozawa, K., Ishikura, T.. Fretting Fatigue Behavior of TiN-Coated Steel. In: Fretting Fatigue: Current Technology and Practices, ASTM STP 1367. West Conshohocken, PA: ASTM International; 2000, p. 465–476. doi:10.1520/STP14748S.

[33] Fouvry, S., Nowell, D., Kubiak, K., Hills, D.. Prediction of fretting crack propagation based on a short crack methodology. Engineering Fracture Mechanics 2008;75(6):1605–1622. doi:10.1016/j.engfracmech.2007.06.011.

[34] Noraphaiphipaksa, N., Manonukul, A., Kanchanomai, C., Mutoh, Y.. Fretting fatigue life prediction of 316L stainless steel based on elastic–plastic fracture mechanics approach. Tribology International 2014;78:84–93. doi:10.1016/j.triboint.2014.04.029.

[35] Alic, J., Hawley, A., M. Urey, J.. Formation of fretting fatigue cracks in 7075-T7351 aluminum alloy. Wear 1979;56(2):351–361. URL: http://linkinghub.elsevier.com/retrieve/pii/0043164879902382. doi:10.1016/0043-1648(79)90238-2.

[36] Waterhouse, R., Noble, B., Leadbeater, G.. The effect of shot-peening on the fretting-fatigue strength of an age-hardened aluminium alloy (2014A) and an austenitic stainless steel (En 58A). Journal of Mechanical Working Technology 1983;8(2):147–153. doi:10.1016/0378-3804(83)90032-3.

[37] Rayaprolu, D., Cook, R.. A Critical Review of Fretting Fatigue Investigations at the Royal Aerospace Establishment. In: Standardization of Fretting Fatigue Test Methods and Equipment. 100 Barr Harbor Drive, PO Box C700, West Conshohocken, PA 19428-2959: ASTM International; 1992, p. 129–152. doi:10.1520/STP25826S.

[38] Szolwinski, M.P., Farris, T.N.. Observation, analysis and prediction of fretting fatigue in 2024-T351 aluminum alloy. Wear 1998;221(1):24–36. doi:10.1016/S0043-1648(98)00264-6.

[39] Shinde, S.R., Hoeppner, D.W.. Fretting fatigue behavior in 7075-T6 aluminum alloy. Wear 2006;261(3):426–434. doi:10.1016/j.wear.2005.12.015.

[40] Hutson, A.L., Nicholas, T., Goodman, R.. Fretting fatigue of Ti–6Al–4V

under flat-on-flat contact. International Journal of Fatigue 1999;21(7):663–669. doi:10.1016/S0142-1123(99)00027-4.

[41] Venkatesh, T.A., Conner, B.P., Suresh, S., Giannakopoulos, A.E., Lindley, T.C., Lee, C.S.. An experimental investigation of fretting fatigue in Ti-6Al-4V: the role of contact conditions and microstructure. Metallurgical and Materials Transactions A 2001;32(5):1131–1146. doi:10.1007/s11661-001-0124-8.

[42] Fouvry, S., Duó, P., Perruchaut, P.. A quantitative approach of Ti–6Al–4V fretting damage: friction, wear and crack nucleation. Wear 2004;257(9):916–929. doi:10.1016/j.wear.2004.05.011.

[43] Golden, P., Grandt, A.. Fracture mechanics based fretting fatigue life predictions in Ti–6Al–4V. Engineering Fracture Mechanics 2004;71(15):2229–2243. doi:10.1016/j.engfracmech.2003.10.005.

[44] Mall, S., Kim, H., Porter, W.J., Ownby, J.F., Traylor, A.G.. High temperature fretting fatigue behavior of IN100. International Journal of Fatigue 2010;32(8):1289–1298. doi:10.1016/j.ijfatigue.2010.01.012.

[45] Matlik, J.F., Farris, T.N., Haynes, J., Swanson, G.R., Ham-Battista, G.. Prediction of fretting crack location and orientation in a single crystal nickel alloy. Mechanics of Materials 2009;41(10):1133–1151. doi:10.1016/j.mechmat.2009.04.002.

[46] Arakere, N.K., Swanson, G.. Fretting Stresses in Single Crystal Superalloy Turbine Blade Attachments. Journal of Tribology 2001;123(2):413–423. doi:10.1115/1.1308032.

[47] Murthy, H., Gao, G., Farris, T.N.. Fretting Fatigue of Single Crystal Nickel at 600 C. Tribology International 2006;39(10):1227–1240. doi:10.1016/j.triboint.2006.02.050.

[48] Dobromirski, J.. Variables of Fretting Process: Are There 50 of Them? In: Attia, M., Waterhouse, R.B., editors. Standardization of Fretting Fatigue

Test Methods and Equipment, ASTM STP 1159. Philadelphia: ASTM Internationalm; 1992, p. 60–66. doi:10.1520/STP25816S.

[49] Rooke, D., Jones, D.. Stress intensity factors in fretting fatigue. The Journal of Strain Analysis for Engineering Design 1979;14(1):1–6. doi:10.1243/03093247V141001.

[50] Hattori, T., Nakamura, M., Sakata, S., Watanabe, T.. Fretting fatigue analysis using fracture mechanics. JSME International Journal Series A 1988;31(1):100–107.

[51] Ciavarella, M., Demelio, G.. A review of analytical aspects of fretting fatigue, with extension to damage parameters, and application to dovetail joints. International Journal of Solids and Structures 2001;38(10-13):1791–1811. doi:10.1016/S0020-7683(00)00136-0.

[52] Chambon, L., Suresh, S.. A unified fracture mechanics approach to fretting fatigue crack growth. Ph.D. thesis; MIT; 2001.

[53] Ciavarella, M., Macina, G.. New results for the fretting-induced stress concentration on Hertzian and flat rounded contacts. International Journal of Mechanical Sciences 2003;45(3):449–467. doi:10.1016/S0020-7403(03)00061-4.

[54] Ciavarella, M., Macina, G.. A note on the crack analogue model for fretting fatigue. International Journal of Solids and Structures 2003;40(4):807–825. doi:10.1016/S0020-7683(02)00652-2.

[55] Mutoh, Y., Xu, J.Q.. Fracture mechanics approach to fretting fatigue and problems to be solved. Tribology International 2003;36(2):99–107. doi:10.1016/S0301-679X(02)00136-6.

[56] Hattori, T., Nakamura, M., Watanabe, T.. Simulation of fretting-fatigue life by using stress-singularity parameters and fracture mechanics. Tribology International 2003;36(2):87–97. doi:http://dx.doi.org/10.1016/S0301-679X(02)00141-X.

[57] Brooks, C., Prost-Domasky, S., Honeycutt, K., Mills, T., Young, N.. Fretting fatigue model. Tech. Rep. February 2003; AFRL-VA-WP-TR-2003-3012; 2003.

[58] Chambon, L., Journet, B.. Modelling of fretting fatigue in a fracture-mechanics framework. Tribology International 2006;39(10):1220–1226. doi:10.1016/j.triboint.2006.02.029.

[59] Ciavarella, M.. Transition from stick to slip in Hertzian contact with "Griffith" friction: The Cattaneo–Mindlin problem revisited. Journal of the Mechanics and Physics of Solids 2015;84:313–324. doi:10.1016/j.jmps.2015.08.002.

[60] Giannakopoulos, A., Lindley, T., Suresh, S.. Aspects of equivalence between contact mechanics and fracture mechanics: theoretical connections and a life-prediction methodology for fretting-fatigue. Acta Materialia 1998;46(9):2955–2968. doi:10.1016/S1359-6454(98)00011-1.

[61] Swalla, D., Neu, R.. Influence of coefficient of friction on fretting fatigue crack nucleation prediction. Tribology International 2001;34(7):493–503. doi:10.1016/S0301-679X(01)00048-2.

[62] Hoeppner, D.W., Salivar, G.C.. The effect of crystallographic orientation on fatigue and fretting-initiated fatigue of copper single crystals. Wear 1977;43(2):227–237.

[63] Murthy, H., Garcia, D.B., Matlik, J.F., Farris, T.N.. Fretting Fatigue of Single Crystal/Polycrystalline Nickel Subjected to Blade/Disk Contact Loading. Acta Astronautica 2005;57:1–9. doi:10.1016/j.actaastro.2004.11.007.

[64] Murthy, H., Harish, G., Farris, T.N.. Efficient Modeling of Fretting of Blade/Disk Contacts Including Load History Effects. Journal of Tribology 2004;126(1):56. doi:10.1115/1.1540125.

[65] Panagopoulos, C., Giannakopoulos, K., Saltas, V.. Wear behavior of nickel superalloy, CMSX-186. Materials Letters 2003;57(29):4611–4616. doi:10.1016/S0167-577X(03)00370-7.

[66] Coskun, M.B., Aksoy, S., Aksit, M.F.. Friction and Wear Characteristics of Haynes 25, 188, and 214 Superalloys Against Hastelloy X up to 540C. Tribology Letters 2012;45(3):497–503. doi:10.1007/s11249-011-9912-5.

[67] Mishra, S.B., Chandra, K., Prakash, S.. Dry sliding wear behaviour of nickel-, iron- and cobalt-based superalloys. Tribology - Materials, Surfaces & Interfaces 2013;7(3):122–128. doi:10.1179/1751584X13Y.0000000038.

[68] Rynio, C., Hattendorf, H., Klöwer, J., Eggeler, G.. The evolution of tribolayers during high temperature sliding wear. Wear 2014;315(1-2):1–10. doi:10.1016/j.wear.2014.03.007.

Chapter 2

Crystallographic aspects on cyclic sliding friction behavior of a single crystal (SC) Ni-base superalloy

Crystallographic aspects of contacting superalloys are investigated on the representative turbine blade and disk assembly. Major emphasis was put on the role of crystallographic orientation with respect to normal loading and tangential loading directions. The experimental observations are related to the basic anisotropic mechanical properties of the material of interest.

2.1 Introduction

Single crystal materials posses anisotropic mechanical properties. The influence of these properties on the frictional behavior of contacting superalloy system is presented in this chapter. Investigation on the effect of crystallographic surface and sliding orientations of CMSX-4 single crystal Ni-base superalloy (SC) on the cyclic sliding friction (CSF) behavior against IN718 polycrystalline Ni-base superalloy (PC) has been carried out at room temperature and at 600 °C. Tests have been conducted on three different surface orientations and two different sliding orientations in order to explore the anisotropic friction response of SC/PC sliding contact pair. The effect of applied normal force and CSF cycles on COF was also explored. Based on these experimental results, discussions were made on the influence of crystallographic orientation of SC on CSF behavior of SC/PC sliding pair.

2.2 Materials

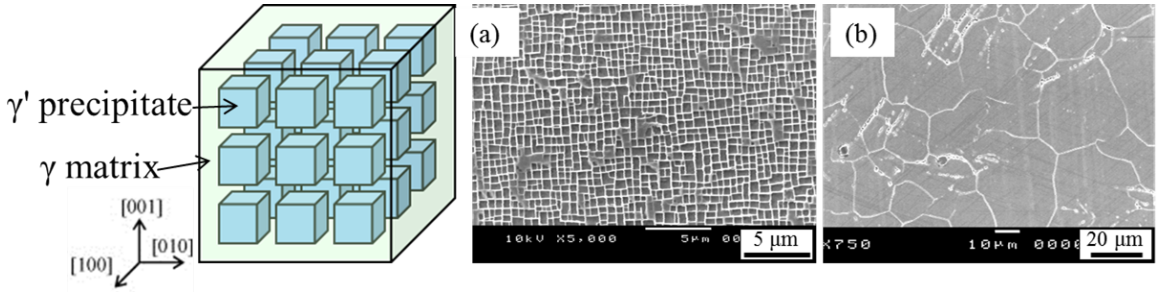

Figure 2-1: Microstructures of Ni-base superalloy system used in this study (a)SC alloy: CMSX-4 (representative material for turbine blades) and (b) PC alloy: IN718 (representative material for turbine disks).

A SC Ni-base superalloy, CMSX-4, representative material for turbine blades, after standard solution heat treatment and aged conditions was used in this study. A PC Ni-base superalloy, IN718, representative material for turbine disks, was used as a counter body. The chemical compositions of the superalloys used in this study are given in Table 3.1. The characteristic microstructures of CMSX-4 and IN718 are shown in Fig. 2-1. In CMSX-4, cuboidal γ' precipitates are uniformly distributed

in the γ matrix. The volume fraction and size of γ' precipitates are approximately 63 % and 0.5 µm, respectively. In IN718, a nickel-iron superalloy rich in niobium, γ'' phase is the primary strengthening precipitate. The average grain size is about 16 µm. The microhardness values of CMSX-4 and IN718 are 490±60 Hv and 480±30 Hv, respectively.

Table 2.1: Chemical compositions (wt%) of Ni-base superalloys used in this study.

Material	Cr	Co	Mo	W	Ti	Al	Ta	Re	Hf	Fe	C	Nb	Ni
CMSX-4	6.4	9.7	0.6	6.4	1.0	5.7	6.5	2.9	0.1	-	-	-	Bal.
IN718	19.0	-	3.0	-	0.9	0.5	-	-	-	18.0	0.04	5.0	Bal.

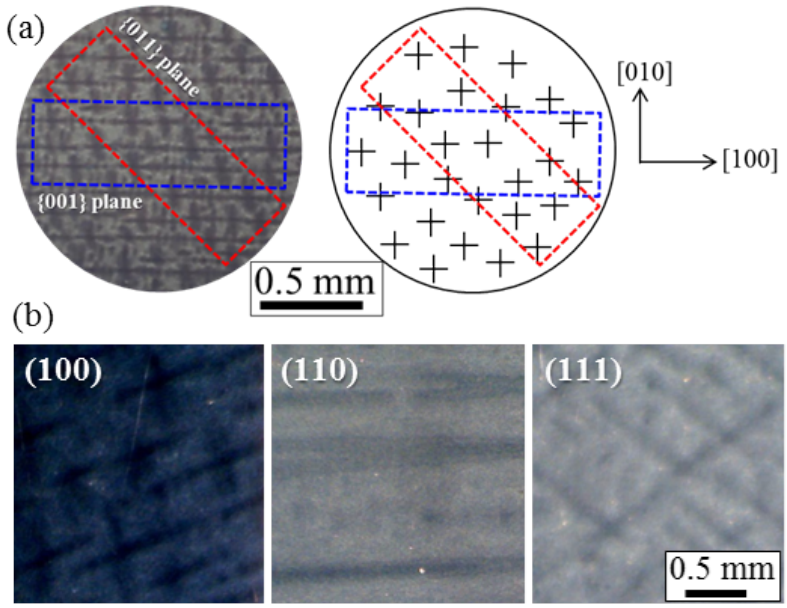

Figure 2-2: CSF test (a) schematic of extracting specimens with different surface orientations (b) optical microscope images of extracted specimens

2.3 Specimen extraction

In this work, specific focus was put on the effects of possible crystallographic factor on the friction behavior. For this purpose, the SC CMSX-4 bars of 13mm diameter and 20mm length were cut from the raw stock. Three specimens with dimensions of

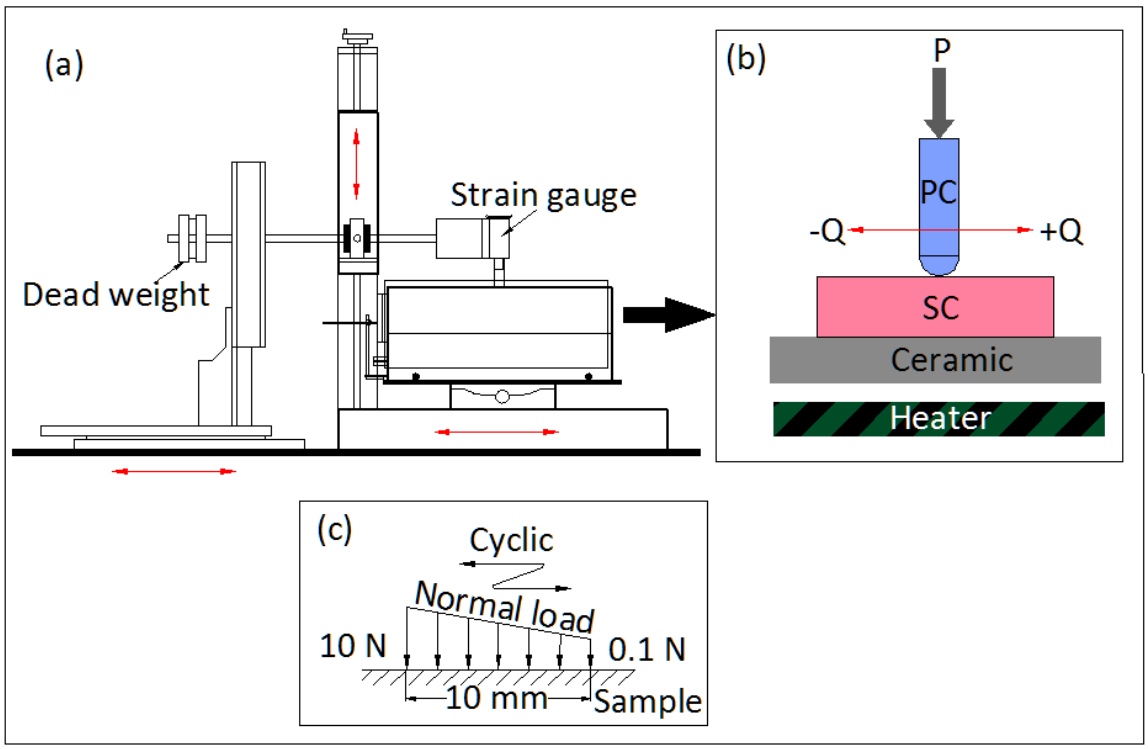

Figure 2-3: Schematic of (a) high temperature CSF test rig, (b) Ball-on-flat contact configuration and (c) cyclic variation of normal load during CSF test. [No. of sliding cycles: 100; Normal load range: 0.1 N-10 N; Sliding distance: 10 mm; Sliding velocity: 1 mm/ sec; Test temperature: RT and 600 °C].

about 15 x 10 x 3 mm were extracted in such a way that their width surfaces (15 x 10 mm surface) are almost aligned within 5 degree from (100), (110) and (111) crystallographic planes, as schematically shown in Fig. 2-2(a). Optical microscope images of obtained specimen surfaces are presented in Fig. 2-2(b). The counter body used was slider balls with hemi-spherical ends of ϕ3mm which were extracted from polycrystalline Ni-base superalloy, IN718. Specimens from IN718 were also extracted. Prior to testing, SC specimens and PC slider ends were mechanically polished to mirror finish.

2.4 Experimental procedure

A ball-on-plate reciprocating sliding friction tester [1] (Made by Shinto Scientific Co., Ltd., HEIDON type HSS2000, managed by NIMS, Japan) equipped with SiC ceramic

heater was used to measure the coefficient of friction (Fig. 2-3(a)). The SC CMSX-4 specimen was fixed on the table which reciprocated to and fro against the PC IN718 slider ball attached to the holder (Fig. 2-3(b)). The position of dead weight was synchronized with the table movement to ensure the application of varying normal load (Fig. 2-3(c)). The normal load was applied using dead weight and lever arm and the resulting friction force up on sliding was measured throughout the test by a strain transducer attached to the slider holder. The coefficient of friction (COF) during sliding was then calculated using (Eq. (2.1)).

$$\text{COF} = \frac{Q}{P} \tag{2.1}$$

Where Q is the frictional or tangential force measured by the strain gage and P is the applied normal force.

2.5 Results

2.5.1 Optical images of sliding traces on SC

The optical images of sliding traces on SC and PC specimen surfaces obtained after testing at room temperature and at 600 °C are shown in Fig. 2-4(a)-(d) and (e)-(h), respectively. The wear trace on SC specimen was broader than PC specimen sliding against PC ball at room temperature. Severe scratching and abrasive wear was observed on all samples tested at room temperature. On the other hand, when tested at 600 °C, the width of wear trace was narrow and grooved deep into the

Table 2.2: Material combination and crystallographic orientations of single crystal specimens used in this study

Material used		Sliding plane and direction		
Specimen	Ball	Code	Plane	Direction
CMSX-4	IN718	SC-1	(100)	<001>
		SC-2	(110)	
		SC-3	(111)	<112>
IN718	IN718	PC-1	-	-

Table 2.3: CSF test conditions

Number of cycles	Normal load [N]	Sliding distance [mm]	Sliding velocity [mm/s]	Test temperature [°C]
100	0.1 - 10	10	1	RT, 600

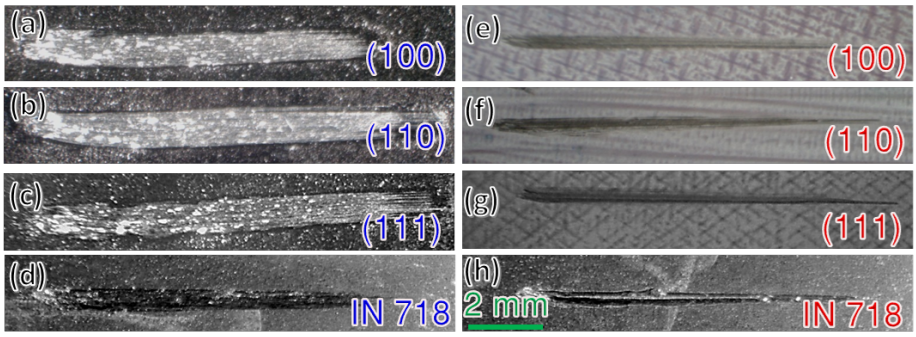

Figure 2-4: Optical images of sliding traces on CSF tested specimens tested at (a)-(d) room temperature, and (e)-(h) 600 °C. Abrasive scratching with broader wear tracks were obtained after sliding at RT, whereas, deep grooves with narrow wear track width were obtained after sliding at 600 °C.

surface. Also up on increasing the temperature to 600 °C, the dendrite pattern was clearly visible in the SC specimens (Fig. 2-4(e)-(g). The wear scars on the counter body (IN718 slider) at room temperature and at 600 °C were presented in Fig. 2-5(a)-(d) and (e)-(h), respectively.

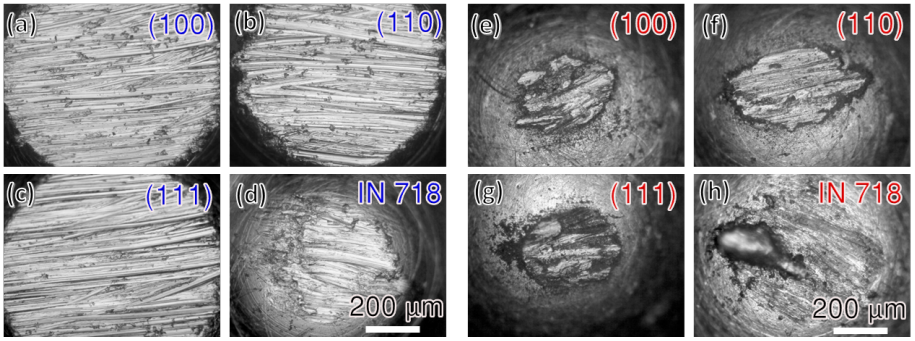

Figure 2-5: Optical microscope images of wear scars on IN718 slider pin ends sliding against (a)-(c) SC at RT, (d) PC at RT, (e)-(g) SC at 600 °C and (h) PC at 600 °C

2.5.2 Effect of contact surface orientation of SC

The evolution of average coefficient of friction over the normal load range of 0.1N – 10N with sliding cycles is shown in Fig. 2-6. Results of the test at room temperature showed notable differences in the coefficient of friction of the crystallographic planes. Cyclic sliding on the (111) plane resulted in the highest coefficient of friction as shown in Fig. 2(a). Noteworthy, the sliding direction on (111) plane specimen was along <011> direction whereas for the (100) and (110) planes the sliding direction was along <001> direction. However, at 600 °C the effect of crystal plane on friction response was not significant (Fig. 2-6(b)). For all the tested samples the coefficient of friction when tested at 600 °C was lower than those tested at room temperature. This can be attributed to the thermal softening and oxidation of the surface.

The change in COF as a function of applied normal force on SC specimens having different surface orientations sliding against PC sliders is presented in Fig. 2-7. The friction response results of PC/PC cyclic sliding contact pair is also plotted for comparison. The error bar in Fig. 2-7(b) represents standard deviation over 100 sliding cycles. A significant orientation dependence is evident at a light load up to 4 N. Under this normal force, the COF increased in the following order: (100) surface < (110) surface < (111) surface. However, COF was observed to be insensitive to surface orientation upon increasing the normal force above 4 N.

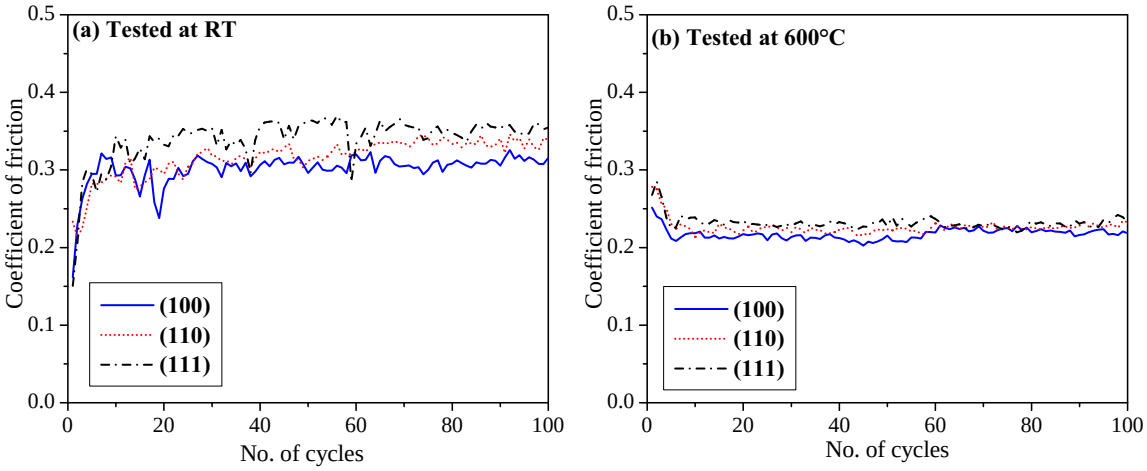

Figure 2-6: Evolution of coefficient of friction with sliding cycles for different surface orientations when tested at (a) room temperature and (b) 600 °C.

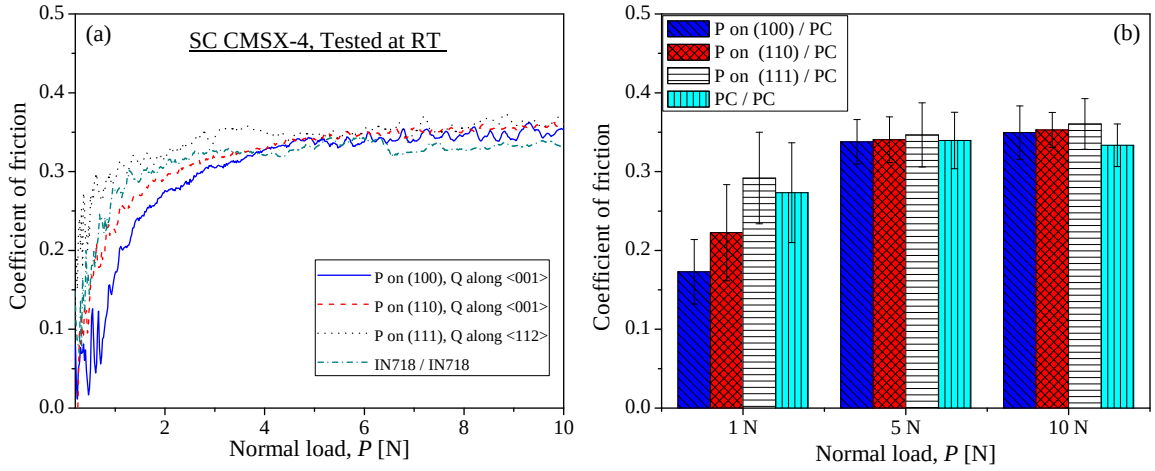

Figure 2-7: Variation of COF as a function of applied normal force on different surface orientations tested at RT (averaged over 100 sliding cycles). A normal force depended surface orientation effect is evident.

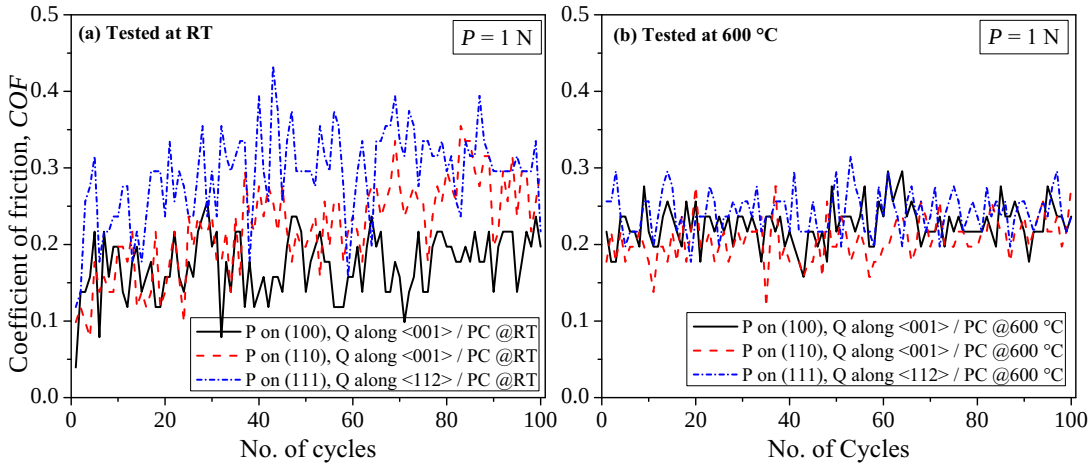

Figure 2-8: Variation of COF as a function of sliding cycles for a constant applied normal force of 1N on different surface orientations tested at (a) RT and (b) 600 °C. Differences and high scatter in during RT test diminished up on increasing test temperature to 600 °C.

The variation of COF is presented in Fig. 2-8(a) and (b) as a function of sliding cycles under a fixed normal force of 1 N tested at RT and at 600 °C, respectively. Cyclic sliding at room temperature is characterized by high scatter as a result of severe abrasive scratching (Fig. 2-4(a)). On the other hand, when tested at 600 °C, the friction response is relatively smooth and stable. Noteworthy, surface orientation effect could not be seen during sliding at 600 °C.

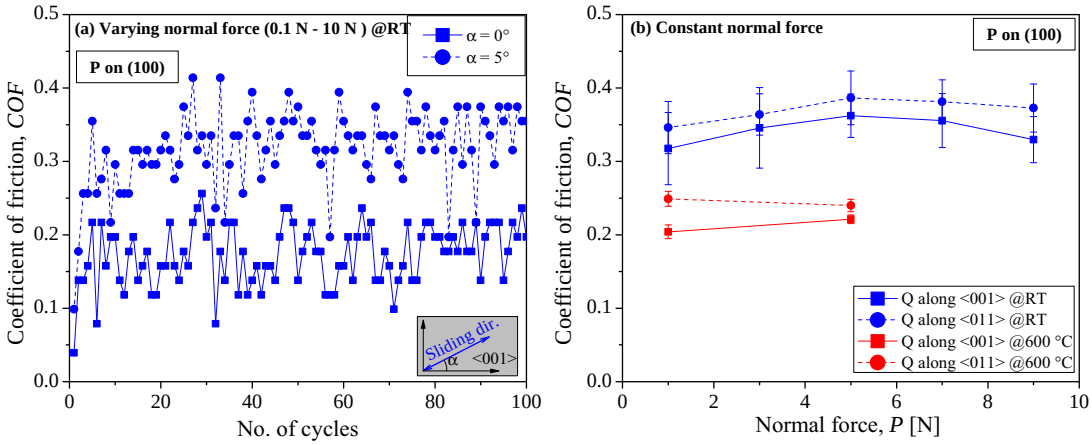

Figure 2-9: Effect of sliding orientation on COF. (a) COF as a function of sliding cycles averaged over the entire normal force range at RT and (b) COF as a function of constant normal forces for two different sliding orientations and two different test temperatures (scatter band represents standard deviation of COF values over 100 sliding cycles). COF for <011> is higher than that for <001>. COF was reduced by about 30% upon increasing the test temperature to 600 °C.

2.5.3 Effect of contact sliding orientation of SC

In addition to CSF tests on different SC surface orientations, tests have also been conducted on two different sliding orientations (crystallographic direction of sliding) on a given surface orientation. Firstly, gradually varying normal force tests have been conducted on (100) SC specimen along two sliding misorientation angles, α, from <001> direction: (i) $\alpha = 0°$ and (ii) $\alpha = 5°$. Figure 6(a) shows RT COF results as a function of sliding cycles on (100) SC specimen. Here, the data represents the average COF over the entire normal force range (0.1 N − 10 N). As shown in Fig. 2-9(a), misorientation of sliding direction from <001> direction revealed higher COF, suggesting the need to explore the role of normal force and temperature on sliding miorientation.

Next, fixed normal force tests have been conducted on (100) SC surface, along two crystallographic sliding orientations: (i) $\alpha = 0°$ i.e. along <001> direction and (ii) $\alpha = 45°$ i.e. along <011> direction. Figure 6(b) shows the CSF response as a function of fixed normal force applied on (100) SC specimen tested at RT and at 600 °C. The error bars in Fig. 2-9(b) show the standard deviation of the COF values averaged

over 100 cycles. When tested at room temperature, sliding along <011> direction showed a higher COF than <001> primary crystallographic direction. This behavior was found to be existing even for higher normal forces. In other words, it is clear from these results that the deviation from the <001> principal crystallographic direction led to an increase in the frictional force for a fixed normal force. The behaviors are in agreement with the results reported by Huang et al. [2] and Flom and Komanduri [3].

2.6 Discussions

The contact tractions and the final state of stress developed during frictional contact are essentially controlled by the elastic properties and compliance of the components in contact. In SC Ni-base superalloys the elastic properties vary with crystallographic orientation, resulting in elastic anisotropy [4]. The anisotropy in mechanical properties of SC Ni-base superalloy is presented in Table 2.4 [4, 5]. In the problem of sliding/fretting of SC/PC contacts, the properties along the direction of application of normal force as well as that along the direction parallel to the contact interface influences the contact behavior. For example, in the specimen denoted as *P on (100) , Q along <001>* in Fig. 2-8(a) , normal load was applied along a direction where Young's modulus is the lowest and the sliding occurs in a direction where the shear modulus and yield strength are the highest in comparison to other directions. This could be the reason for the severe wear on the PC ball sliding against (111) plane where the Young's modulus was about 1.5 times the same for IN718 ball. The wear volume on the PC ball sliding against (111) plane was 25% higher than for the ball sliding against (110) plane (Fig. 2-4). It is clear from the above discussion that the elastic properties of the counter body in relation to the single crystal face could also have an impact on the resulting contact traction.

From the CSF tests, a significant crystallographic effect was observed at low normal loads applied on different crystal planes (Fig. 2-7(b)). Buckley [6] reported similar load dependent orientation effect on matched planes and directions of Cu FCC single

crystals tested at a normal load of 1 N. In the case of matched planes and directions, lowest adhesive forces (minimum adhesion) were observed on {111} planes, which are the highest atomic packing and lowest surface energy planes of a FCC crystal. Thus, Buckley [6] suggested that the surface energy might have more influence than mechanical property of elasticity for matched planes and directions of single crystal (SC/SC contact) adhesive contact. However, in this work, a quite opposite trend was observed via CSF tests (SC/PC contact), where sliding on (111) plane exhibited higher COF despite being the lowest surface energy plane. As will be seen later, elastic properties seem to have a greater influence for the the case of dissimilar SC/PC elastic contact. However, the orientation dependence observed at light loads gradually disappeared with increasing applied normal forces. This trend is also in agreement with the results of Buckley [6], where up on repeated unidirectional sliding, SC COF approaches PC COF.

Also, during this transition, the wear state changed from a "mild wear state" to a "severe wear state" upon increasing the mean contact pressure (σ_{mean}) which is proportional to the applied normal force on SC surface [6, 7]. In this work, the COF increased with mean contact pressure until a transition regime followed by a steady value of COF (Fig. 2-7(a)). Thus it is clear that the effect of crystallographic contact plane should be more sensitive when the magnitude of σ_{mean} is sufficiently low. In other words, when the present SC/PC contact condition is in an elastic state, the stress field around the contact must be more sensitive to crystallographic surface orientation of SC.

It is well known that the contact conditions primarily depended on the elastic properties and the compliance of the bodies in contact. The mechanical properties along the direction of normal load can alter the contact tractions. Also, the properties along the sliding/fretting directions can alter the tangential load distribution and in turn the peak fretting stress at the edge of contact. In this work, a crystallographic effect on the CSF response was observed at low normal load of 1 N (Fig. 2-7(b)). Similar load depended orientation effect was also reported by Buckley et al., where coefficient of friction in sliding contact is quite dependent on crystallographic orien-

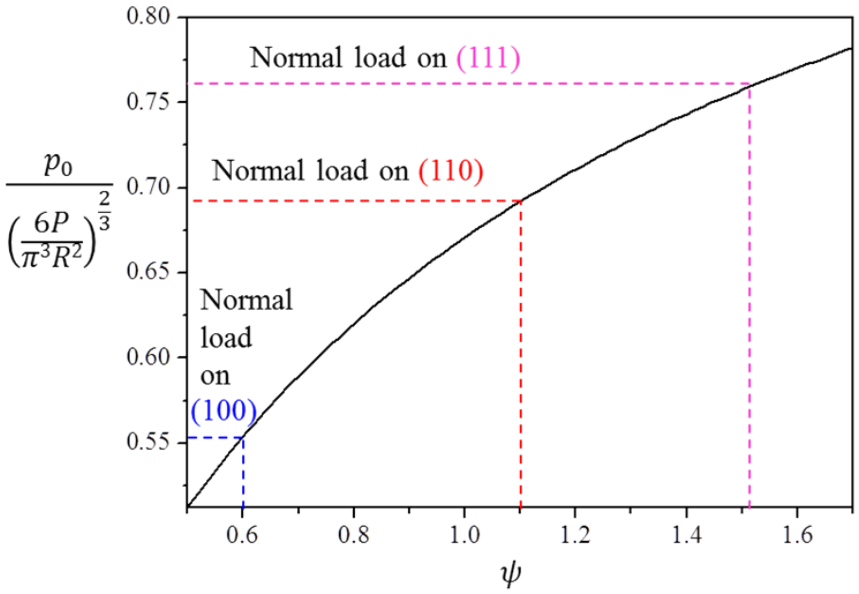

Figure 2-10: Effect of elastic properties on Hertz pressure. ψ is defined by Eq. (2.4)

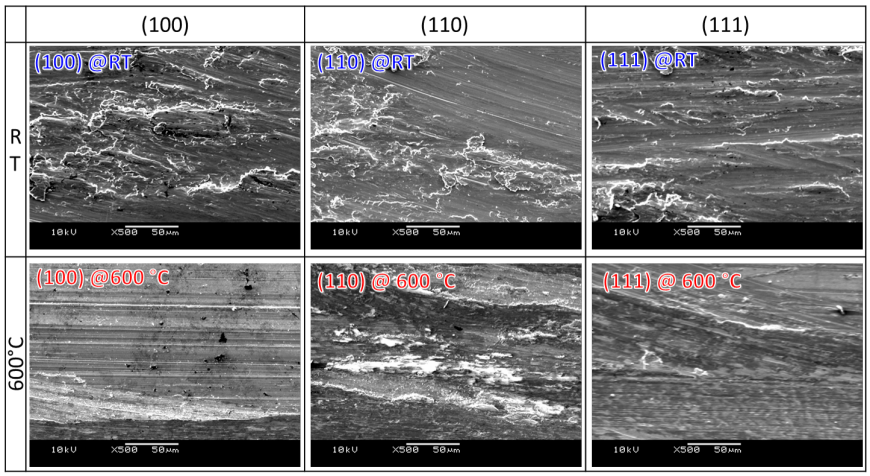

Figure 2-11: SEM micrographs of sliding traces on different SC specimen surfaces tested at RT and 600 °C.

tation of Cu at about 1 N [6]. According to Figure 2-8(a), sliding on (100) plane specimen exhibited lowest coefficient of friction of all tested plane samples. Similar behavior was also reported by Huang et al., where fretting on (100) crystal face along <001> direction was lower than <011> direction. At higher loads, the surface layers were highly deformed, thus might lost its single crystal properties [2]. The load depended friction behavior was much significant in (100) plane specimen, whereas in the case of (111) plane specimen, normal load dependence diminished.

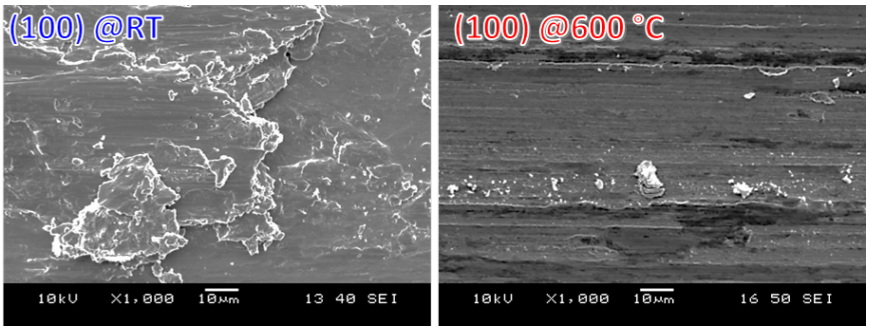

Figure 2-12: SEM micrographs of sliding traces on (100) SC specimen tested at (a) RT and (b) 600 °C.

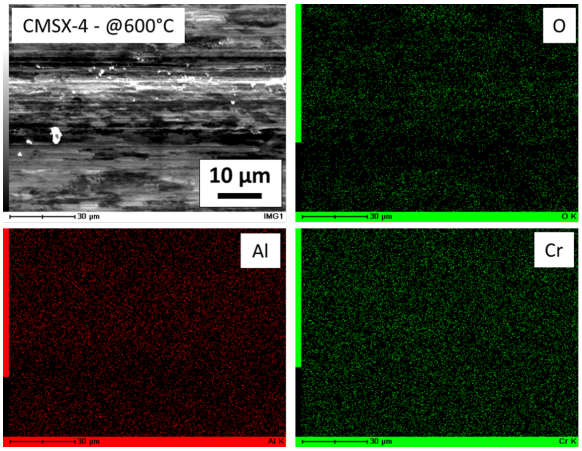

Figure 2-13: Effects of crystallographic sliding direction and test temperature on coefficient of friction when normal load is applied on (100) plane.

Table 2.4: Mechanical properties of CMSX-4 SC alloy and IN718 PC alloy [4, 5].

		CMSX-4			IN718
		<100>	<110>	<111>	
Longitudinal modulus	E [GPa]	124	226	311	204
Shear modulus	G [GPa]	127	66	57	78
Yield strength	σ_Y [MPa]	1150	1020	1100	925

These differences can be explained by a simplified Hertzian elastic analysis [8]. Consider an elastic contact between a sphere indenter (PC alloy) and an elastic half-space (SC alloy). The maximum contact pressure p_0 due to applied normal load P

by the indenter of radius R on the half-space is given by [8],

$$p_0 = \left(\frac{6PE^{*2}}{\pi^3 R^2}\right)^{\frac{2}{3}} \equiv 1.5\sigma_{mean} \tag{2.2}$$

where, σ_{mean} is the average contact stress, and E^* is the effective Young's modulus which is related to the elastic properties of contacting bodies as follows,

$$E^* = \left(\frac{1-\nu_p^2}{E_p} + \frac{1-\nu_s^2}{E_s}\right)^{-1} \tag{2.3}$$

where, ν_p, E_p - Elastic properties of PC alloy in this study, and ν_s, E_s - Elastic properties of SC alloy in this study. Introducing a parameter ψ that represents the relative elastic ratio of SC to PC alloy, defined by,

$$\frac{E_s}{E_p} = \psi, \tag{2.4}$$

we have a normalized contact stress p_0,

$$p_0 = \left(\frac{6P}{\pi^3 R^2}\right)^{\frac{2}{3}} [f(\psi)]^{\frac{2}{3}}, \tag{2.5}$$

where,

$$f(\psi) = \left(1 - \nu_p^2 + \frac{1-\nu_s^2}{\psi}\right)^{-1}. \tag{2.6}$$

Using the mechanical properties listed in Table 2.4, the value of p_0 is calculated in Fig. 2-10, which shows higher contact pressures when the contacting plane and sliding orientation deviates from the primary crystallographic direction. This trend can provide a reasonable explanation on the results in Fig. 2-8(a), where the sliding on (111) plane exhibited the highest COF followed by (110) and (100) planes.

As shown in Fig. 2-9(b), for a given crystal plane of contact, sliding along the <011> direction resulted in an increased tangential resistance and, in turn, increased the COF. In other words, the COF increases with the increase in misorientation of sliding direction from the <001> primary crystallographic orientation. These behav-

iors are in agreement with the results reported by Huang et al. [2], in which COF during fretting on (100) cubic crystal face along <011> direction was higher than that along <001> direction. Flom and Komanduri [3] reported results of indentation and sliding experiments on different SC materials. A 6.35 mm diameter sapphire ball sliding on (100) face of SC copper at a load of 0.981 N resulted in 16% increase in COF in going from the <001> direction to the <011> direction [3]. Qualitatively similar trend was observed in the current work, where the increase in COF was about 10% when tested at RT and 21% at 600 °C (Fig. 2-9(b)). This sliding friction behavior is also in agreement with anisotropic rolling resistance of SC copper with respect to rolling orientation reported by several researchers [3, 9, 10]. Tanaka and Oda [11] studied sliding friction behavior of SC copper against hard sliders of copper and steel. They reported an increase in sliding resistance due to the formation of bulge in front of the slider when sliding along <011> direction, as schematically shown in Fig. 2-14(b). On the other hand, when sliding along <001> direction, the bulges formed at either side of the slider resulting in concave wear track which offer less resistance to sliding in that direction. This anisotropy in surface deformation has also been confirmed by Huang et al. [2] using finite element simulation of rigid sphere indenting on a (100) plane of SC Ni-base superalloy, where residual deformation along <011> direction was more extensive, thereby forming a bulge on all four <011> directions, as shown in Fig. 2-14(a). This behavior was also attributed to the reorientation of initial fretting direction from <110> to <100> direction when the the specimen is allowed certain degrees of freedom [2].

Since the anisotropic formation of bulges should be due to the anisotropies in material yield strength as suggested by Huang et al. (2009), it seems reasonable to consider that the differences in tangential force resistance in present experiments would have been resulted from multiple material responses: relatively higher elastic modulus, lower shear modulus, lower yield strength and work hardening along <011> orientation, in comparison to those along <001> orientation (see Table 2.4). Based on the above discussion, as evident from the Fig. 2-9, the sliding direction with respect to crystal orientation in a SC/PC contact also appear to have substantial influence

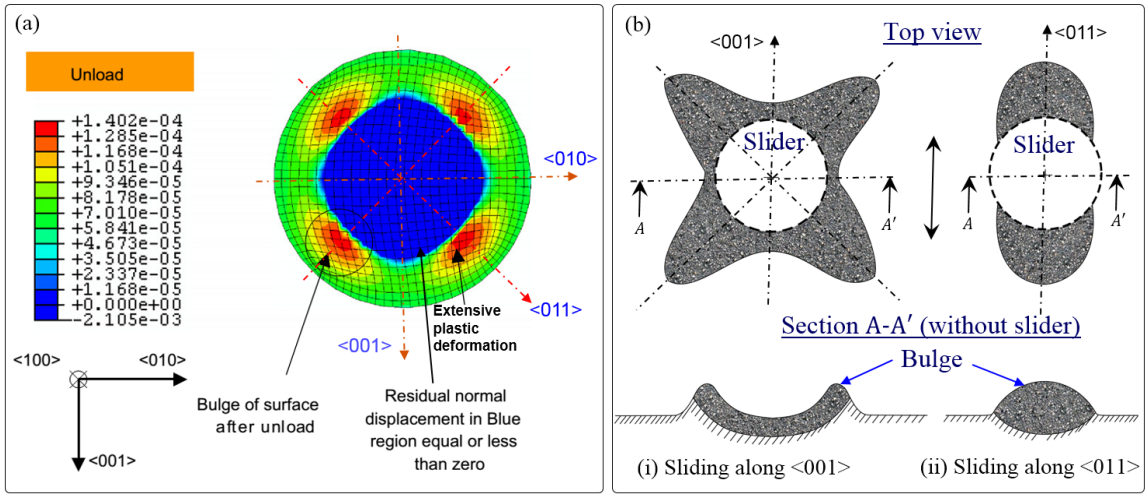

Figure 2-14: Residual deformation of single crystal (a) FE simulation of rigid sphere indenting the cubic face of a SC [2] and (b) Schematic of residual bulge formation on SC up on sliding along different sliding orientations.

on the tribo performance. Thus, as a primary postulation, relatively higher elastic modulus and lower shear modulus along <110> orientation in comparison to <100> orientation could increase the tangential force resistance.

This sliding orientation depended friction behavior was continued to exist even after increasing the test temperature to 600 °C despite oxidation (Fig. 2-13) and plastic deformation (Fig. 2-12(b)). From the EDS analysis results presented in Fig. 2-13, it is clear that the role of oxidation at high temperature is to reduce the width of wear trace and in turn reducing the effective contact area covered by thin glaze layer consist of oxides of Ni, Al and Cr. Nanoindentation test of glaze oxide layer on Ni-base superalloy formed up on cyclic sliding against cast iron revealed higher hardness than that of the bulk material [12]. Latief et al. [13] reported the anisotropy in the oxidation behavior of SC Ni-base superalloys where the thickness of oxide layer on (110) surface oriented specimen was smaller than (100) surface at 1100 °C. Thus the reduction in COF found in this study at 600 °C could be due to the formation of hard oxide layer on the sliding tracks, though the layers might have removed and replenished with sliding cycles as can be seen in Fig. 2-13.

This knowledge can give useful insight on the importance of considering both the crystallographic orientation of sliding direction together with the contact surface

orientation of SC/PC mating parts such as gas turbine SC blades and PC disk assemblies, where friction/fretting induced stress concentration leads to early fatigue crack nucleation and growth, resulting in premature failure of components.

2.7 Chapter summary

The influence of surface orientation and sliding orientation of SC/PC Ni-base superalloy system on the CSF behavior was investigated at room temperature and at 600 °C. The findings of this work are summarized as follows:

- The contact surface orientation was found to have a very significant influence on the room temperature CSF behavior of SC/PC superalloy system, especially when the contact is under mild wear condition. On the other hand, the contact surface orientation had negligible effect on COF when tested at 600 °C
- Not only the contact surface orientation but also the sliding orientation along SC plane had a strong influence under all normal loads and test temperatures. Also, the COF measured at 600 °C was lower than that at RT.
- The variation of mechanical properties of SC along loading and sliding orientations were compared and with the differences in experimental results were addressed in terms of elastic properties and resistance to deformation of SC. It is suggested that both the stress and the deformation field near the contact area which are closely influenced by the anisotropic mechanical properties in longitudinal and transverse elastic moduli and in yield strength would play extrinsic roles there.

2.8 Chapter references

[1] Goto, M., Kasahara, A., Tosa, M.. Low-Friction Coatings of Zinc Oxide Synthesized by Optimization of Crystal Preferred Orientation. Tribology Letters 2011;43(2):155–162. doi:10.1007/s11249-011-9792-8.

[2] Huang, X., Gibson, T.E., Zhang, M., Neu, R.W.. Fretting on the cubic face of a single-crystal Ni-base superalloy at room temperature. Tribology International 2009;42(6):875–885. doi:10.1016/j.triboint.2008.12.003.

[3] Flom, D.G., Komanduri, R.. Some indentation and sliding experiments on single crystal and polycrystalline materials. Wear 2002;252:401–429. doi:10.1016/S0043-1648(01)00879-1.

[4] Shah, D., Duhl, D.. The Effect of Orientation, Temperature and Gamma Prime Size on the Yield Strength of a Single Crystal Nickel Base Superalloy. In: Et al., M.G., editor. Superalloys 1984 (Fifth International Symposium). TMS; 1984, p. 105–114. doi:10.7449/1984/Superalloys_1984_105_114.

[5] Zhang, X., Stoddart, P.R., Comins, J.D., Every, A.G.. High-temperature elastic properties of a nickel-based superalloy studied by surface Brillouin scattering. Journal of Physics: Condensed Matter 2001;13(10):2281–2294. doi:10.1088/0953-8984/13/10/320.

[6] Buckley, D.H.. Surface Effects in Adhesion, Friction, Wear and Lubrication; vol. 0. Amsterdam, NY.: Elseiver Scientific Publishing Company; 1981.

[7] Degnan, C.C., Shipway, P.H., Wood, J.V.. Elevated temperature sliding wear behaviour of TiC-reinforced steel matrix composites. Wear 2001;251(1–12):1444–1451. doi:10.1016/S0043-1648(01)00772-4.

[8] Johnson, K.. Contact Mechanics; vol. 19. Cambridge: Cambridge University Press; 1985. ISBN 9781139171731. doi:10.1016/0301-679X(86)90085-X.

[9] Dyer, L.. Rolling friction on single crystals of copper in the plastic range. Acta Metallurgica 1961;9(10):928–936. doi:10.1016/0001-6160(61)90111-0.

[10] Bailey, J.M., Gwathmey, A.T.. Friction and Surface Deformation During Sliding on a Single Crystal of Copper. A S L E Transactions 1962;5(1):45–56. doi:10.1080/05698196208972452.

[11] Tanaka, K., Oda, Z.. Friction and deformation of copper single crystal. Journal of the Japan Society of Applied Physics 1973;42(4):347–356. doi:10.11470/oubutsu1932.42.347.

[12] Rynio, C., Hattendorf, H., Klöwer, J., Eggeler, G.. The evolution of tribolayers during high temperature sliding wear. Wear 2014;315(1-2):1–10. doi:10.1016/j.wear.2014.03.007.

[13] Latief, F., Kakehi, K., Fu, X.. Influence of Surface Orientation on Oxidation Resistance of Ni- based Single Crystal Superalloy CM186LC at 1100 C in Air. International Journal of Electrochemical Science 2012;7:7608–7618.

THIS PAGE INTENTIONALLY LEFT BLANK

Chapter 3

Fretting fatigue failure behavior of contacting Ni-base superalloys

Fretting fatigue failure behavior of similar contacting superalloys is studied in order to estimate the fatigue strength of superalloys subjected to fretting loading. The plain fatigue strength of the materials is compared with observed fretting fatigue strength and severity of fretting process is highlighted. Specific role of developed contact tractions controlled by secondary crystallographic orientations is characterized by means of stick-slip area fraction and fracture morphologies of failed specimens.

3.1 Introduction

Fretting and friction properties are known to be influenced by displacement modes such as partial slip, mixed mode and gross slip/sliding [1]. Here, the coefficient of friction between sliding/fretting contacts is one of the main factors that could control the failure mechanism, that is, either material removal by wear, crack nucleation from frictional interface or both [2, 3]. In order to characterize the orientation induced anisotropy on normal load direction, fretting fatigue (FF) failure tests were conducted on single crystal specimens having different secondary crystallographic orientations to estimate the fatigue life under fretting conditions.

In this chapter, the roles of fretting induced tangential force evolution and secondary crystallographic orientation on fretting fatigue failure behavior were investigated by using a combined single crystal and polycrystalline superalloy contacting pair at ambient (RT) and high temperature (HT) conditions. The effects of contacting superalloys and applied bulk stress amplitude on developed contact tractions were characterized in terms of tangential force coefficient and stick-slip area fraction. Failed specimens were observed using SEM in order to investigate the anisotropic behavior in fracture morphology influenced by fretting stresses.

3.2 Materials

Table 3.1: Chemical compositions (wt%) of Ni-base superalloys used in this study.

Material	Cr	Co	Mo	W	Ti	Al	Ta	Hf	Fe	C	Nb	Ni
SC CMSX-2	7.9	4.6	0.6	7.9	1.0	5.6	6.0	0.1	-	-	-	Bal.
PC IN718	19.0	-	3.0	-	0.9	0.5	-	-	18.0	0.04	5.0	Bal.

Single crystal (SC) Ni-base superalloy, CMSX-2; a representative material for gas turbine blades, was used in this study after standard solution heat treatment and aged conditions. A polycrystalline (PC) Ni-base superalloy, IN718; a representative material for gas turbine disks, was used as a contacting body. The chemical compositions of the superalloys used in this study are presented in Table 3.1. The characteristic

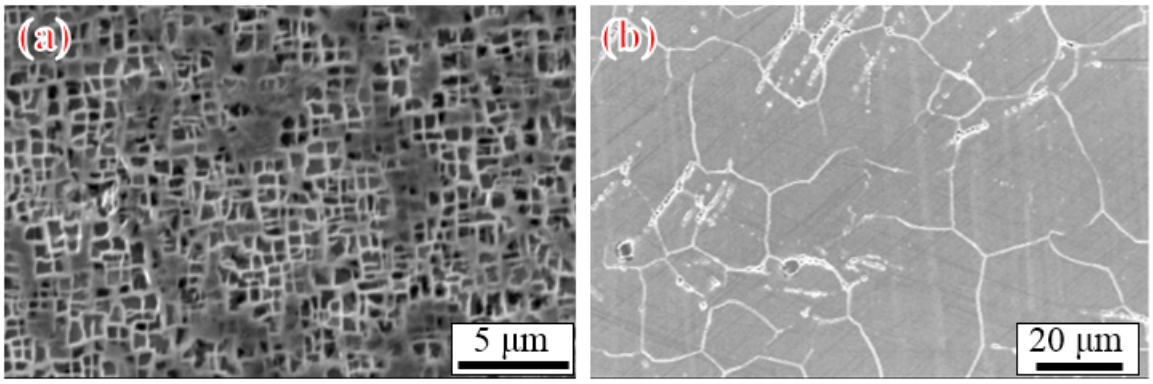

Figure 3-1: Microstructures of Ni-base superalloys used in this study (a) CMSX-2 and (b) IN718.

microstructures of CMSX-2 and IN718 are shown in Fig. 3-1. In CMSX-2, cuboidal γ' precipitates are uniformly distributed in the γ matrix. The volume fraction and size of γ' precipitates are approximately 75 % and 0.5 µm, respectively. In IN718, a nickel-iron superalloy rich in niobium, γ'' phase is the primary strengthening precipitate. The average grain size is about 16 µm.

3.3 Specimens and contact pads

SC specimens for fretting fatigue tests were machined from CMSX-2 bar stock as per dimensions shown in Fig. 3-2(a). The [001] crystallographic orientation was within $\pm 5^\circ$ of the longitudinal axis of the specimen. The dimensions of PC contact pad is shown in Fig. 3-2(b). Specimens from PC IN718 superalloy were also machined. Contact surfaces of specimen and contact pads were polished with SiC papers up to P-600 along the fretting direction.

3.4 Experimental procedure

3.4.1 Fretting fatigue tests

The fretting fatigue tests were conducted by applying cyclic bulk loading (Stress ratio, $R = -1$ and Frequency, $f = 10$ Hz) to the longitudinal axis and contact pressure to

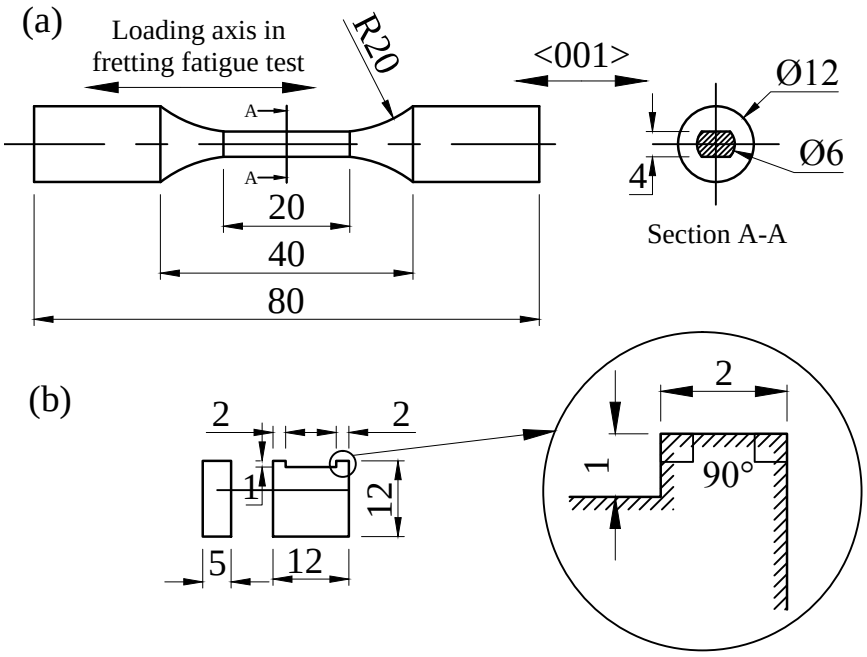

Figure 3-2: Geometries of (a) CMSX-2 fretting fatigue test specimen (b) IN718 contact pad. All dimensions are in *mm*.

the transverse axis using a flat-on-flat fretting contact arrangement [4] on a servo-hydraulic test machine as shown in Fig. 3-3. Two set of contact combinations were tested: (i) SC specimen vs PC contact pad (SC/PC) and (ii) PC specimen vs PC contact pad (PC/PC). For the tests at 600 °C, the specimen and contact pads were heated using a high frequency induction heating equipment. A constant contact pressure (σ_p = 100 MPa) was applied by pressing a pair of contact pads on either side of the specimen surface using a calibrated proving ring. Fretting fatigue test was carried out until failure to determine the fretting fatigue life for a given stress amplitude.

3.4.2 Secondary crystallographic orientation, β

The secondary crystallographic orientation (β) with respect to fretting contact plane normal of SC specimen is schematically shown in Fig. 3-4 and in Fig. 3-5. β angles of the SC specimens were not controlled but measured values are presented in Table 3.2.

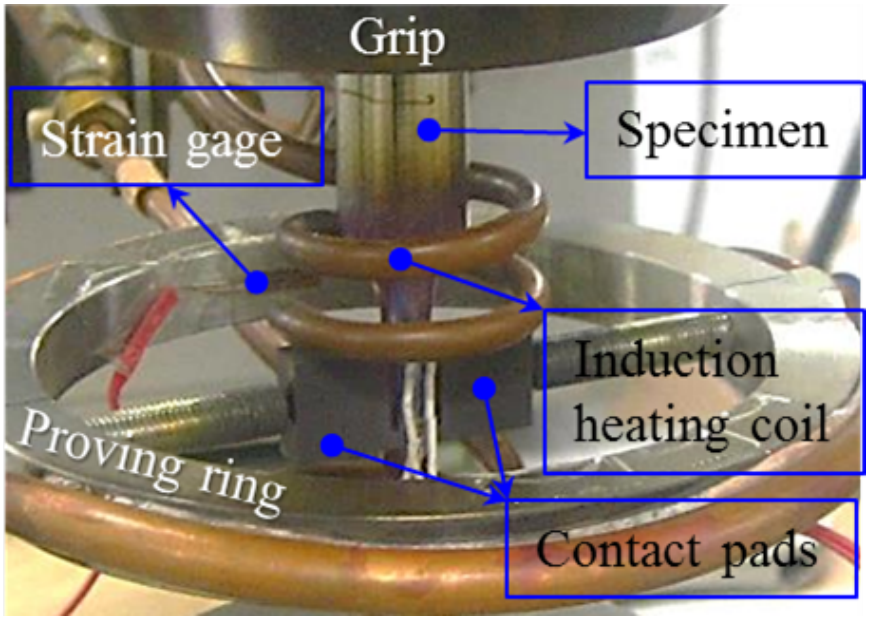

Figure 3-3: Photograph of high temperature fretting fatigue test rig system utilized in this study.

Table 3.2: Secondary crystallographic orientations (β) of SC specimens used in fretting fatigue tests.

Test temperature	Stress amplitude, σ_{app} [MPa]	β (from <010>, see Fig. 3-4)
RT	100	~25°
	150	~40°
	250	~5°
	400	~20°
600 °C	200	~15°
	300	~45°

3.4.3 Measurement of tangential force

The tangential force between the specimen and contact pad was continuously measured using a pair strain gages attached to the groove part of the contact pads. For this purpose, prior to testing, fretting pads were calibrated using a split specimen technique. Then, the tangential force coefficient (TFC) was calculated using Eq. (3.1).

$$TFC = \frac{Q}{P} \tag{3.1}$$

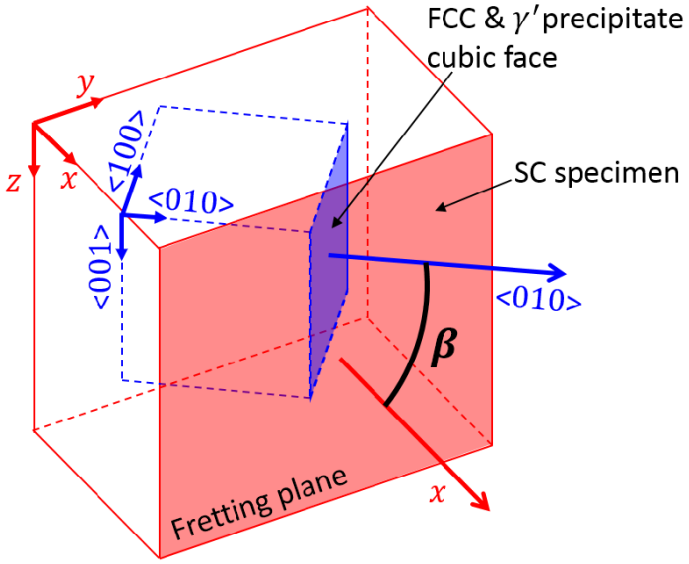

Figure 3-4: Schematic representation of secondary crystallographic orientation (β) angle between fretting plane normal and FCC SC cubic principal direction

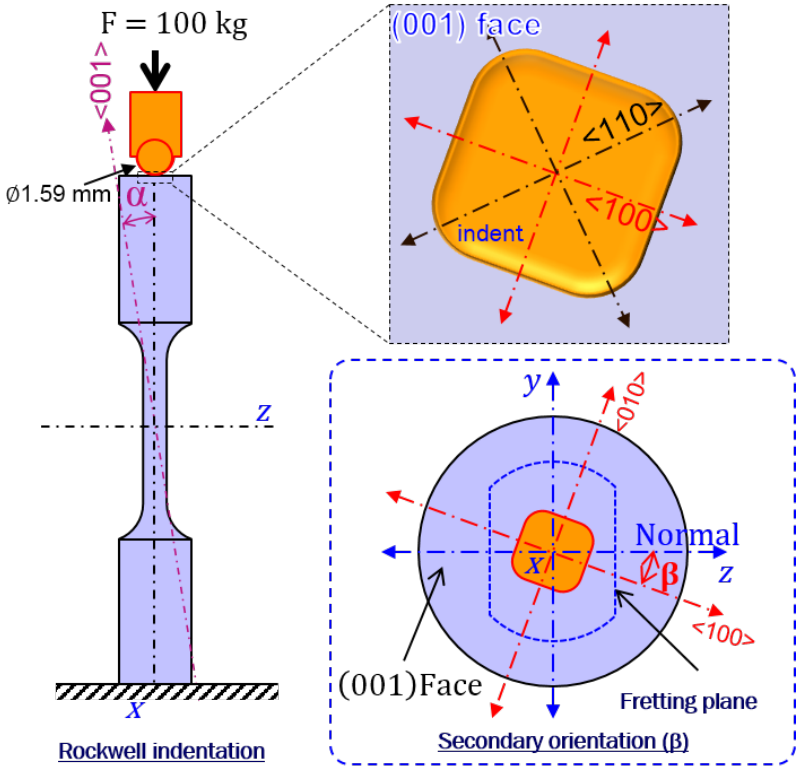

Figure 3-5: Schematic of rockwell indentation of (001) crystal face

where Q is the measured tangential force amplitude per unit length and P is the normal force per unit length applied on the specimen surface via proving ring.

3.5 Results and discussion

3.5.1 Dependence of orientation on mechanical properties

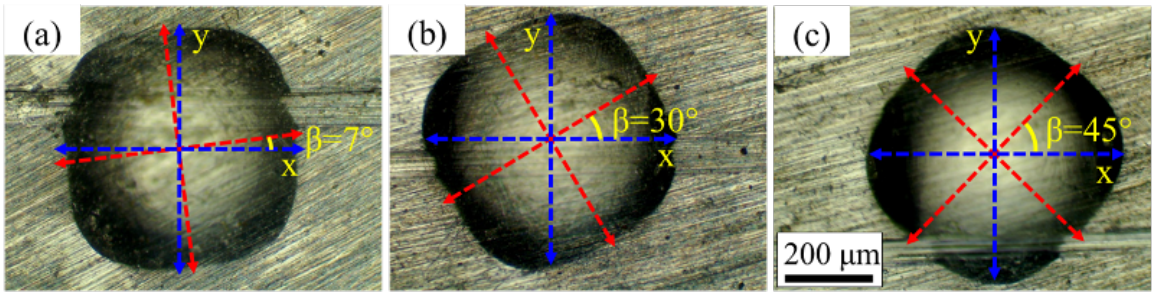

Figure 3-6: Spherical indentation shapes on (001) plane sensitive to secondary misorientation angle (β) from <100> axis (a) $\beta = 7°$, (b) $\beta = 30°$ and (c) $\beta = 45°$

Ball indention was carried out on the (001) face of FF test specimens and the topography of plastic deformation was studied. When indenting an isotropic material, the plastic deformation around the indentation is uniform. On the other hand, in the case of indentation on a single crystal material, the plastic deformation is not uniform [5]. In this study, indentations were made on CMSX-2 specimens by Rockwell hardness tester. Standard steel ball of diameter 1.59 mm was used to produce indents under a load of 100 kg (Rockwell B scale). The resulting indents on (001) face of CMSX-2 specimen is shown in Fig. 3-6, which have the shape of square with rounded edges. The location of rounded diagonals were depended on the secondary crystallographic orientation with respect to fretting plane normal (see Fig. 3-5). The amount of plastic deformation was excessive on corners for the uniform strain applied by axi-symmetric indenter. This anisotropic behavior was a result of difference in mechanical properties with crystallographic orientation. Higher elastic modulus and lower yield strength in the <110> direction facilitated excessive plastic deformation when compared to <100> direction. The normal to the straight edges correspond to the <100> direction [1, 2]. The maximum stress at the contact is strongly depended on the primary and secondary crystallographic orientation with respect to contact plane normal. It is evident that the normal stress distribution during fretting contact was also varied with secondary crystallographic orientation [6].

3.5.2 Experimental fretting fatigue life: S-N curve

Fig. 3-7 shows the relationship between applied bulk stress amplitude (σ_{app}) and number of cycles to failure (N_f) of SC and PC superalloys fretted against PC superalloy. All of the fretting fatigue tests were conducted under a constant contact pressure (σ_p) of 100 MPa. Reference room temperature plain fatigue tests were also conducted and high temperature plain fatigue results of SC alloy are taken from literatures [7, 8]. Overall fatigue lives under fretting conditions were reduced by a factor of 0.2∼0.3. With respect to contact pair, fretting fatigue strength of SC/PC contact pair was found to be lower than that of PC/PC contact pair. Fretting fatigue strength (at $N = 1 \times 10^7$) was 150 MPa for PC/PC and was 100 MPa for SC/PC. Noteworthy, test temperature did not affect the plain fatigue life of the superalloys. On the other hand, fretting fatigue life was improved slightly at high temperature when the applied bulk stress amplitude was low enough. Little is known on the effect of secondary crystallographic orientation from the S-N curve, as the SC specimens tested at different stress amplitudes had different secondary orientations (Table 3.2). Possible influence of secondary crystallographic orientation of SC specimen on the fretting fatigue life will be discussed in Chapter 4.

Mall et al. [9] reported a significant improvement in plain fatigue and fretting fatigue performance of IN100 alloy at 600 °C. Such temperature dependent fatigue behavior was linked to the increase in yield and tensile strengths of Ni-base superalloys at intermediate temperatures [9]. Waterhouse [10] reported the formation of glaze oxide layer on the surface of IN718 alloy subjected to fretting at 540 °C that resulted in low *COF* and wear rate. Similar response was observed in the current study, where the formation of oxide glaze layer at high temperature reduced the tangential force at the interface which must have delayed the crack nucleation process. However, such a temperature dependent behavior was observed only under lower stress amplitudes. Fleury et al. [2] noted possible effect of exposure time in forming the oxide layer on the contact interface, where longer exposure time would increase the thickness of oxide

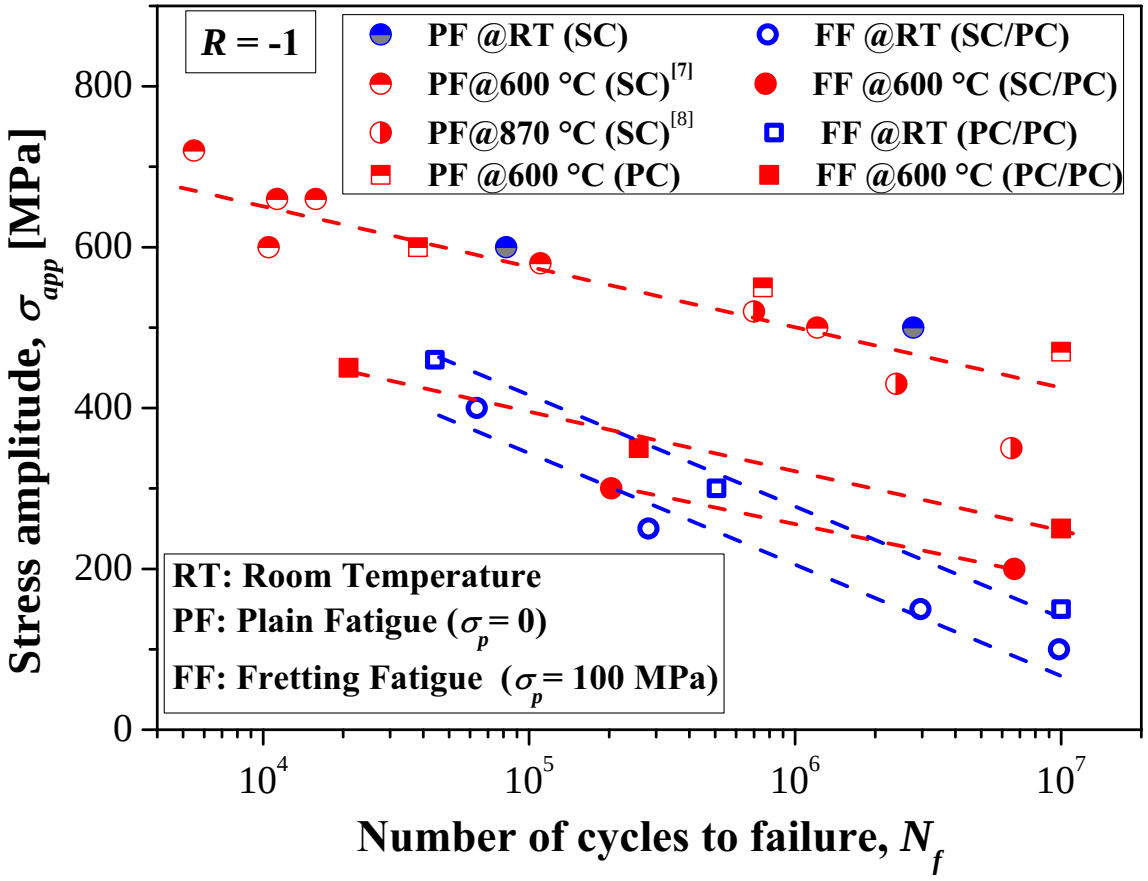

Figure 3-7: S-N data for plain fatigue and fretting fatigue of Ni-base superalloy combinations ($\sigma_p = 100\,\text{MPa}$).

layer. Hence, longer exposure time (number of cycles) under lower stress amplitudes resulted in the reduction of *TFC*. Thus, the knowledge of contact tractions at the interface with respect to contacting materials and operating environment is inevitable.

3.5.3 Contact tractions during fretting fatigue test: *TFC*

Fig. 3-8 shows the variation of mean *TFC* with applied bulk stress amplitude for a constant contact pressure of 100 MPa at RT. The increase in TFC was found to be linearly proportional to stress amplitude (at least in the range of tested stress amplitudes). Similar proportional relationship was also found in fretting fatigue of steel/steel contact pair [11]. Mean TFC for SC/PC fretting pair was higher than that of PC/PC pair. The increase in TFC for SC/SC pair could be the reason for the reduction in fretting fatigue life (Fig. 3-7). Thus, it is clear that the influence of

stress amplitude on TFC (i.e. TFC as a function of stress amplitude) which could control fretting fatigue crack initiation needs to be taken into account for a better life prediction methodology. In Chapter 4, an attempt was made to estimate the fretting fatigue life of superalloys by incorporating experimentally measured TFC values into an analytical model based on crack analogue, which was proposed by Giannakopoulos et al. [12].

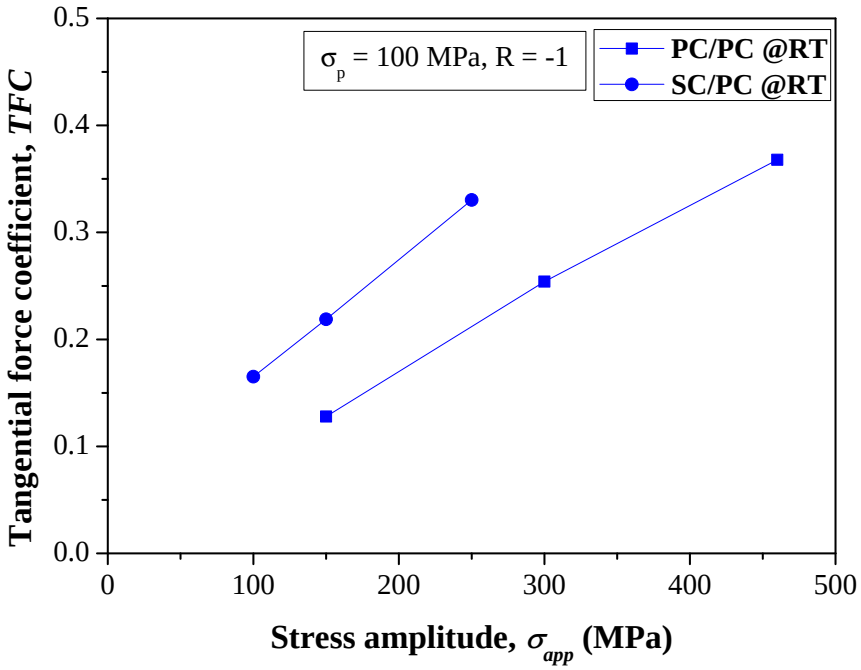

Figure 3-8: Relationship between applied stress amplitude σ_{app} and measured mean tangential force coefficient TFC at room temperature ($\sigma_p = 100\,\mathrm{MPa}$).

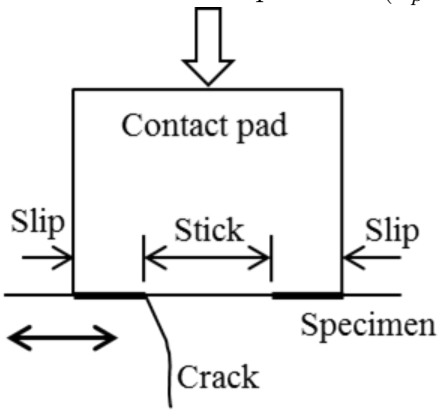

Figure 3-9: Schematic of stick-slip interface crack initiation

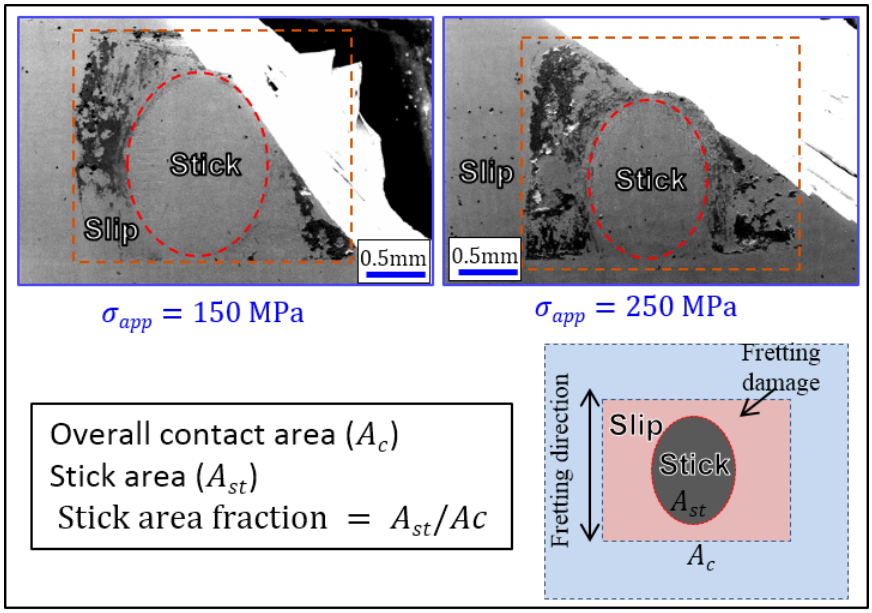

Figure 3-10: Variation of stick-slip contact area on SC specimens with different stress amplitudes. Stick area fraction is defined as the ratio of stick area to total contact area

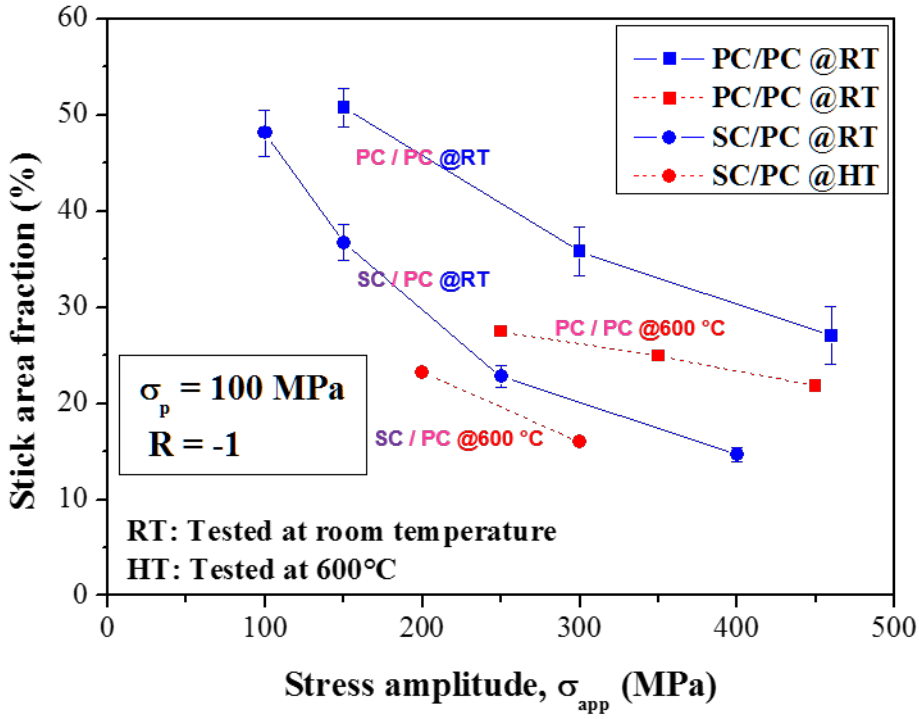

Figure 3-11: Measured stick area fraction values for specimens tested different stress amplitudes

3.5.4 Stick-slip area fraction

The crack initiation under fretting conditions generally occurs either at the outer edge of the contact area or at the interface between stick-slip region [13–16]. During the fretting fatigue test, the fretting fatigue surface consisted of two layers: a slipping, or, worn layer; and an adhered, or an elastically contact layer. Note that the fretting fatigue crack was nucleated from the interface between the two layers, so-called the stick-slip region (Fig. 3-9). Fig. 3-10 shows the fretting contact area on the SC specimen surface subjected to two different stress amplitudes. Here, the stick area decreased with the increase in stress amplitude. In order to quantify the variation of stick-slip area with stress amplitude, stick area fraction is defined as a ratio of stick area to total contact area as schematically shown in Fig. 3-10. The variation of stick area fraction with stress amplitude for different contacting superalloy combination is presented in Fig. 3-11. SAF was higher for PC/PC contact pair than SC/PC contact pair. This implies that for PC/PC contact slip amplitude was lower than SC/PC which had better life. This behavior in SAF is inversely proportional to the *TFC* evolution.

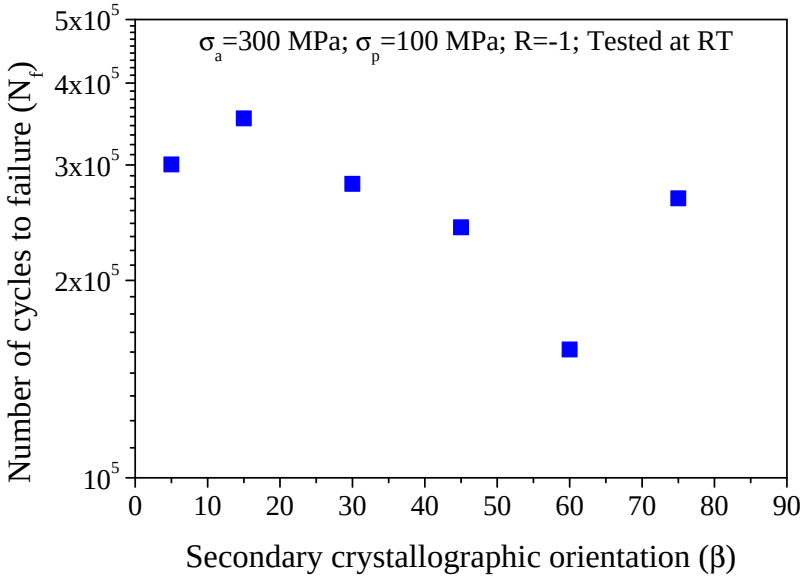

Figure 3-12: Effect of secondary orientation, β on cycles to failure

3.5.5 Effect of secondary orientation, β

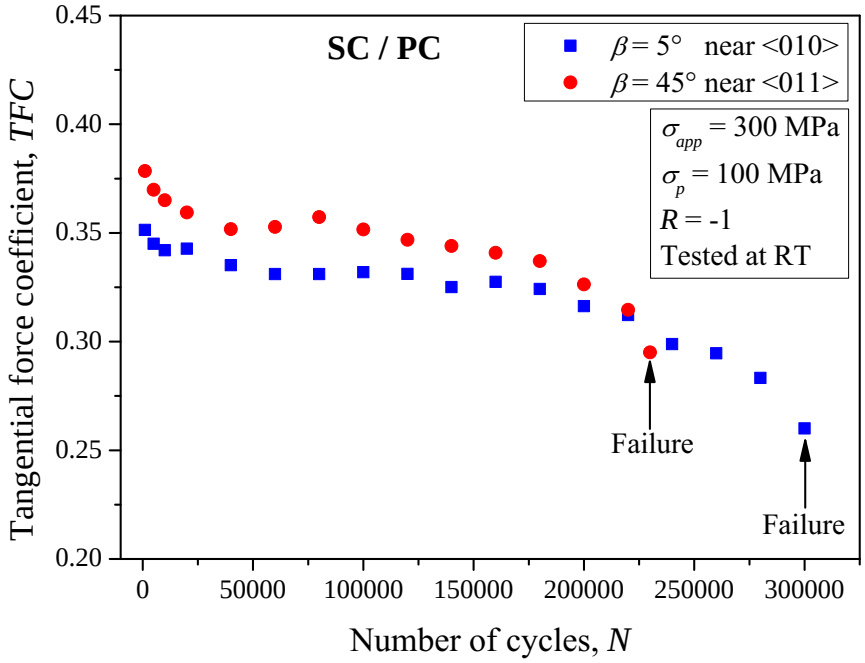

Figure 3-13: Evolution of TFC with fretting fatigue cycles on SC specimens having two different secondary orientations under identical loading conditions.

For the case of contact between SC and PC alloys, the stress state below the contact must be sensitive to secondary crystallographic orientation of SC with respect to contact pressure direction (or fretting plane normal) [17, 18]. In order to explore this aspect, fretting fatigue tests (under identical loading conditions) were carried out with SC specimens having different secondary crystallographic orientations β as schematically shown in Fig. 3-4. Although the applied contact pressure (σ_p) for all these tests was maintained constant at 100 MPa, the resulting contact shear traction at the interface must be different and dependent on the contact orientation. In order to isolate the effect of contact orientation on fretting fatigue strength, tests were conducted under a constant bulk stress amplitude and contact pressure on SC alloy specimens having different secondary orientations (β). The change in fretting fatigue life with the angle β is presented in Fig. 3-12. Only one specimen was used for each β angle specimen, hence only a qualitative analysis could be carried out. However, the results provide a clear trend to the fretting fatigue strength affected by the angle β.

Fig. 3-13 shows the evolution of TFC with fretting fatigue cycles for two different β orientations. Note that the applied contact pressure σ_p was 100 MPa, for both orientations. However, the TFC was observed to be higher for $\beta = 45°$ specimen than that of $\beta = 5°$ specimen. As one would expect, the specimen with higher *TFC* ($\beta = 45°$) failed faster than the other specimen. Similar trends in cyclic sliding friction behavior and contact stress field with respect to secondary crystal orientation was confirmed in the CSF behavior, presented in Chapter 2.

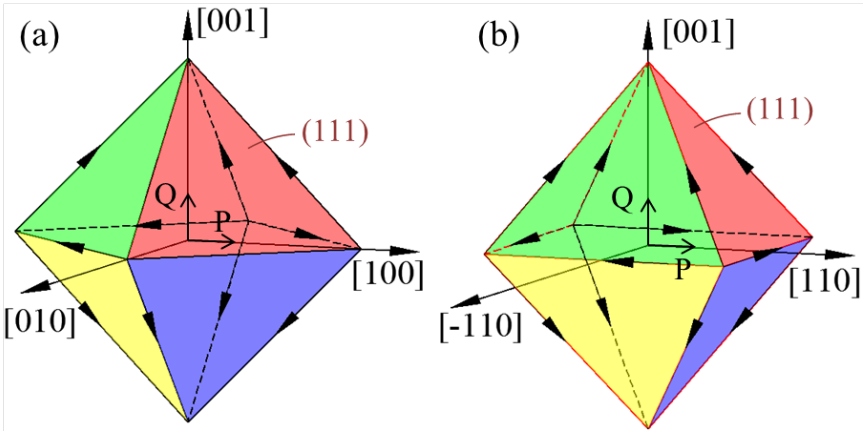

Figure 3-14: Schematic of arrangement of octahedral slip systems in FCC crystal when (a) Normal force P from [100] with $\beta = 0°$ and (b) Normal force P from [110] with $\beta = 45°$.

3.5.6 Fracture surfaces

The examination of macroscopic fracture surfaces of the SC specimens in the FF tests revealed features sensitive to secondary crystallographic orientations. Fig. 3-15 shows the appearance of fretted region and fracture morphology of two specimens with different secondary orientations. The cracks were nucleated from the interface between stick-slip region, which is one of the common modes of crack nucleation in fretting fatigue [13–16, 19]. Furthermore, cracks initiated from the contact edge shifted to slip-stick interface, as a result of wear of contact edge [13, 20–22]. Note the orientation of fracture planes with respect to axial bulk stress axis was found to be influenced by the secondary crystallographic orientation of the fretting contact planes. The fracture plane was perpendicular to the fretting plane in near (110) specimen,

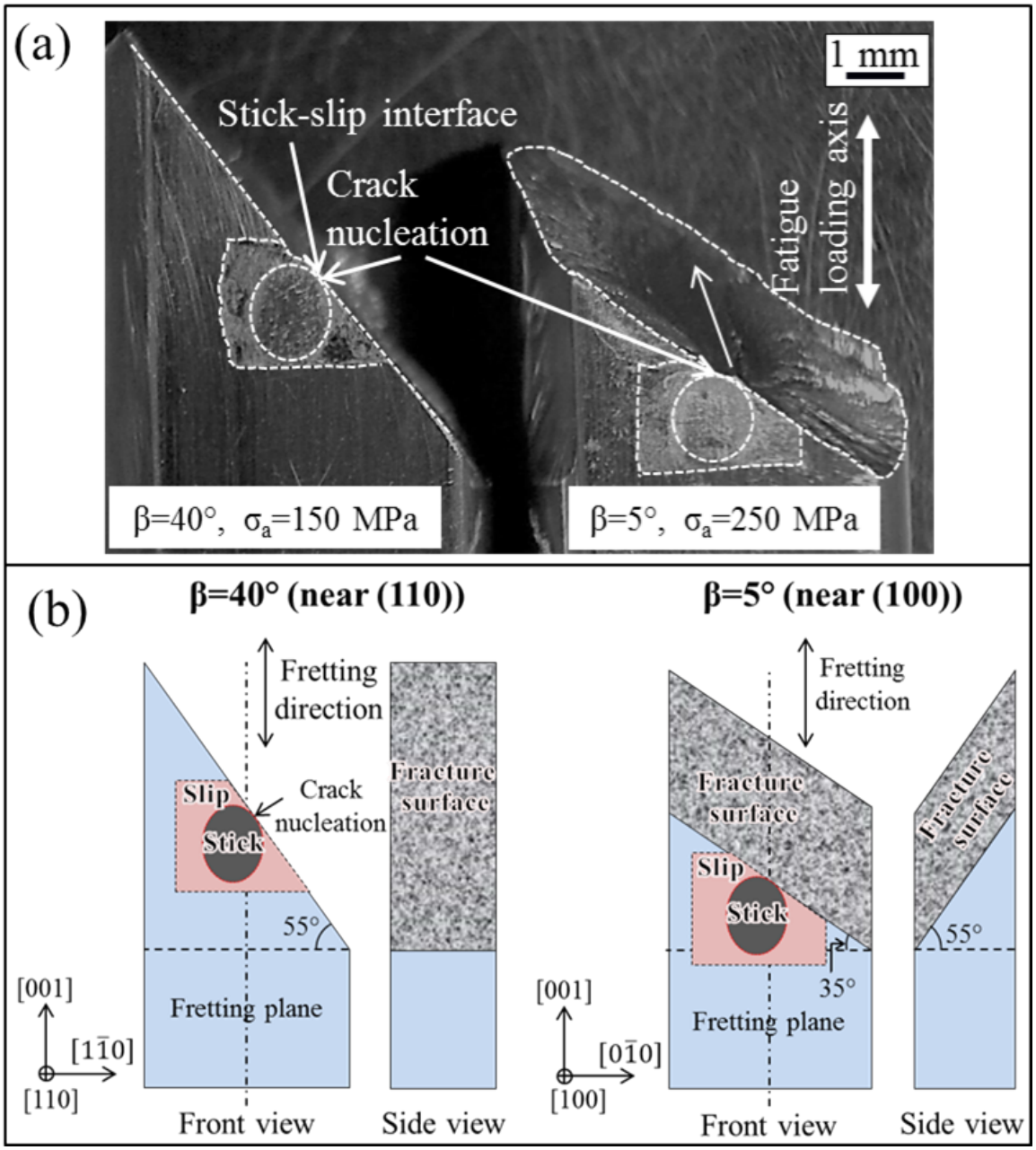

Figure 3-15: Macroscopic FF fracture morphology of CMSX-2 at the room temperature (a) Optical microscope images of typical fracture surfaces and (b) Schematic of the influence of macroscopic crystallographic orientation on fracture behavior.

whereas, in the (100) specimen, the fracture plane was inclined at an angle of about 55° to the fretting plane. Furthermore, the angle between the fracture plane and bulk stress axis was approximately 55° in near (110) specimen, whereas, the same was about35° in near (100) specimen (Fig. 3-15(b)). The arrangement of octahedral

slip systems of FCC crystal with respect to contact normal is schematically shown in Fig. 3-14. The relative angles of fracture planes correspond to the {111} octahedral slip planes on which the cracks were propagated [3, 23].

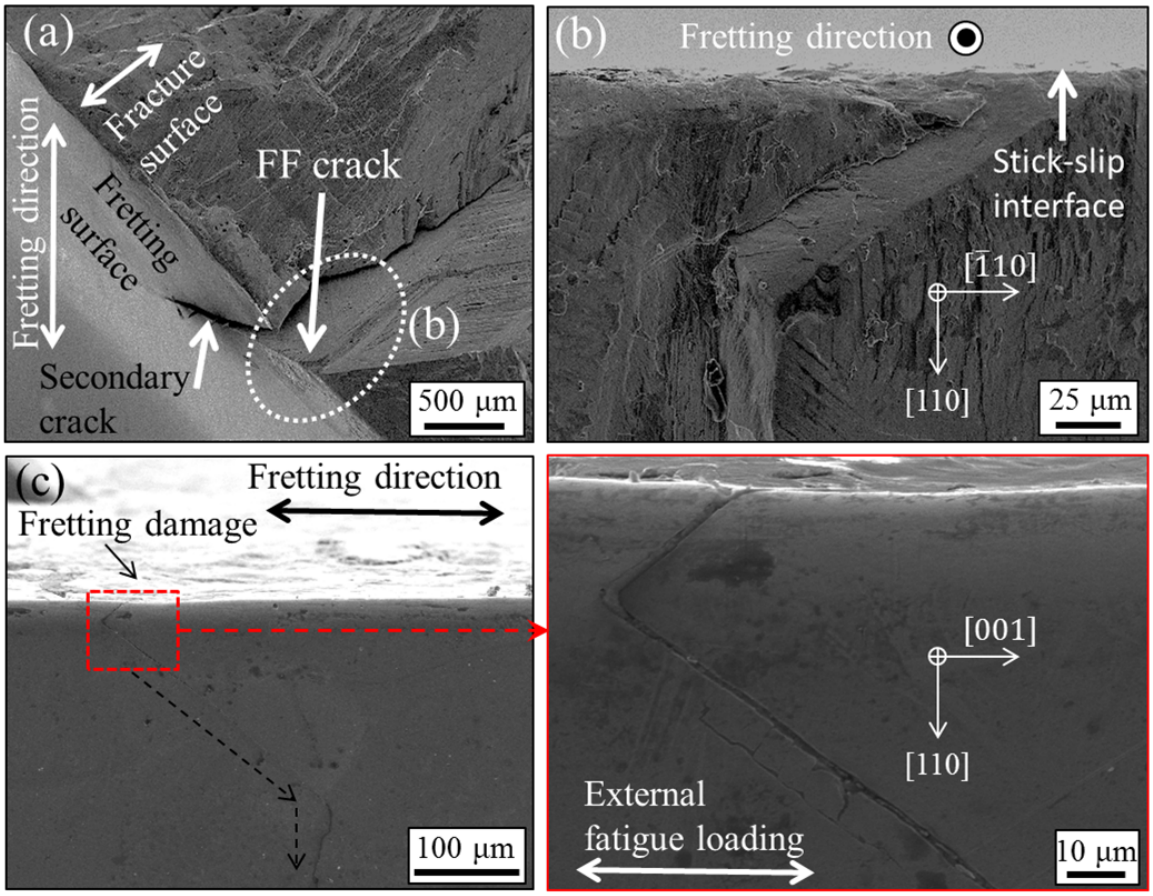

Figure 3-16: SEM fractographs of fretting fatigue crack in CMSX-2 tested at room temperature ($\beta = 45°$, $\sigma_{app} = 300\,\text{MPa}$) (a) fracture surface showing the crack initiation from the contact edge at surface, (b) closer view of fracture surface marked in (a) and (c) longitudinal transverse cross section, showing a crack nucleated from the fretting damaged area and growing along different slip planes.

Fig. 3-16(a) shows the SEM image of the fracture surface of the CMSX-2 specimen subjected to fretting fatigue. Secondary cracks were developed beside a primary crack that were nucleated from the fretted surface. This can be attributed to the activation of multiple slip systems during the crack propagation period where the resolved shear stresses acting on the crack tip were altered. Fig. 3-16(c) shows the longitudinal cross section of the CMSX-2 specimen in which the crack nucleation location and propagation path can be clearly seen. Fretting fatigue crack nucleated from the

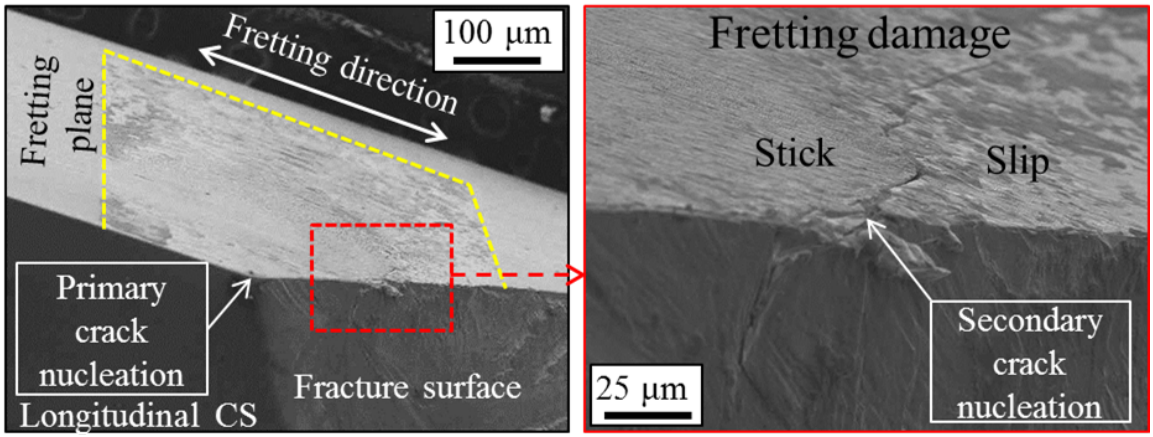

Figure 3-17: SEM image of secondary surface crack propagating along stick-slip interface ($\beta = 30°$, $\sigma_{app} = 300$ MPa, Tested at RT).

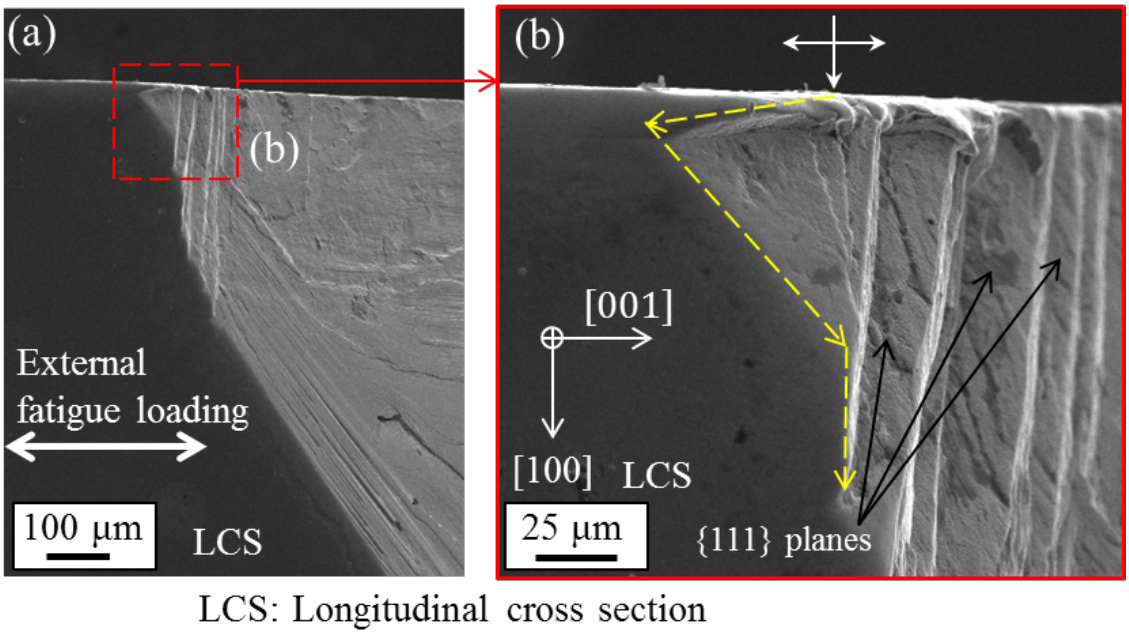

Figure 3-18: SEM image of longitudinal cross section of failed specimen showing shallow crack initiation from the stick-slip interface and crack kinking. Macroscopic crack propagation was found to occur along a set of {111} octahedral planes ($\beta = 5°$, $\sigma_{app} = 250$ MPa, Tested at RT).

localized fretting damaged region and grew at a sharp angle to the surface by 20 µm and then it kinked to grew along {111} plane for a length of 220 µm before deflecting in a direction normal to the bulk stress axis.

In addition to the crack propagation into the material, surface cracks were also found to be grown along the stick-slip interface, where localized stress concentration

caused a singular state of stress at the interface [24], as shown in Fig. 3-17. It is interesting to note that, similar to Figs. 3-15 and 3-16, the direction of crack growth at the surface was not perpendicular to the bulk stress direction but along the severe contact traction direction, i.e. along the direction of stress singularity [24]. As the crack grows away from the stick-slip interface it branches out along crystallographic slip planes and along the plane normal to bulk stress direction (Fig. 3-18).

3.5.7 Electron Back Scattered Diffraction (EBSD) analysis of subsurface microstructure

In addition to the understanding of macroscopic fretting fatigue failure behavior, it is necessary to understand the effect of fretting contact stresses on the subsurface microstructure on a crystallographic scale (such as, extent of highly deformed regions, local misorientation, Euler orientation, crystallographic orientation in relation to a specific specimen axis), which might in turn, influence the crack initiation and propagation behavior. The automated Electron Back Scattered Diffraction (EBSD) technique, a sophisticated technique to obtain crystallographic orientation patterns [25, 26], can be utilized to analyze the effect of fretting induced damage on the subsurface crystallographic microstructure of the specimen material. Also, the automated EBSD pattern is especially useful in quantifying the local changes in misorientation of deformed layers just below the fretting surface [1].

Small blocks were cut through the fretting contact area along the longitudinal axis of the fractured specimens. These representative subsurfaces were polished to reveal high surface finish using 0.06 µm colloidal silica. A SEM system (JEOL JSM6510) equipped with a EBSD detector (Oxford Instruments) was used to capture the diffracted patterns and a post processing software (HKL Channel 5) was used to obtain the orientation maps.

Fig. 3-19(a) shows the SEM image of longitudinal transverse cross section of a SC specimen tested at a stress amplitude of 300 MPa at room temperature. Fig. 3-19(b) and Fig. 3-19(c) show the magnified SEM images of area *away from* fretting-disturbed

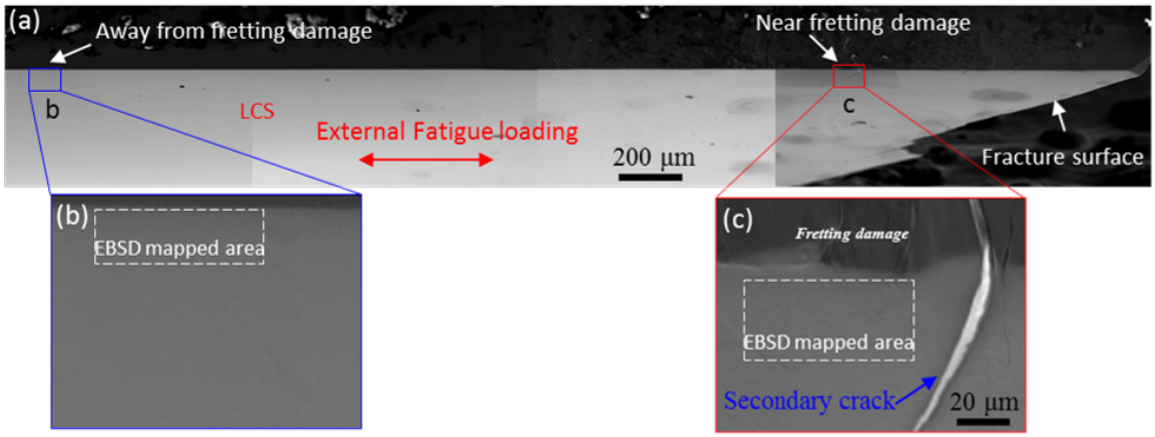

Figure 3-19: SEM image of longitudinal cross section of CMSX-2 specimen used in EBSD analysis (a) overall inclined view of LCS which shows the surface damage due to fretting, (b) magnified image of inset denoted as *b* in *a* and (c) magnified image of inset denoted as *c* in *a* ($\beta = 15°$, $\sigma_{app} = 300\,\text{MPa}$, Tested at RT).

region and area *in* fretting-disturbed region, respectively. In the latter image, the fretting damage and associated secondary cracks can be seen which initiated at the surface and propagated in a direction parallel to the primary crack. EBSD analyses were carried out on the longitudinal transverse cross section of specimens subjected to fretting loading conditions.

Fig. 3-20 shows the EBSD analysis results of an area *away from* fretting-disturbed region presented in Fig. 3-19(b). Fig. 3-20(c) shows the band contrast (BC) image, also called as the pattern quality map, of the area highlighted in Fig. 3-20(a), which is related to the brightness level of diffraction bands above a normalized background. Generally dark regions in a BC image represents highly deformed regions where the diffraction patterns are too diffuse to index the orientation [25]. Fig. 3-20(d) shows the changes in local misorientation. Fig. 3-20(e) shows the all Euler orientation map representing the orientation of the mapped area in Euler space. Fig. 3-20(f) shows the inverse pole figure (IPF) map with reference to the direction normal to fretting surface. Fig. 3-20(b) shows the orientation of the mapped area in stereographic triangle. From these figures, it is clear that crystallographic orientation near the surface away from fretting-disturbed region is uniform and same (Fig. 3-20(e)). Also the variation in local misorientation angles is insignificant (Fig. 3-20(d)) and negligible deviation of

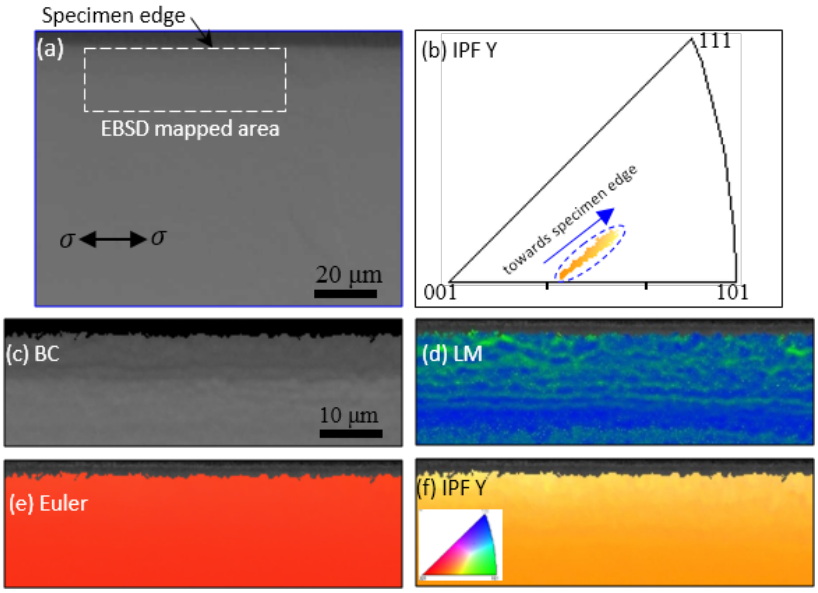

Figure 3-20: EBSD analysis results of the area away from fretting-disturbed region (a) SEM image showing the EBSD mapped area, (b) crystallographic orientation of the mapped area in stereographic triangle (color code corresponds to (f)), (c) Band contrast map, (d) Local misorientation map, (e) All Euler orientation map, and (f) inverse pole figure map with reference to the orientation normal to the fretting contact surface ($\beta = 15°$, $\sigma_{app} = 300$ MPa, Tested at RT).

orientation with reference to the fretting surface normal is evident (Fig. 3-20(f)). However, a tendency of orientation shift from <001>-<101> line of the stereographic triangle (deeper from surface) towards the center of the triangle (near surface) can be seen in Fig. 3-20(b).

Fig. 3-21 shows the EBSD analysis of results of an area *just below* the fretting-disturbed region presented in Fig. 3-19(c). The EBSD mapped area is marked with a white dashed rectangle in the SEM image. In contrast to the EBSD results of the area away from fretting-disturbed region, a significant scatter in orientation distribution can be seen from Fig. 3-21(b). Although the SEM image of the EBSD mapped area is smooth in appearance, dark regions just below the fretting surface in Fig. 3-21(c) suggest highly deformed microstructure as a result of fretting contact stresses. In addition to the highly deformed region, a set of darker lines parallel to secondary crack can be seen which could be slip traces. A relatively higher local misorientation angles were observed along these slip traces suggesting lattice rotation and activation

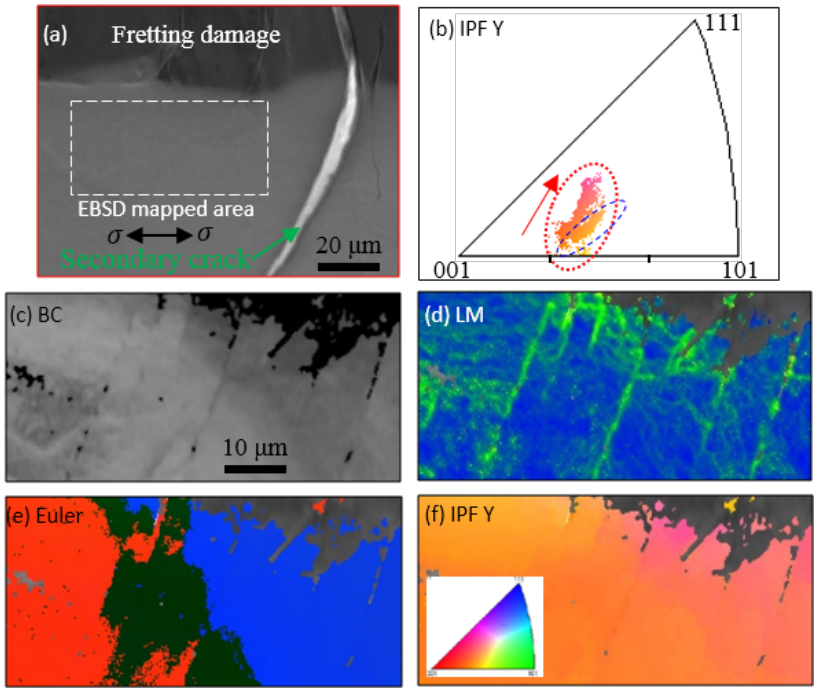

Figure 3-21: EBSD analysis results of the area away from fretting-disturbed region (see Fig. 3-20 for details)

of multiple slip systems (Fig. 3-21(d)). Also the all Euler orientation map shows significant differences in crystallographic orientations just below the highly deformed region (Fig. 3-21(e)), suggesting the tendency to form new sub-grains.

In order to stabilize the fretting-damaged region, fractured specimens were subjected to reheat treatment at 1080 °C in Ar atmosphere for 12 hours. Fig. 3-22 shows the EBSD analysis results of the fretting-damaged areas in SC CMSX-2 tested at both RT and at 600 °C after reheat treatment. In comparison to the specimen tested at RT, the specimen tested at 600 °C showed thicker highly deformed layer. Fatigue cracks were found to be nucleated right away from the contact interface with relatively little plastic deformation and wear when tested at RT. In other words, under ambient testing conditions, fretting stresses are concentrated over a small area around the stick-slip interface resulting in a singular state of stress, thereby facilitating the early initiation of fatigue crack rather than fretting wear.

On the other hand, when tested at 600 °C, small grains with random orientations were also formed as a result of recrystallization. It can be inferred that lattice rotation

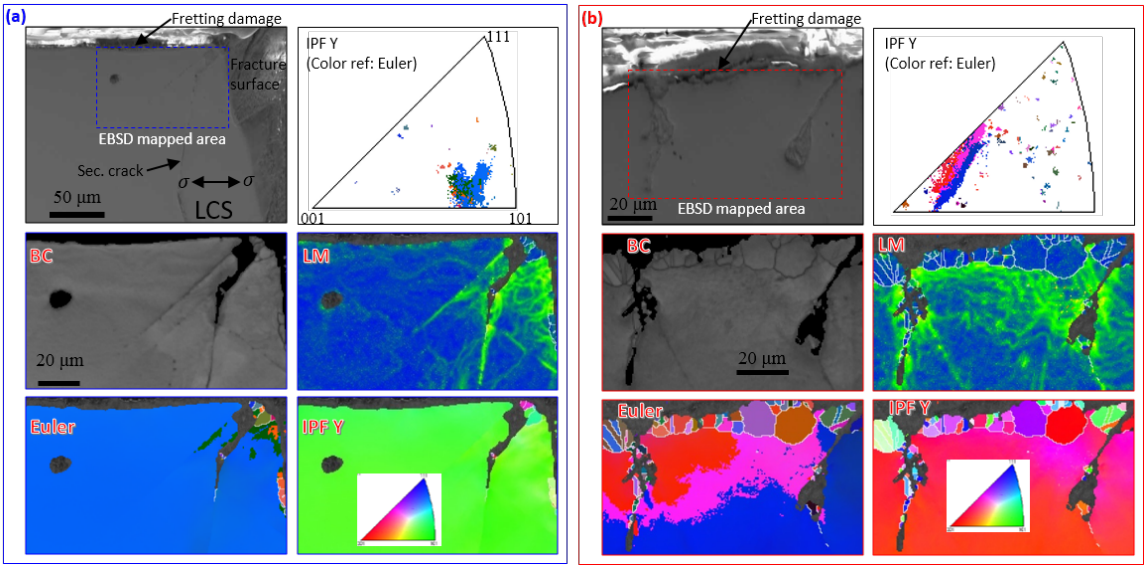

Figure 3-22: EBSD analysis results of the fretting-damaged areas in SC CMSX-2 after post-test solution heat treatment (a) tested at RT [$\sigma_{app} = 150\,\text{MPa}$], and (b) tested at 600 °C [$\sigma_{app} = 200\,\text{MPa}$].

had occurred as a result of severe fretting wear at contact interface and associated material transfer aided in the formation of new grains, when tested at high temperature. The lattice rotation due to fretting stresses increased towards the fretting contact surface. Also, the formation fine-grains just below the plastically deformed region show the increase in intragranular misorientation [27]. A significant amount of energy might be spent on fretting wear process prior to the initiation of fatigue crack which resulted in higher fretting fatigue life for superalloy specimens tested at 600 °C [18]. It is also reported that the formation of thicker mechanically mixed layers could delay the initiation of surface cracks as a result of continuous mixing of material which might as well remove small cracks within this layer [1]. Fretting wear process was dominated when tested at high temperature resulting in delayed fatigue crack nucleation. As a result, fretting fatigue life of superalloys were found to be slightly improved at high temperature (see Fig. 3-7).

It is also interesting to note that the small cracks nucleated from fretting damage region were transformed into localized cellular microstructure after re-heat treatment. The cellular transformation can occur in single crystal Ni-base superalloys subjected to prior damage by fatigue, thermomechanical fatigue, and creep, upon specific re-

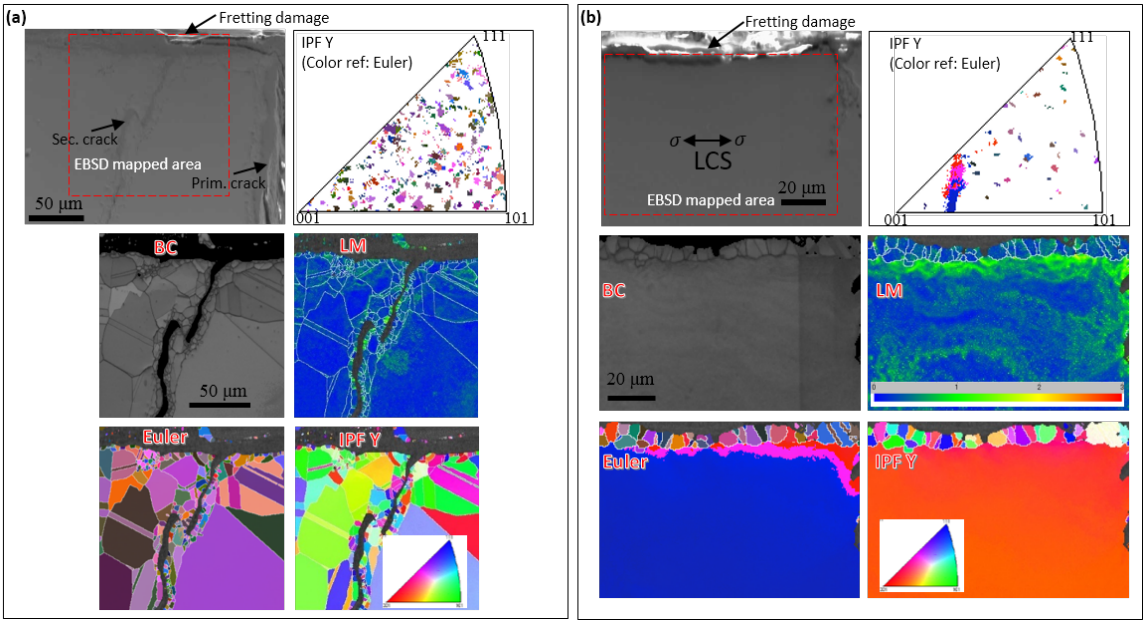

Figure 3-23: EBSD analysis results of the fretting-damaged areas in different superalloy materials tested at 600 °C after post-test solution heat treatment (a) PC IN718 [$\sigma_{app} = 350$ MPa], and (b) SC CMSX-2 [$\sigma_{app} = 200$ MPa].

heat treatment conditions [28–30]. So it is clear that the non-critical secondary fatigue cracks nucleated from fretting damage could also result in degradation of high temperature strength of the material by facilitating the formation of undesirable cellular microstructure.

The formation of finer recrystallized grains below the highly deformed layer was also observed in PC IN718 specimen tested at 600 °C, as shown in Fig. 3-23(a). Also, the mechanically mixed layer was thicker in PC IN718 than SC CMSX-2. In addition to the sub-grains parallel to the highly deformed layer, fine grains were formed along the crack faces as a result of localized recrystallization of the bulk polycrystalline material. This could have been triggered by the remaining plastic deformation along the crack path [31].

Fig. 3-24 summarizes the results of EBSD analysis, which clearly shows the deformed microstructure below fretting surface in the following order: a mechanically mixed layer as a result of severe deformation, new sub-grain layer, and original single crystal or polycrystalline material. Highly deformed layers can be identified by the absence or diffuseness of EBSD patterns [32]. An increase in low-angle misorientations

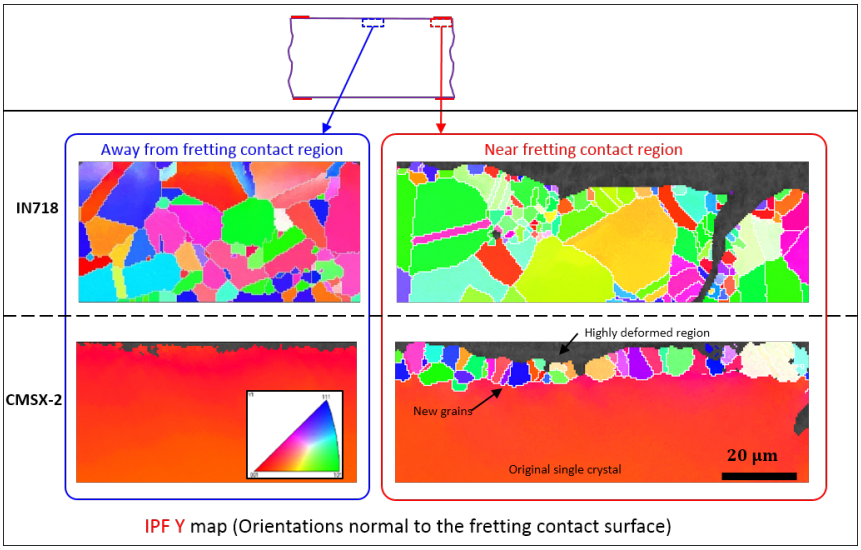

Figure 3-24: IPF maps with reference to the orientations normal to the fretted surface for different superalloy materials used in this study.

in the subsurface regions is the first step towards sub-grain formation as a result of fretting strain. It is clear from the above EBSD analysis that the stress concentration around stick-slip interface as a result of fretting contact stresses resulted in highly deformed layers from which the fretting fatigue cracks were initiated. These layers were formed as a result of fretting of contact pads on the specimen surface. Here, the contacting superalloy combination and loading conditions influenced the extent of plastic deformation below surface. Especially for the case of single crystal material, the formation of distinct polycrystalline layer suggest that the fretting disturbed region had eventually lost its single crystal properties with continued loading [1]. The extent of deformation must be a function of contact tractions quantified in terms of TFC. Also, the presence of slip traces and secondary cracks suggest the activation of multiple slip systems and indicate the necessity of analyzing the stresses acting on the FCC slip systems which will be covered in the following chapters.

3.6 Chapter summary

The fretting fatigue failure behavior of two different Ni-base superalloys was investigated. The following conclusions are drawn.

- Significant reduction in fretting fatigue life was observed in comparison to plain fatigue life.
- For a given contact pressure, *TFC* increased with increasing bulk stress amplitude. Fretting fatigue life of superalloys was found to be controlled by *TFC*.
- At both room temperature and 600 °C, fretting fatigue life of SC/PC was lower than PC/PC fretting contact pair. Fretting fatigue life was slightly improved when tested at 600 °C, only under low stress amplitudes.
- Possible effect of contact traction and secondary orientation on the fracture behavior was noted, where early crack nucleation from the localized stress concentration points followed by macroscopic crack propagation along crystallographic planes were observed.
- A layered texture was found which was controlled by the extent of fretting contact tractions. New finer sub-grains were formed by recrystallization of remaining plastic deformation.
- A significant difference in mechanism of subsurface damage was found between the specimens tested at RT and 600 °C. Fretting fatigue crack nucleation was dominant at RT whereas, fretting wear was dominant at high temperature.

3.7 Chapter references

[1] Huang, X., Gibson, T.E., Zhang, M., Neu, R.W.. Fretting on the cubic face of a single-crystal Ni-base superalloy at room temperature. Tribology International 2009;42(6):875–885. doi:10.1016/j.triboint.2008.12.003.

[2] Fleury, R.M.N., Paynter, R.J.H., Nowell, D.. The Influence of Contacting Ni-based Single-crystal Superalloys on Fretting Fatigue of Ni-based Polycrystalline Superalloys at High Temperature. Tribology International 2014;76:63–72. doi:10.1016/j.triboint.2014.01.011.

[3] Murthy, H., Garcia, D.B., Matlik, J.F., Farris, T.N.. Fretting Fatigue of Single Crystal/Polycrystalline Nickel Subjected to Blade/Disk Contact Loading. Acta Astronautica 2005;57:1–9. doi:10.1016/j.actaastro.2004.11.007.

[4] JSME Standard method of fretting fatigue testing, JSME S 015-2002. The Japan Society of Mechanical Engineers; 2002.

[5] Liu, Y., Varghese, S., Ma, J., Yoshino, M., Lu, H., Komanduri, R.. Orientation effects in nanoindentation of single crystal copper. International Journal of Plasticity 2008;24(11):1990–2015. doi:10.1016/j.ijplas.2008.02.009.

[6] Savage, M.W.R.. The Influence of Crystal Orientation on the Elastic Stresses of a Single Crystal Nickel-Based Turbine Blade. Journal of Engineering for Gas Turbines and Power 2012;134(1):012501: 1–7. doi:10.1115/1.4004129.

[7] Okazaki, M., Imai, T., Satoh, T., Nohmi, S.. Fatigue Small Crack Growth in a Single Crystal NI-Base Superalloy at Elevated Temperature. Journal of The Society of Materials Science Japan 1992;41(467):1261–1267. doi:10.2472/jsms.41.1261.

[8] Harris, K.. High temperature alloys committee: Session on recent advanvces in Superalloy Technology. Tech. Rep.; 1982.

[9] Mall, S., Kim, H., Porter, W.J., Ownby, J.F., Traylor, A.G.. High temperature fretting fatigue behavior of IN100. International Journal of Fatigue 2010;32(8):1289–1298. doi:10.1016/j.ijfatigue.2010.01.012.

[10] Waterhouse, R.B.. Fretting at high temperatures. Tribology International 1981;14(4):203–207. doi:10.1016/0301-679X(81)90041-4.

[11] Okane, M., Shiozawa, K., Ishikura, T.. Fretting Fatigue Behavior of TiN-Coated Steel. In: Fretting Fatigue: Current Technology and Practices, ASTM STP 1367. West Conshohocken, PA: ASTM International; 2000, p. 465–476. doi:10.1520/STP14748S.

[12] Giannakopoulos, A., Lindley, T., Suresh, S.. Aspects of equivalence between contact mechanics and fracture mechanics: theoretical connections and a life-prediction methodology for fretting-fatigue. Acta Materialia 1998;46(9):2955–2968. doi:10.1016/S1359-6454(98)00011-1.

[13] Nakazawa, K., Sumita, M., Maruyama, N.. Effect of Contact Pressure on Fretting Fatigue of High Strength Steel and Titanium Alloy. In: Standardization of Fretting Fatigue Test Methods and Equipment. 100 Barr Harbor Drive, PO Box C700, West Conshohocken, PA 19428-2959: ASTM International; 1992, p. 115–125. doi:10.1520/STP25824S.

[14] Giannakopoulos, A.E., Venkatesh, T.A., Lindley, T.C., Suresh, S.. Role of adhesion in contact fatigue. Acta Materialia 1999;47(18):4653–4664. doi:10.1016/S1359-6454(99)00312-2.

[15] Fouvry, S., Duó, P., Perruchaut, P.. A quantitative approach of Ti–6Al–4V fretting damage: friction, wear and crack nucleation. Wear 2004;257(9):916–929. doi:10.1016/j.wear.2004.05.011.

[16] Yang, B., Mall, S.. On Crack Initiation Mechanisms in Fretting Fatigue. Journal of Applied Mechanics 2001;68(1):76. doi:10.1115/1.1344901.

[17] Arakere, N.K., Knudsen, E., Swanson, G.R., Duke, G., Ham-Battista, G.. Subsurface Stress Fields in Face-Centered-Cubic Single-Crystal Anisotropic Contacts. Journal of Engineering for Gas Turbines and Power 2006;128(4):879. doi:10.1115/1.2180276.

[18] Balavenkatesh, R., Baba, S., Okazaki, M.. Influence of Crystal Orientation on Cyclic Sliding Friction and Fretting Fatigue Behavior of Single Crystal Ni-Base Superalloys. In: Superalloys 2016. Hoboken, NJ, USA: John Wiley & Sons, Inc.; 2016, p. 395–404. doi:10.1002/9781119075646.ch43.

[19] Waterhouse, R.. Fretting fatigue. Applied Science Publishers; 1981.

[20] Sabelkin, V., Martinez, S.A., Mall, S., Sathish, S., Blodgett, M.P.. Effects of shot-peening intensity on fretting fatigue crack-initiation behaviour of Ti-6Al-4V. Fatigue and Fracture of Engineering Materials and Structures 2005;28(3):321–332. doi:10.1111/j.1460-2695.2005.00871.x.

[21] Takeda, J., Niinomi, M., Akahori, T., Gunawarman, . Fretting Fatigue Characteristics with Relating Contact Pressure and Surface Roughness of Highly Workable Titanium Alloy, Ti-4.5Al-3V-2Mo-2Fe. MATERIALS TRANSACTIONS 2004;45(5):1586–1593. doi:10.2320/matertrans.45.1586.

[22] Madge, J.J., Leen, S.B., Shipway, P.H.. A combined wear and crack nucleation-propagation methodology for fretting fatigue prediction. International Journal of Fatigue 2008;30(9):1509–1528. doi:10.1016/j.ijfatigue.2008.01.002.

[23] Murthy, H., Gao, G., Farris, T.N.. Fretting Fatigue of Single Crystal Nickel at 600 C. Tribology International 2006;39(10):1227–1240. doi:10.1016/j.triboint.2006.02.050.

[24] Nishioka, K., Hirakawa, K.. Fundamental Investigations of Fretting Fatigue : Part 3, Some Phenomena and Mechanisms of Surface Cracks. Bulletin of JSME 1969;12(51):397–407. doi:10.1299/jsme1958.12.397.

[25] Schwartz, A.J., Kumar, M., Adams, B.L., Field, D.P., editors. Electron Backscatter Diffraction in Materials Science. Boston, MA: Springer US; 2009. ISBN 978-0-387-88135-5. doi:10.1007/978-0-387-88136-2.

[26] Prasad, S., Michael, J., Christenson, T.. EBSD studies on wear-induced subsurface regions in LIGA nickel. Scripta Materialia 2003;48(3):255–260. doi:10.1016/S1359-6462(02)00376-7.

[27] Zhou, J.M., Bushlya, V., Peng, R.L., Stahl, J.E.. Identification of Subsurface Deformation in Machining of Inconel 718. Applied Mechanics and Materials 2011;117-119:1681–1688. doi:10.4028/www.scientific.net/AMM.117-119.1681.

[28] Okazaki, M., Hiura, T., Suzuki, T.. Effect of Local Cellular Transformation on Fatigue Small Crack Growth in CMSX-4 and CMSX-2 at High Temperature. Proceedings, Superalloys 2000, TM Pollock et al, TMS 2000;:505–514.

[29] Okazaki, M., Ohtera, I., Harada, Y.. Damage Repair in CMSX-4 Alloy without Fatigue Life Reduction Penalty. Metallurgical and Materials Transactions A 2004;35A(2):535–542. doi:10.1007/s11661-004-0364-5.

[30] Rettberg, L.H., Pollock, T.M.. Localized recrystallization during creep in nickel-based superalloys GTD444 and René N5. Acta Materialia 2014;73:287–297. doi:10.1016/j.actamat.2014.03.052.

[31] Kuhn, F., Zeismann, F., Brueckner-Foit, A.. Crack growth mechanisms in an aged superalloy at high temperature. International Journal of Fatigue 2014;65:86–92. doi:10.1016/j.ijfatigue.2013.05.014.

[32] Swalla, D.R., Neu, R.W., McDowell, D.L.. Microstructural Characterization of Ti-6Al-4V Subjected to Fretting. Journal of Tribology 2004;126(4):809. doi:10.1115/1.1792677.

THIS PAGE INTENTIONALLY LEFT BLANK

Chapter 4

Estimation of fretting fatigue crack propagation life and crack initiation stress state

Analytical study on the fretting fatigue crack propagation and crack initiation stress state is detailed. The influence of tangential tractions between the contacting superalloys on the crack propagation behavior are studied using a model based on crack analogue approach. Furthermore, the variation of sub-surface stress state under the action of fretting stresses acting on different crystallographic orientations which control the crack nucleation process is formulated. The role of tangential force coefficient and orientation on the resolved stresses on single crystal slip systems are analyzed in detail. Correlations with experimental findings are shown to have good agreement.

4.1 Introduction

This chapter deals with the analytical investigation on the estimation of fretting fatigue crack propagation life and crack initiation stress state. Thus, the chapter is divided into two sections:

1. Analysis of crack propagation process - life estimation based on experiments.
2. Analysis of crack initiation process - sub-surface stress field acting on FCC slip systems.

4.2 Analysis of crack propagation process

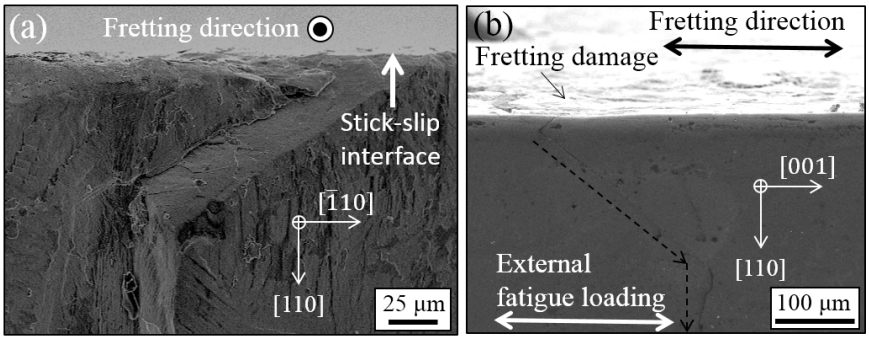

Figure 4-1: Fracture morphology of CMSX-2 tested at RT (a) cross section of fracture surface showing inclined crack nucleation and (b) longitudinal cross section of the same specimen showing two stage crack propagation ($\sigma_{app} = 300\,\text{MPa}$)

Typical fracture morphology observed in SC CMSX-2 specimen subjected to fretting fatigue is shown in Fig. 4-1. The primary crack was nucleated from the stick-slip interface (location of high stress concentration) at an inclined angle to the surface (Stage A). Then, the crack was reoriented to grow in a direction normal to the external fatigue loading axis (Stage B). This transition can be attributed to the competition between contact stresses arising from fretting action and the bulk stress amplitude. Several authors proposed fracture mechanics based approaches for the prediction of fretting fatigue life of polycrystalline alloys [1–8]. Giannakopoulos et al. [9] used the analogy in stress state between contact mechanics and fracture mechanics, thereby

introducing a methodology to estimate fretting fatigue life, by considering the two stages of crack growth, as shown in Fig. 4-2. They also highlighted the influence of *COF* on the crack initiation angle and effective stress intensity factors acting on the crack tip. Crack analogue (CA) model is employed in this work to estimate the fretting fatigue life by incorporating experimentally measured TFC values (Fig. 3-8). For the sake of completeness, this section derives the important parameters considered in the CA model [9].

4.2.1 Crack analogue (CA) model

This model is based on the analogy between the stress state due to fretting forces in terms of contact mechanics domain and that of due to stress intensity factors for double-edge cracked specimen in fracture mechanics domain. By identify the equivalence between the two cases it is possible to convert the fretting contact problem into fracture mechanics problem of crack kinking, which is schematically shown in .

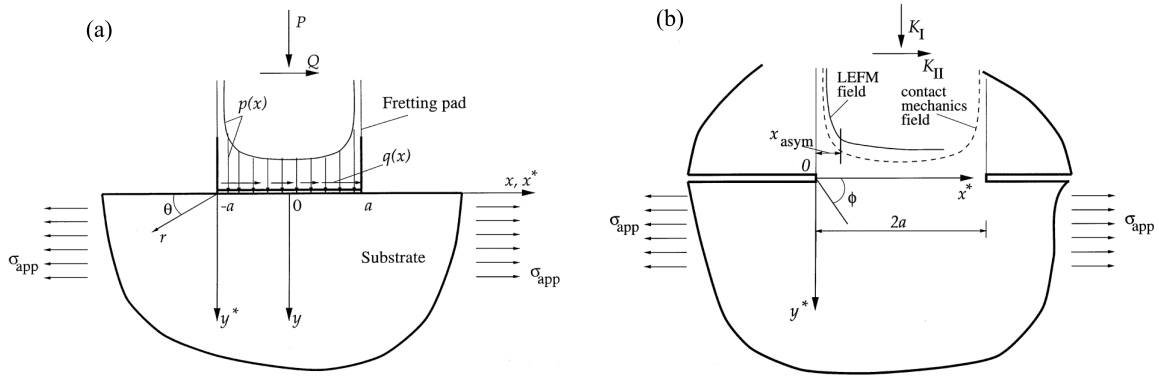

Figure 4-2: Crack analogue model (a) fretting contact of flat punch (contact pad) and infinite half-plane (specimen) subjected to normal and tangential forces, (b) crack analogue of (a) as a double-edge cracked specimen subjected to mode I and mode II SIFs [9].

(a) Stress intensity factors

The remote stress intensity factors, K_I and K_{II} due to normal line force P and tangential line force Q are given by,

$$K_I = -\frac{P}{\sqrt{\pi a}}, \qquad K_{II} = \frac{Q}{\sqrt{\pi a}}. \tag{4.1}$$

where, a is the half-width of the contact pad foot.

The local stress intensity factors at the tip of incipient small crack initiating from the surface, k_1 and k_2 can be computed in terms of remote K_I and K_{II} by [10]:

$$\begin{aligned} k_1 &= a_{11}(\phi)K_I + a_{12}(\phi)K_{II} \\ k_2 &= a_{21}(\phi)K_I + a_{22}(\phi)K_{II} \end{aligned} \tag{4.2}$$

where, a_{ij} - dimensionless factors (function of crack initiation angle) for the infinitesimal kink (after Cotterell and Rice [10]).

$$\begin{aligned} a_{11}(\phi) &= \frac{1}{4}\left(3\cos\frac{\phi}{2} + \cos\frac{3\phi}{2}\right), \\ a_{12}(\phi) &= -\frac{3}{4}\left(\sin\frac{\phi}{2} + \sin\frac{3\phi}{2}\right), \\ a_{21}(\phi) &= \frac{1}{4}\left(\sin\frac{\phi}{2} + \sin\frac{3\phi}{2}\right), \\ a_{22}(\phi) &= \frac{1}{4}\left(3\cos\frac{\phi}{2} + 3\cos\frac{3\phi}{2}\right). \end{aligned} \tag{4.3}$$

(b) Crack initiation angle ϕ_{in}

It is assumed that the crack is initiating in a direction along which k_2 is zero, i.e. maximum shear energy direction. Thus the crack initiation angle ϕ_{in} can be computed by solving the equations in Eq. (4.2) by invoking the condition that $k_2 = 0$ and is

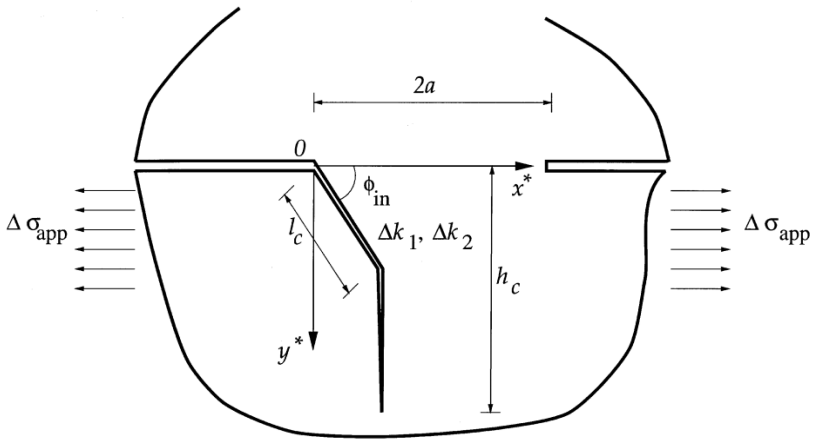

Figure 4-3: schematic of two stage crack propagation analysis using crack analogue model [9].

given by,

$$\left(\sin\frac{\phi_{in}}{2}+\sin\frac{3\phi_{in}}{2}\right)\times\left\{\left|\cos\frac{\phi_{in}}{2}+3\cos\frac{3\phi_{in}}{2}\right|\right\}^{-1} = \frac{Q_{max}}{P}=TFC \tag{4.4}$$

where, TFC - tangential force coefficient

(c) Stage A crack growth life N_A

A fatigue crack initiating at ϕ_{in} is subjected to an effective stress intensity factor (arising from static P and cyclic Q), Δk_1, given by,

$$\Delta k_1 = \pm\frac{3}{4}\Delta K_{II}\left(\sin\frac{\phi_{in}}{2}+\sin\frac{3\phi_{in}}{2}\right) \tag{4.5}$$

The fatigue crack initiated at angle of ϕ_{in} would first propagate under the influence of P and ΔQ over a distance of l_c, before deflecting to propagate in a direction perpendicular to $\Delta\sigma_{app}$. This transition in crack growth occurs when the local *driving force* for fatigue crack growth due solely to $\Delta\sigma_{app}$ begins to exceed that due solely to P and ΔQ. At the critical length l_c, the local Δk_1 due to $\Delta\sigma_{app}$ is [11]:

$$(\Delta k_1)_{\Delta\sigma_{app}} = 1.12\Delta\sigma_{app}\sqrt{\pi(l_c \sin\phi_{in})} \geq (\Delta k_1)_{P,\ \Delta Q} \tag{4.6}$$

Now number of cycles for stage I crack length can be computed using Paris law as follows,

$$N_A = \int_0^{l_c} \frac{dl}{C\left(\Delta k_1\right)^m} \approx \frac{l_c}{C\left(\Delta k_1\right)^m} \tag{4.7}$$

where, C and m are Paris law constants.

(d) Stage B crack growth life N_B

Stage B of crack propagation is solely under the influence of $\Delta\sigma_{app}$ until a critical length, h_c, at which maximum SIF reaches the fracture toughness of the material, K_c (for a very deep substrate):

$$K_{max} = 1.12[\sigma_{app}]_{max}\sqrt{\pi h_c} \rightarrow K_c \tag{4.8}$$

where, K_c - fracture toughness of the material.
Stage B life can be calculated as follows,

$$N_B = \int_{l_c \sin\phi_{in}}^{h_c} \frac{dl}{C\left(1.12\Delta\sigma_{app}\sqrt{\pi l}\right)^m} \tag{4.9}$$

(e) Comparison: Application of CA model to present work

The variation of TFC with applied bulk stress amplitude during fretting fatigue tests is plotted in Fig. 3-8. It is clear that the TFC can be fitted as a linear function of bulk stress amplitude as follows:

$$TFC = m_1\sigma_{app} + c_1 \tag{4.10}$$

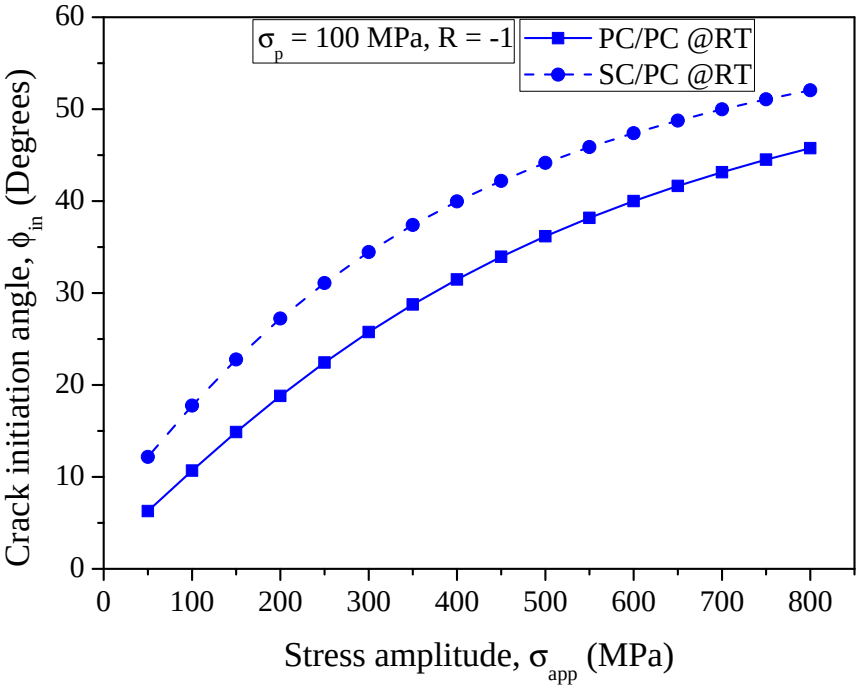

Figure 4-4: Crack initiation angle as a function of applied bulk stress amplitude

where m_1 and c_1 are experimental constants that depend on contact pair and loading conditions.

Now the *TFC* can be used to solve for ϕ_{in} in Eq. (4.4). The calculated values of ϕ_{in} for two different contacting pairs are presented in Fig. 4-4, where ϕ_{in} (angle from the surface) gradually increased with the increase in bulk stress amplitude σ_{app}. The ϕ_{in} was fitted as a quadratic function of σ_{app} as follows:

$$\phi_{in} = a_2 {\sigma_{app}}^2 + b_2 \sigma_{app} + c_2 \tag{4.11}$$

where a_2, b_2 and c_2 are curve fitting constants. The calculated values of empirical constants from the current fretting fatigue experiments on two contact pairs are presented in Table 4.1.

The total number of cycles to failure ($N_{CA} = N_A + N_B$) can now be calculated by incorporating Eqs. (4.10) and (4.11) together with the fatigue properties listed in Table 4.2, to calculate local SIFs through Eq. (4.1) to Eq. (4.8). Estimated cycles

Table 4.1: Curve fit parameters calculated from room temperature fretting fatigue experiments

Pair	m_1	c_1	a_2	b_2	c_2
PC/PC	8×10^{-3}	0.0152	-5×10^{-5}	0.0926	2.0432
SC/PC	1.1×10^{-3}	0.0542	-7×10^{-5}	0.1077	7.8196

to failure curves for two different contacting superalloys pairs are plotted in Fig. 4-5 and are compared with experimental lives. The upper and lower scatter band curves (dashed) on either side of the predicted life curve (dotted-dashed) in Fig. 4-5, represent 1/3 and 3 times the predicted fretting fatigue lives, respectively. A good correlation was found between predicted and experimental fretting fatigue lives. Note that the length of stage I and stage II cracks calculated in CA model are for deep substrate (under the assumption of infinite half-plane) although the actual specimens have finite width. However, CA model could still be effective for estimation of fretting fatigue life in terms of total number of cycles to failure.

Table 4.2: Fatigue properties of PC superalloy [12].

Property	Value
C $[(\text{MPa})^{-3}\text{m}^{-1/2}]$	3×10^{-13}
m [-]	4
K_c $[\text{MPa}\sqrt{\text{m}}]$	130.8

4.2.2 Extension of CA model to estimate the effect of secondary crystallographic orientation of SC

For the case of contact between SC and PC alloys, the stress state below the contact must be sensitive to secondary crystallographic orientation of SC with respect to contact pressure direction (or fretting plane normal) [13, 14]. In order to explore this aspect, fretting fatigue tests (under identical loading conditions) were carried out with SC specimens having different secondary crystallographic orientations β as schematically shown in Fig. 3-4.

Fig. 4-6 shows the evolution of TFC with fretting fatigue cycles for two different

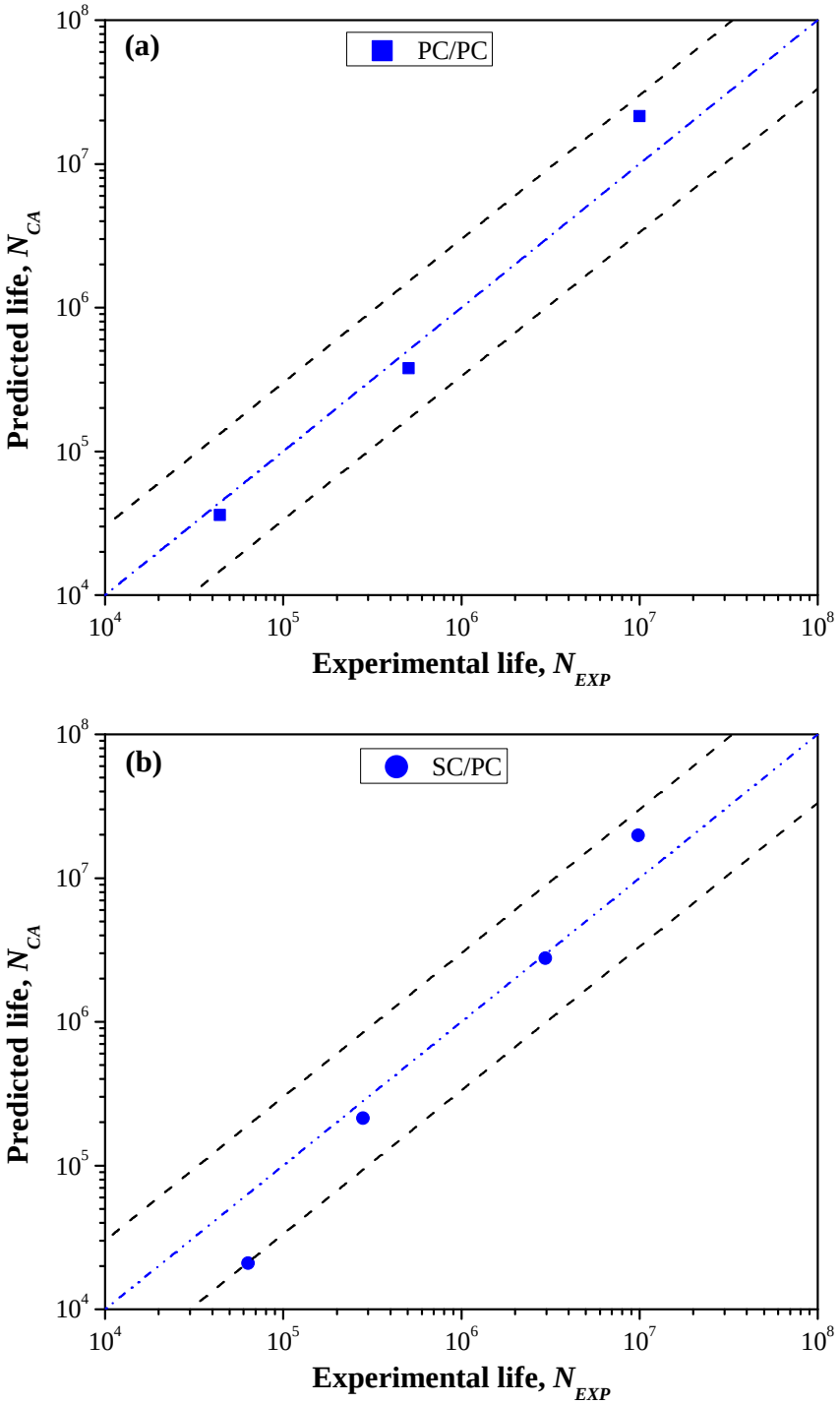

Figure 4-5: Room temperature experimental life versus predicted life using CA model for (a) PC IN718 and (b)SC CMSX-2

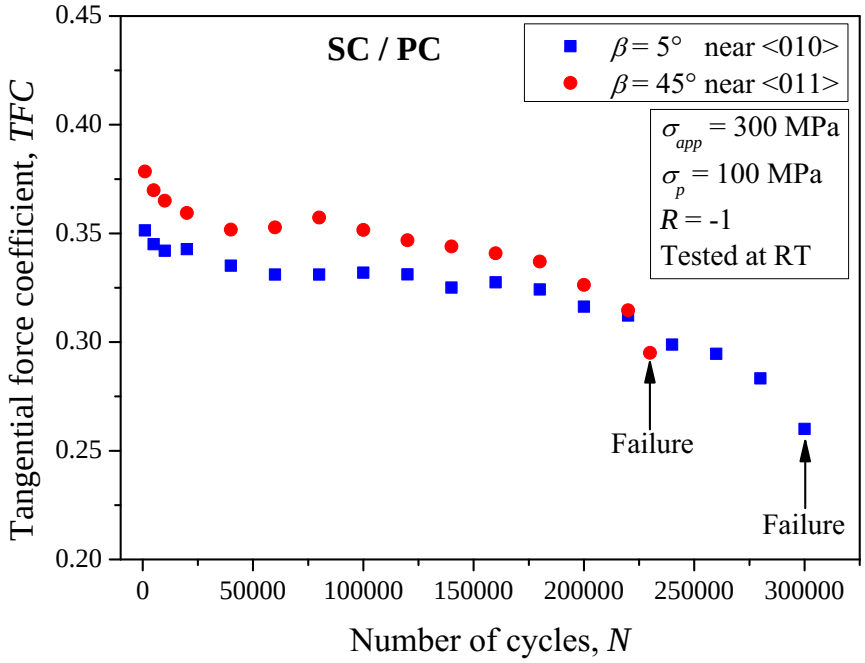

Figure 4-6: Evolution of TFC with fretting fatigue cycles on SC specimens having two different secondary orientations under identical loading conditions.

β orientations. Note that the applied contact pressure σ_p was 100 MPa, for both orientations. However, the TFC was observed to be higher for $\beta = 45°$ specimen than that of $\beta = 5°$ specimen. As one would expect, the specimen with higher *TFC* ($\beta = 45°$) failed faster than the other specimen. Similar trends in cyclic sliding friction behavior and contact stress field with respect to secondary crystal orientation were confirmed in a previous study by the authors [13]. Thus, it is possible to estimate the fretting fatigue life of SC/PC fretting contact using CA model by incorporating the experimental knowledge of tangential force coefficient *TFC* evolution with respect to secondary crystallographic orientation.

Limitations of crack analogue model

In the previous section, life estimation based on crack analogue model is described. However, there are certain limitations to the model despite its attractiveness in simplicity. Cycles to crack initiation is set to zero i.e. crack initiation is neglected. Furthermore, the model is based on macroscopic treatment of contact tractions where

sub-surface stress state is not taken in to account. However, in the single crystal alloys slip deformation occurs according to the stress state on preferred slip planes. The knowledge of sub-surface stress state in single crystal material due to fretting stresses become inevitable. Also, it is necessary to investigate the effect of secondary orientation on stress state. In order to extend the analysis to a microscopic level, next section elaborates an approach based on point forces.

4.3 Analysis of crack initiation stress state

4.3.1 Stress concentration at stick-slip interface

The previous discussion primarily focused on the effect of crystal plane and sliding orientation on the macroscopic friction/fretting along the contact interface. The above discussion based on macroscopic theory cannot be quantitatively applied for the case of fretting contact where the stress state beneath the contact and sub-surface region should also be taken into account. In this work, significant differences in fretting fatigue fracture with different orientations were observed, as presented in and Fig. 3-15 and Fig. 3-16. Murthy et al. [15] highlighted the fractographic features and preferential crack growth planes sensitive to secondary crystallographic orientations. In spite of the contact pressure being applied over a definite area, stress singularity occurs at a point along the interface between the stick-slip region, which then acted as potential crack nucleation sites (Fig. 4-7). In order to make discussion on the singularity, an analysis based on point forces acting along normal and tangential directions is helpful for further understanding of stress field due to fretting forces.

4.3.2 Boussinesq-Cerruti stress analysis: Role of secondary orientation

As suggested in the experimental observations in Figs. 3-15, 3-16 and 4-7 it must be very effective to expand discussions on the FF failure (Figs. 3-7 and 3-12) from crystallographic mechanistic view point, based on stress field at a stick/slip point

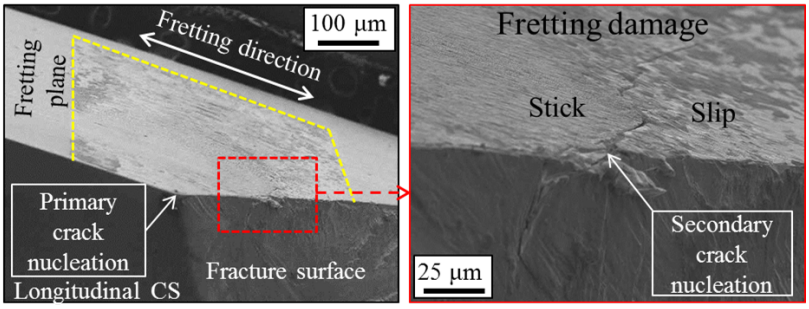

Figure 4-7: SEM image of secondary surface crack propagating along stick-slip interface ($\beta = 30°$, $\sigma_{app} = 300\,\text{MPa}$, Tested at RT).

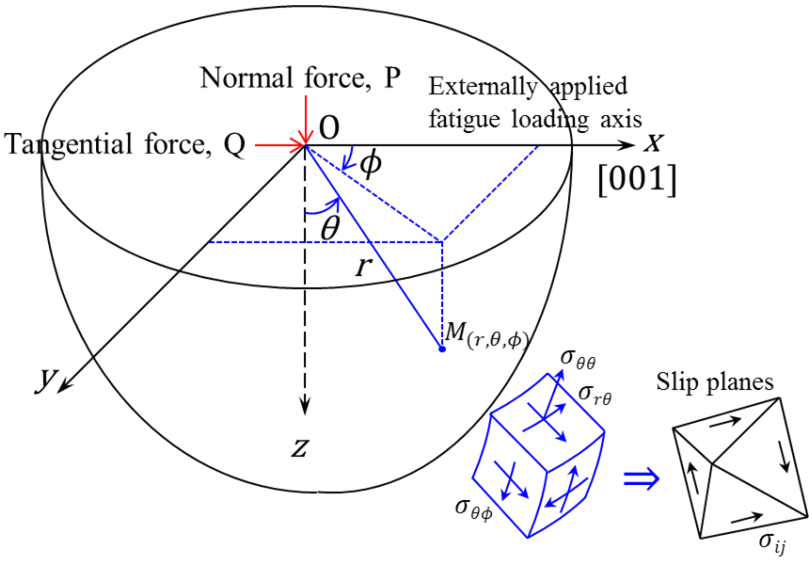

Figure 4-8: Illustration of point loading of elastic half-space with respect to single crystal cubic axes. $x - y$ plane represents the contact surface

(Figs. 3-15 and 4-7). The sub-surface stress field due to a normal point force can be estimated by solving Boussinesq's problem whereby the stress field due to tangential point force can be computed by solving Cerruti's problem [16, 17]. The stress state at any given point M (Fig. 4-8), due to applied normal and tangential forces, is given in spherical coordinate system,

$$\sigma_{rr} = -\frac{sin\theta}{\pi r^2}(Qcos\phi)\left(2 - \nu - \frac{1-2\nu}{1+cos\theta}\right) + \frac{P}{2\pi r^2}\left[1 - 2\nu - 2\,(2-\nu)\,cos\theta\right] \tag{4.12}$$

$$\sigma_{\theta\theta} = \frac{1-2\nu}{2\pi r^2}(Qcos\phi)\frac{cot\theta cos\theta}{1+cos\theta}(1-cos\theta) + \frac{P}{2\pi r^2}\frac{(1-2\nu)cos^2\theta}{(1+cos\theta)} \tag{4.13}$$

$$\sigma_{\phi\phi} = \frac{1-2\nu}{2\pi r^2}Qcos\phi\frac{cot\theta(1-cos\theta)}{1+cos\theta}(2+cos\theta) + \frac{P(1-2\nu)}{2\pi r^2}\left[cos\theta - \frac{1}{1+cos\theta}\right] \tag{4.14}$$

$$\sigma_{r\theta} = \sigma_{\theta r} = \frac{1-2\nu}{2\pi r^2}Qcos\phi\frac{cos\theta(1-cos\theta)}{1+cos\theta} + \frac{P(1-2\nu)}{2\pi r^2}\frac{sin\theta cos\theta}{1+cos\theta} \tag{4.15}$$

$$\sigma_{\theta\phi} = \sigma_{\phi\theta} = \frac{1-2\nu}{2\pi r^2}Qsin\phi\frac{cot\theta(1-cos\theta)}{1+cos\theta} \tag{4.16}$$

$$\sigma_{r\phi} = \sigma_{\phi r} = \frac{1-2\nu}{2\pi r^2}Qsin\phi\frac{1-cos\theta}{1+cos\theta}. \tag{4.17}$$

Where, P is the normal force acting along z axis, Q is the tangential force acting along x axis and ν is the Poisson's ratio. Note from Eqs. (4.12)-(4.17) that when only P is applied the $\sigma_{r\theta}$ in xz plane shows the maximum at $\theta = 52°$, and when only Q is applied the $\sigma_{r\theta}$ shows the maximum at $\theta = 66°$.

The stress components in local spherical coordinate system can be converted into single crystal cubic axes (x,y,z) as represented in Fig. 4-8 through tensor transformation which is given by,

$$\sigma_{ij} = \mathbf{A}\sigma_{st}\mathbf{A}^T \tag{4.18}$$

where, $s,t = r,\theta,\phi$ and i,j=slip plane, slip direction. The matrix $\mathbf{A}$ is the tensor transformation matrix which represent the direction cosines between two coordinate systems.

Table 4.3: Primary octahedral slip systems in FCC crystals [18].

Slip system no. (s^i)	Slip plane	Slip direction
a1	(1 1 1)	[$\bar{1}$ 1 0]
a2	(1 1 1)	[1 0 $\bar{1}$]
a3	(1 1 1)	[0 $\bar{1}$ 1]
b1	(1 $\bar{1}$ 1)	[$\bar{1}$ $\bar{1}$ 0]
b2	(1 $\bar{1}$ 1)	[1 0 $\bar{1}$]
b3	(1 $\bar{1}$ 1)	[0 1 1]
c1	(1 $\bar{1}$ $\bar{1}$)	[$\bar{1}$ $\bar{1}$ 0]
c2	(1 $\bar{1}$ $\bar{1}$)	[1 0 1]
c3	(1 $\bar{1}$ $\bar{1}$)	[0 1 $\bar{1}$]
d1	(1 1 $\bar{1}$)	[$\bar{1}$ 1 0]
d2	(1 1 $\bar{1}$)	[1 0 1]
d3	(1 1 $\bar{1}$)	[0 $\bar{1}$ $\bar{1}$]

4.3.3 Stresses acting on slip systems due to fretting forces

In the case of single crystal Ni-base superalloys which have FCC crystal structure, slip occurs on crystal planes which possess high atomic density and in a direction where the atoms are closely packed [18]. Thus the primary slip systems consist of 12 independent {111} <110> group of slip systems as listed in Table 4.3. The normal stress on each plane, σ_{rns}, and shear stress on each slip system, $\tau_{rss,i}$, can be calculated by Eq.(4.18) and Eqs.(4.12)-(4.17)[18].

Resolved normal Stresses (σ_{rns})

$$\sigma_{rns} = \begin{pmatrix} \sigma_{(111)} \\ \sigma_{(\bar{1}1\bar{1})} \\ \sigma_{(1\bar{1}\bar{1})} \\ \sigma_{(\bar{1}\bar{1}1)} \end{pmatrix} = \begin{pmatrix} \sigma^A \\ \sigma^B \\ \sigma^C \\ \sigma^D \end{pmatrix} = \frac{1}{\sqrt{9}} \begin{bmatrix} 1 & 1 & 1 & 2 & 2 & 2 \\ 1 & 1 & 1 & -2 & 2 & -2 \\ 1 & 1 & 1 & -2 & -2 & 2 \\ 1 & 1 & 1 & 2 & -2 & -2 \end{bmatrix} \begin{Bmatrix} \sigma_{11} \\ \sigma_{22} \\ \sigma_{33} \\ \sigma_{12} \\ \sigma_{31} \\ \sigma_{23} \end{Bmatrix} \tag{4.19}$$

Resolved shear stresses (τ_{rss})

$$\tau_{rss} = \begin{pmatrix} \tau^{a1} \\ \tau^{a2} \\ \tau^{a3} \\ \tau^{b1} \\ \tau^{b2} \\ \tau^{b3} \\ \tau^{c1} \\ \tau^{c2} \\ \tau^{c3} \\ \tau^{d1} \\ \tau^{d2} \\ \tau^{d3} \end{pmatrix} = \frac{1}{\sqrt{6}} \begin{bmatrix} 1 & 0 & -1 & 1 & 0 & -1 \\ 0 & -1 & 1 & -1 & 1 & 0 \\ 1 & -1 & 0 & 0 & 1 & -1 \\ -1 & 0 & 1 & 1 & 0 & -1 \\ -1 & 1 & 0 & 0 & -1 & -1 \\ 0 & 1 & -1 & -1 & -1 & 0 \\ 1 & -1 & 0 & 0 & -1 & -1 \\ 0 & 1 & -1 & -1 & 1 & 0 \\ 1 & 0 & -1 & -1 & 0 & -1 \\ 0 & -1 & 1 & -1 & -1 & 0 \\ -1 & 0 & 1 & -1 & 0 & -1 \\ -1 & 1 & 0 & 0 & 1 & -1 \end{bmatrix} \begin{Bmatrix} \sigma_{11} \\ \sigma_{22} \\ \sigma_{33} \\ \sigma_{12} \\ \sigma_{31} \\ \sigma_{23} \end{Bmatrix} \tag{4.20}$$

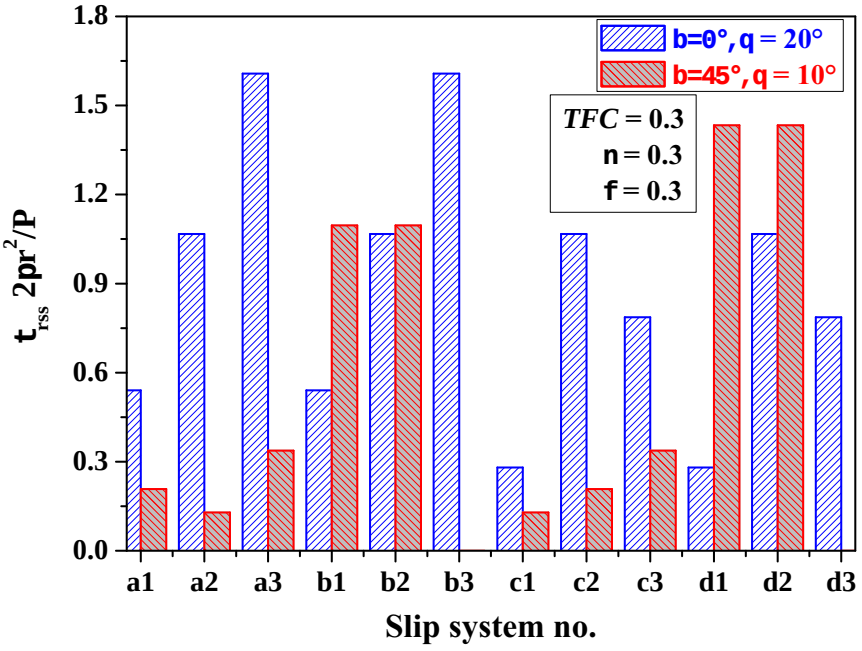

Figure 4-9: Resolved shear stresses on all octahedral slip systems for different β orientations (<001> tangential force, $TFC = 0.3$, $\nu = 0.3$).

4.3.4 Distribution of resolved shear stress amplitude

Fig. 4-9 shows the variation of resolved shear stresses on all possible primary octahedral slip systems due to the applied normal load along [100] and [110] directions for the case of $TFC = 0.3$. Note that the activated slip systems depend on the secondary orientation angle, β, and the θ angle. The maximum of $\tau_{rss,i}$, $(\tau_{rss})_{max}$ over unit area with respect to θ is plotted in Fig. 4-10, where the region with $\theta = 90°$ corresponds to the specimen surface. The distance from the origin corresponds to the magnitude of the maximum $\tau_{rss,i}$. The τ_{rss} shown in Fig. 4-10 is supposed to act when the external load reaches maximum during the cyclic fretting fatigue test. Noteworthy, $(\tau_{rss})_{max} \neq 0$ and it was 25% higher for $\beta = 45°$ than for $\beta = 0°$, at the surface.

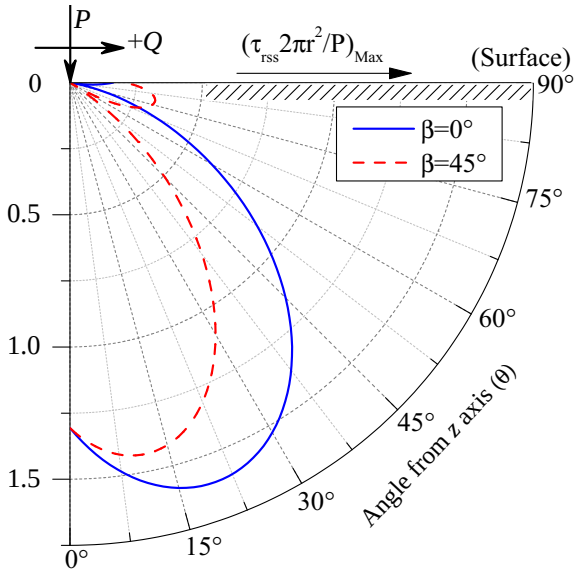

Figure 4-10: Distribution of the maximum resolved shear stress as function of angle θ from z axis ($TFC = 0.3$, $+Q$ direction, $\nu = 0.3$).

4.3.5 Distribution of resolved shear stress range

During the present fretting fatigue test, the tangential force is oscillated between $-Q$ and $+Q$ in a mechanistic mode. Thus not only the τ_{rss} given in Fig. 4-10 but also the range, $\Delta\tau_{rss}$, should be considered. Fig. 4-11 shows the $(\Delta\tau_{rss})_{max}$ for $TFC = 0.3$, where the higher $\Delta\tau_{rss}$ area spreads near the surface with a maximum at an angle of

15° from the surface. The corresponding most activated slip systems are found to be the slip systems $a3$ and $b3$ for $\beta = 0°$, and $b3$ and $c2$ for $\beta = 45°$ respectively, which contain newly activated slip systems due to fretting fatigue.

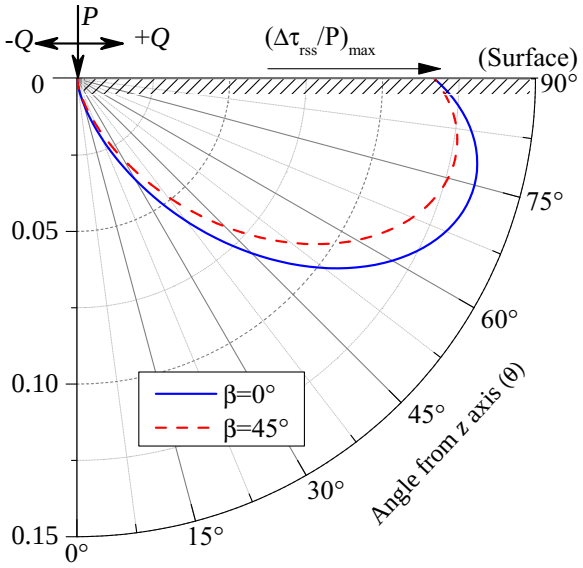

Figure 4-11: Distribution of the maximum resolved shear stress range as function of angle θ from z axis during cyclic Q ($TFC = 0.3, \nu = 0.3$).

4.3.6 Effect of elastic modulus of contacting materials

The influence of elastic modulus of SC alloy (E_{ijkl}), can be estimated as shown in Fig. 4-12 for a fretting fatigue test combination between the present SC/PC alloys. It is noteworthy to note that the distance from the origin corresponds to the magnitude of $\Delta\tau_{rss}$ in which a possible effect of elastic modulus of contact plane is taken into account by Eq.(2.5). It is evident from Fig. 4-12 that the elastic modulus along loading direction essentially controls the magnitude of $(\Delta\tau_{rss})_{max}$ and the most activated slip systems which in turn influence the crack nucleation and growth life. These differences were well reflected in the crack growth and fracture regions observed in Fig. 3-15.

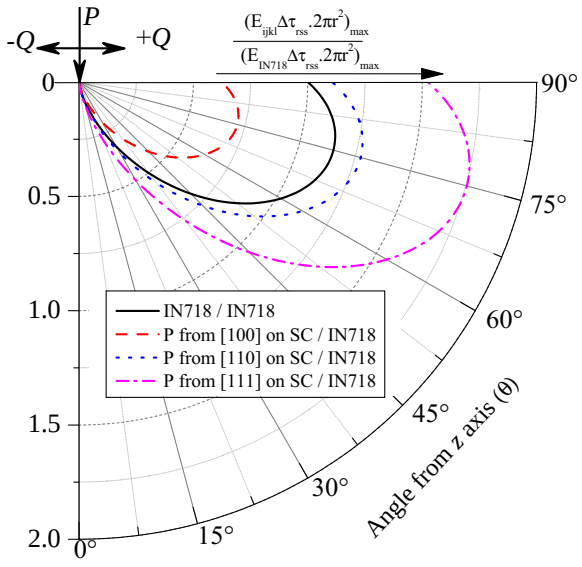

Figure 4-12: Effect of elastic modulus of contacting bodies on the maximum shear stress range ($TFC = 0.3, \nu = 0.3$).

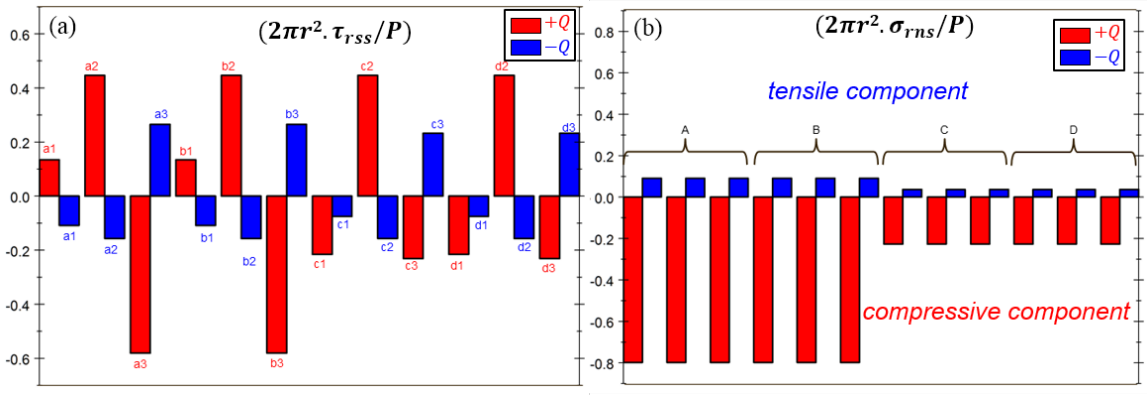

Figure 4-13: Magnitude and direction of resolved stresses on all possible primary slip systems (a) resolved shear stress and (b) resolved normal stress.

4.3.7 Role of resolved normal stresses

So far discussions are made based on the distribution of resolved shear stress range. However, the normal stress acting perpendicular to the slip plane could have an effect in the stress state [19–21]. The contribution of normal stresses are taken in to account and are plotted in Fig. 4-13. while, the sign of τ_{rss} has no physical sense, but it is very important in case of normal stress. For example, in Fig. 4-13(b), σ_{rns} is positive when Q is negative. The positive component of σ_{rns} can aid in mode I crack opening. Thus,

it is necessary to study the effect of resolved normal stresses on TFC and secondary orientation.

4.3.8 Role of TFC on magnitude and direction of resolved stresses

Fig. 4-14 shows the magnitude and direction of resolved shear and normal stresses on most activated slip systems during a fretting cycle when β=0°. The positive component of normal stress increases in magnitude with increasing TFC. Furthermore, with continued fretting cycles most activated slip systems are continuously changing with the direction of fretting. The fact that the TFC can modify the normal stress give rise to the justification for characterization based on TFC.

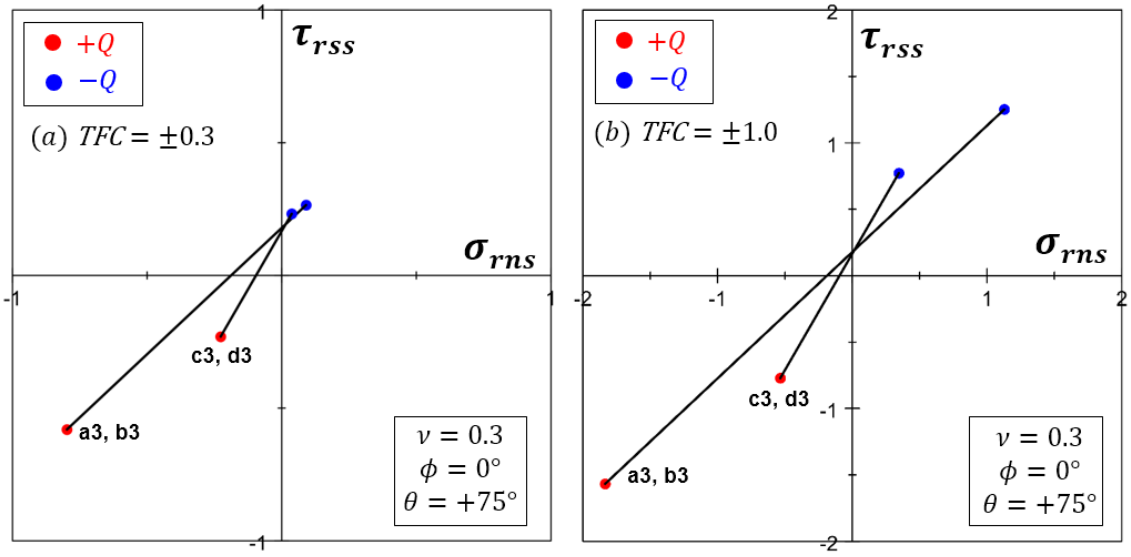

Figure 4-14: Relationship between resolved shear stress and resolved normal stress during a fretting cycle for (a) TFC=0.3 and (b) TFC=1.0.

4.3.9 Normal stress ratio as a function of TFC

Let us define a normal stress ratio, R_{rns}, given by,

$$R_{rns} = \frac{(\sigma_{rns})_{min}}{(\sigma_{rns})_{max}} \tag{4.21}$$

where, $(\sigma_{rns})_{min}$ and $(\sigma_{rns})_{min}$ are minimum and maximum values of σ_{rns} during a fretting cycle. From Eq. (4.21), it can be seen that $R_{rns} < 0$ when one of the normal stress component is positive (Tensile). Many researchers have reported that the TFC can be reach unity or higher, due to the addition of bulk loads applied to the specimen [22–25]. The variation of R_{rns} with TFC is plotted in Fig. 4-15. A set of curves are also plotted for different β values. R_{rns} increases with TFC.

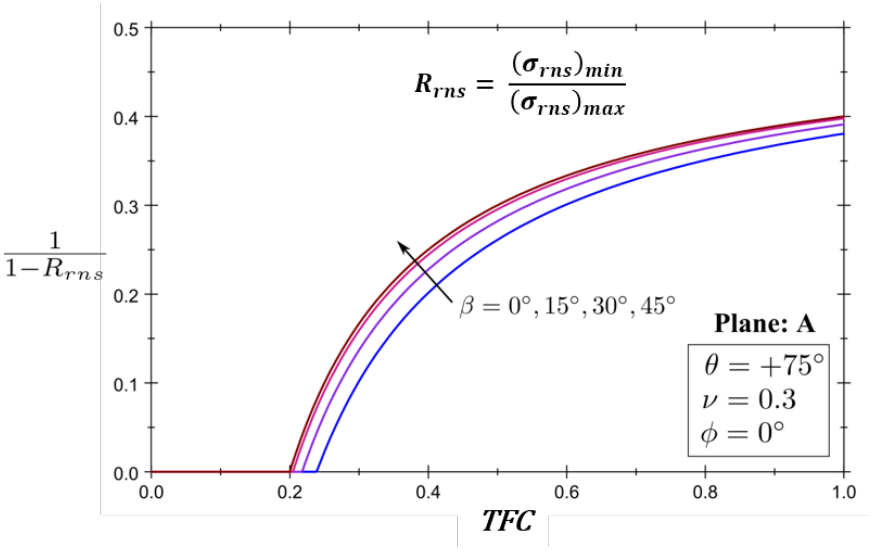

Figure 4-15: Variation of normal stress ratio as a function of TFC for different β values.

4.3.10 Equivalent stress range parameter

Brown and Miller [26] proposed an equivalent stress range parameter to evaluate multi-axial fatigue stresses. Similar parameter is used in this study which take in to account the positive component of normal stress, as defined by,

$$\Delta S_{eqv} = \begin{cases} |\Delta\tau_{rss}| + m|\Delta\sigma_{rns}| \left(\frac{1-R_{rns}}{2}\right)^C, & \text{if } R_{rns} < 0 \\ |\Delta\tau_{rss}|, & \text{otherwise} \end{cases} \tag{4.22}$$

where, $\Delta\tau_{rss}$ is the resolved shear stress range, $\Delta\sigma_{rns}$ is the resolved normal stress range, R_{rns} is the normal stress ratio defined by Eq. (4.21) and m, C are empirical constants.

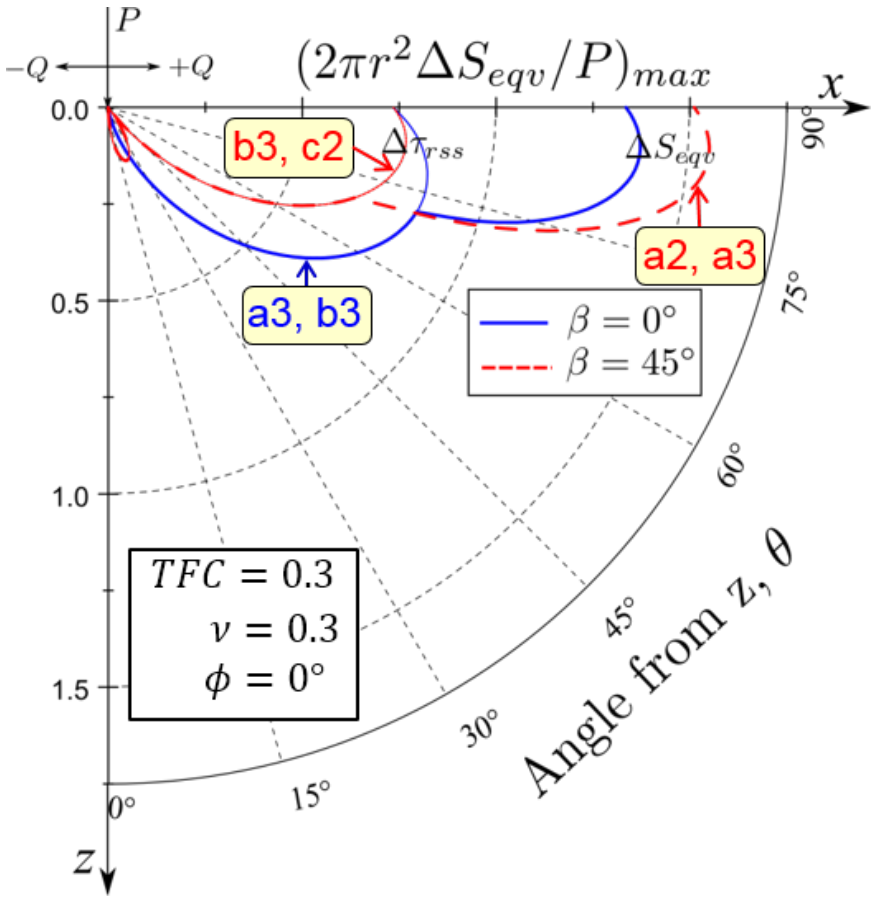

Figure 4-16: Comparison of maximum resolved shear stress range and equivalent stress range for different β values. Respective most activated slip systems are also denoted.

Distribution of equivalent stress range for most activated slip systems is presented in Fig. 4-16 together with the plot of $\Delta\tau_{rss}$. The normal stress is positive up to 15° from the surface. Due to this, magnitude of ΔS_{eqv} is higher than $\Delta\tau_{rss}$ at shallow angles to the surface. Noteworthy, most activated slip systems have not changed when $\beta = 0°$, on the other hand, $b3$ and $c2$ are activated at $\beta = 45°$ when considering only $\Delta\tau_{rss}$. New slip systems ($a2$ and $a3$) are activated when σ_{rns} is taken into account by means of ΔS_{eqv}.

A clear competition between resolved shear stresses and resolved normal stresses is evident with respect to secondary crystallographic orientation. Furthermore, the mode of deformation itself altered from shear mode to opening mode under the influence of normal stress. Thus, the additional component of resolved normal stress

induced with increasing misorientation angle from primary directions could accelerate crack initiation and facilitate faster crack propagation rate.

4.3.11 Correlation with experiments

The direction of maximum equivalent stress range is comparable with experimentally observed crack initiation angles. Comparing the fracture surfaces of SC specimens shown in Fig. 3-18, it is clear that the crack nucleated (microscopic crack nucleation) from the stick-slip interface started to grow at a shallow angle to the surface along which the equivalent stress range is maximum. Once the crack grown to sufficient length, it kinks to grow (macroscopic crack propagation) along a set of {111} slip planes. From the above discussions, increase in elastic modulus with increasing misorientation angle results in higher stress concentration at critical point. This is confirmed by the increasing trend of coefficient of friction measured in CSF tests. The increase in equivalent stress range with misorientation was found to be controlled by resolved normal stress component which could accelerate crack growth.

4.4 Chapter summary

Analytical investigations on the estimation of fretting fatigue crack propagation life and crack initiation stress state were carried out. The findings of this chapter are summarized as follows:

- Analysis of crack propagation process was performed by utilizing an analytical model based on crack analogue to estimate the fretting fatigue crack propagation life using measured TFC and plain fatigue properties of the material. It was shown that material dependent *TFC* could be successfully employed to estimate the fretting fatigue life. The effect of secondary orientation in terms of *TFC* variation is also highlighted.

- Analysis of crack initiation process was carried out to compute sub-surface stress field acting on FCC crystallographic slip systems. The shallow fretting

fatigue crack nucleation was found to be influenced by equivalent stress range parameter. A competition between resolved shear stresses (shear mode) and resolved normal stresses (opening mode) was found to be controlled by the secondary crystallographic orientation and the magnitude of TFC.

4.5 Chapter references

[1] Asai, K.. Fracture Mechanics Analysis of Fretting Fatigue Considering Small Crack Effects, Mixed Mode, and Mean Stress Effect. In: Applied Fracture Mechanics. 1; InTech; 2012, p. 177–196. doi:10.5772/51463.

[2] Attia, M.H.. Prediction of Fretting Fatigue Behavior of Metals Using a Fracture Mechanics Approach With Special Consideration to the Contact Problem. Journal of Tribology 2005;127(4):685. doi:10.1115/1.2000265.

[3] Chambon, L., Journet, B.. Modelling of fretting fatigue in a fracture-mechanics framework. Tribology International 2006;39(10):1220–1226. doi:10.1016/j.triboint.2006.02.029.

[4] Fouvry, S., Nowell, D., Kubiak, K., Hills, D.. Prediction of fretting crack propagation based on a short crack methodology. Engineering Fracture Mechanics 2008;75(6):1605–1622. doi:10.1016/j.engfracmech.2007.06.011.

[5] Hattori, T., Nakamura, M., Sakata, S., Watanabe, T.. Fretting fatigue analysis using fracture mechanics. JSME International Journal Series A 1988;31(1):100–107.

[6] Nix, K.J., Lindley, T.C.. The application of fracture mechanics to fretting fatigue. Fatigue & Fracture of Engineering Materials and Structures 1985;8(2):143–160. doi:10.1111/j.1460-2695.1985.tb01200.x.

[7] Jeung, H.K., Kwon, J.D., Lee, C.Y.. Crack initiation and propagation under fretting fatigue of inconel 600 alloy. Journal of Mechanical Science and Technology 2015;29(12):5241–5244. doi:10.1007/s12206-015-1124-8.

[8] Wei, D.S., Wang, Y.R.. Analysis of fretting fatigue life of dovetail assemblies based on fracture mechanics method. Engineering Failure Analysis 2012;25:144–155. doi:10.1016/j.engfailanal.2012.05.005.

[9] Giannakopoulos, A., Lindley, T., Suresh, S.. Aspects of equivalence between contact mechanics and fracture mechanics: theoretical connections and a life-prediction methodology for fretting-fatigue. Acta Materialia 1998;46(9):2955–2968. doi:10.1016/S1359-6454(98)00011-1.

[10] Cotterell, B., Rice, J.. Slightly curved or kinked cracks. International Journal of Fracture 1980;16(2):155–169. doi:10.1007/BF00012619.

[11] Suresh, S.. Fatigue of Materials. Cambridge: Cambridge University Press; 1998. doi:10.1017/CBO9780511806575.

[12] Xian-feng MA, Zheng DUAN, Hui-ji SHI, Ryosuke MURAI, E.Y.. Fatigue and fracture behavior of nickel-based superalloy Inconel 718 up to the very high cycle regime. Journal of Zhejiang University-SCIENCE A (Applied Physics & Engineering) 2010;11(10):727–737. doi:10.1631/jzus.A1000171.

[13] Balavenkatesh, R., Baba, S., Okazaki, M.. Influence of Crystal Orientation on Cyclic Sliding Friction and Fretting Fatigue Behavior of Single Crystal Ni-Base Superalloys. In: Superalloys 2016. Hoboken, NJ, USA: John Wiley & Sons, Inc.; 2016, p. 395–404. doi:10.1002/9781119075646.ch43.

[14] Arakere, N.K., Knudsen, E., Swanson, G.R., Duke, G., Ham-Battista, G.. Subsurface Stress Fields in Face-Centered-Cubic Single-Crystal Anisotropic Contacts. Journal of Engineering for Gas Turbines and Power 2006;128(4):879. doi:10.1115/1.2180276.

[15] Murthy, H., Garcia, D.B., Matlik, J.F., Farris, T.N.. Fretting Fatigue of Single Crystal/Polycrystalline Nickel Subjected to Blade/Disk Contact Loading. Acta Astronautica 2005;57:1–9. doi:10.1016/j.actaastro.2004.11.007.

[16] Okumura, I.A.. On the Generalization of Cerruti's Problem in an Elastic Half-space. Japan Society of Civil Engineers 1995;12(2):1–10. doi:10.2208/jscej.1995.519_1.

[17] Mindlin, R., Deresiewicz, H.. Elastic Spheres in Contact Under Varying Oblique Forces. ASME Journal of Applied Mechanics 1953;20:327–344.

[18] Stouffer, D., Dame, L.. Inelastic Deformation of Metals: Models, Mechanical Properties, and Metallurgy. NewYork: Wiley; 1996. ISBN 978-0-471-02143-8.

[19] Koss, D., Chan, K.. Fracture along planar slip bands. Acta Metallurgica 1980;28(9):1245–1252. doi:10.1016/0001-6160(80)90080-2.

[20] Chan, K., Davidson, D., Jr, S.H.. A fracture mechanics approach to high cycle fretting fatigue based on the worst case fret concept–I. Model development. International journal of fracture 2001;:299–330.

[21] Chan, K.S.. A microstructure-based fatigue-crack-initiation model. Metallurgical and Materials Transactions A 2003;34(1):43–58. doi:10.1007/s11661-003-0207-9.

[22] Nishioka, K., Hirakawa, K.. Fundamental Investigations of Fretting Fatigue : Part 3, Some Phenomena and Mechanisms of Surface Cracks. Bulletin of JSME 1969;12(51):397–407. doi:10.1299/jsme1958.12.397.

[23] Rayaprolu, D., Cook, R.. A Critical Review of Fretting Fatigue Investigations at the Royal Aerospace Establishment. In: Standardization of Fretting Fatigue Test Methods and Equipment. 100 Barr Harbor Drive, PO Box C700, West Conshohocken, PA 19428-2959: ASTM International; 1992, p. 129–152. doi:10.1520/STP25826S.

[24] Swalla, D., Neu, R.. Influence of coefficient of friction on fretting fatigue crack nucleation prediction. Tribology International 2001;34(7):493–503. doi:10.1016/S0301-679X(01)00048-2.

[25] Proudhon, H., Fouvry, S., Yantio, G.R.. Determination and prediction of the fretting crack initiation: introduction of the (P, Q, N) representation and definition of a variable process volume. International Jour-

nal of Fatigue 2006;28(7):707–713. doi:10.1016/j.ijfatigue.2005.09.005. arXiv:0810.4096.

[26] Brown, M.W., Miller, K.J.. A theory for fatigue failure under multiaxial stress–strain conditions. Proceedings of the Institution of Mechanical Engineers 1973;187(1):745–755. doi:10.1243/PIME_PROC_1973_187_161_02.

THIS PAGE INTENTIONALLY LEFT BLANK

Chapter 5

Conclusions and Future Work

5.1 Conclusions

Investigations on the influence of crystallographic orientation of single crystal Ni-base superalloys on friction and fretting fatigue behavior were carried out. So far, studies on the crystal orientation dependence on creep, TMF and HCF behavior have been reported. However, the fretting behavior of single crystal material is still not clear. This work focuses on the role of secondary crystallographic orientation in influencing the frictional tractions and in turn fretting fatigue lives at ambient and high temperature conditions. The major findings of this research work are as follows:

In **Chapter 2:** The cyclic sliding friction behavior of SC superalloy was found to be significantly influenced by the crystallographic plane of contact and sliding direction. Crystal plane (surface orientation) with higher elastic modulus revealed higher COF, especially when the contact is under mild wear condition. Crystal direction of sliding (sliding orientation) with lower yield strength also revealed higher COF. This orientation depended friction response was attributed to the differences in mechanical properties and resistance to deformation of SC along loading and sliding orientations under elastic state. Overall COF was reduced at 600 °C as a result of oxidation (formation of hard oxide layer) and thermal softening.

In **Chapter 3:** Significant reduction in fretting fatigue life was observed in comparison to plain fatigue life. For a given contact pressure, *TFC* increased with increasing bulk stress amplitude. Fretting fatigue life of superalloys was found to be controlled by *TFC*. At both room temperature and 600 °C, fretting fatigue life of SC/PC was lower than PC/PC contact pair. A relatively higher *TFC* for SC/PC resulted in life reduction. A slight improvement of life at 600 °C was attributed to the reduction in *TFC* as a result of oxidation, only under low stress amplitudes. A decreasing trend of fretting fatigue life with increasing secondary orientation angle was observed. Possible effect of contact traction and secondary orientation on the fracture behavior was noted, where early crack nucleation from the localized stress concentration points followed by macroscopic crack propagation along crystallographic planes were observed. A layered subsurface texture was formed by fretting deformation and new finer sub-grains were formed by recrystallization of remaining plastic deformation. The effect of test temperature on subsurface damage mechanism was as follows: fretting fatigue crack nucleation was dominant at RT whereas, fretting wear was dominant at high temperature.

In **Chapter 4:** An analytical model based on crack analogue was utilized to estimate the fretting fatigue crack propagation life using the measured *TFC* values and plain fatigue properties of the material. Estimated lives were in good agreement with experimental fretting fatigue lives of superalloys. Analysis on crack initiation stress state due to fretting forces on single crystal slip systems revealed significant differences with crystallographic orientation. A competition between resolved shear stresses (shear mode) and resolved normal stresses (opening mode) was found to be controlled by the secondary crystallographic orientation. The magnitude of *TFC* at the contact interface and resolved normal stresses on slip planes play a critical role in accelerating crack initiation and propagation with increasing misorientation angle. An equivalent stress range parameter was proposed to incorporate the effect of varying resolved normal stresses with secondary orientation and *TFC*. The magnitudes and directions of equivalent stress range were compared with experimental crack nucleation directions and propagation planes.

5.2 Fututre work

The findings in this study showed that the cyclic sliding friction and fretting fatigue behavior of SC superalloys are significantly influenced by secondary crystallographic orientation. Thus, it is necessary to consider the crystallographic orientation of contacting single crystal and polycrystalline superalloys during the fretting fatigue strength design process. With the knowledge of orientation effect, it would be possible to avoid premature failure of blade-disk assembly due to fretting fatigue. Furthermore, the results obtained in this study give way to the possible scope for further work. The following are the suggestions for future work:

- High temperature experiments carried out in this study (chapter 2 and 3) revealed a significant effect of oxide layers. Hence, it becomes necessary to consider the oxidation properties of the superalloys. More specifically, analysis on fretting induced oxidation (Tribo-oxidation) is suggested. Previous studies on the oxidation of single crystal superalloys reported an orientation dependent behavior. It would be of great interest to know any dependency of tribo-oxidation on crystallographic orientation. Also, the nature of interface oxides and their thicknesses could be different with respect to orientation. Given the knowledge of *COF* or *TFC* for different oxide layers, it would be possible to choose a suitable surface processing which could reduce the frictional stresses between contacting superalloys.

- In the analytical investigations (chapter 4), influence of *TFC* and secondary orientation on the crack initiation stress state were analyzed. Next step would be to quantify the number of fretting cycles for fatigue crack initiation with respect to secondary orientation. For this purpose, the stress singularity at the stick-slip interface needs to be correlated with finite stress concentration at the crack tip. However, the order of stress states are quite different between both cases. In order to normalize the stress state, wedge or point force stress field analysis in which elastic anisotropic effect is taken into consideration, combining with path integrals might be useful to estimate stress intensity factors. With

the knowledge of stress intensity factors it is straightforward to compute the cycles to crack initiation under the action fretting contact forces.

- Although the fretting fatigue tests conducted in chapter 3 provided reasonable qualitative trend, further experiments deemed necessary for improved quantitative reliability. Furthermore, significant differences in *TFC* with respect to contacting superalloys (i.e. SC/PC or PC/PC) were found. Generally, frictional properties are depended on not only the specimen material but also the slider/pad material i.e. material combination chiefly determines the frictional behavior. Further experiments at room temperature as well as at high temperature are needed to clarify this material dependent *TFC* behavior and also oxidation response.

- In addition to stress amplitude, future work should also consider the influence slip amplitude on *TFC*. In the current study, the effect of slip amplitude have been indirectly taken into account in terms of stick-slip area fraction which is a function of slip amplitude. Based on the CSF results from chapter 2, where orientation dependent residual displacements on SC were discussed, any likely behavior on fretting fatigue slip amplitude would be useful.

- Surface treatments are generally proposed as one of the palliatives for fretting fatigue. Shot peening and protective coatings have been shown to improve the fretting fatigue strength by reducing the COF at the contact interface. Another promising method is the use of abradable coatings at the contact interface, which could reduce the relative displacement between the mating parts thereby reducing the deleterious effect of fretting. Furthermore, metal-to-metal contact can also be avoided, thereby reducing surface damage. However, the compatibility of abradable coatings with single crystal superalloys needs be studied for successful application of this technology.